

Tel Aviv University

The Iby and Aladar Fleischman Faculty of Engineering
Department of Solid Mechanics, Materials and Systems

Delamination In Periodically Layered Bi-material Composites

by

Leonid Kucherov

THESIS SUBMITTED FOR THE DEGREE
"DOCTOR OF PHILOSOPHY"

SUBMITTED TO THE SENATE OF TEL AVIV UNIVERSITY

This research was carried out under supervision of

Dr. Michael Ryvkin

Monday, August 11, 2003

Acknowledgments

It has been a great pleasure working with the staff and students of the Faculty of Engineering and, in particular, of the Department of Solid Mechanics, Materials and Systems at the Tel Aviv University, during my tenure as a doctoral student.

This work could have never been if it were not the freedom I was given to pursue my research interests, thanks to the kindness and considerable supervision provided by Dr. Michael (Shmuel) Ryvkin, my scientific advisor. It is my pleasure to express gratitude to him for willingness and generosity in sharing his knowledge with me, for his insightful guidance and open mindedness, care and precision in editing my drafts.

I must especially thank Prof. Moshe Fuchs, former head of the department for his concern. Particular thanks go to Israel Sheinberger and Udi Motello for technical assistance and to Daniel Rubin and Michael Slavutin for moral support.

I owe a great deal to my teachers, Dr Michael Chebakov, and Prof. Iosif Vorovich who have played a pivotal role in my education in mechanics. I am grateful to Prof. Boris Nuller for his invaluable suggestions and encouragement, without which this dissertation would possibly not have come to fruition.

I would like to offer my appreciation to the Hammerly Family Trust that has provided the continued financial support, due to which this research has been being carried out and has been successfully finished.

I thank my family for fortifying my confidence to do what I love and for believing in me. This thesis is dedicated to my wife, Olga who deserves much more for her patience and for all the things she filled my life with.

Abstract. Delamination in periodically layered materials occurs as an intra-layer crack propagating parallel to the layering, or as an interface debonding. In this research both types of delamination are examined.

A general scheme for analysis of delamination cracks in periodically layered composites consisting of an arbitrary finite or infinite number of layers is presented. The crack is viewed as a superposition of distributed dislocations. The problem of a composite consisting of a finite number of layers is replaced by an equivalent one for a periodically layered plane. The Green's function for a single dislocation is obtained in a closed form. By means of the representative cell method based on the discrete Fourier transform, the Green's function problem is reduced to the analysis of a single bi-layered cell, the elastic solution of which is found in the form of Laplace integrals. Using this result, the problem is formulated as a system of two singular integral equations, which are solved numerically.

A number of basic delamination problems for a periodically layered bi-material plane and a periodically layered strip are examined. An extensive parametric investigation reveals, in particular, that for the interface debonding, as opposed to the case of non-interface delamination, increasing the stiffness of the thin layers can raise the stress intensity, producing some maximum. For the case of a large material mismatch between thin stiff layers and thick compliant ones, this maximum can significantly exceed the corresponding value for the crack in a homogeneous material. The results obtained in the considered delamination problems meet the asymptotes for a semi-infinite crack in the anisotropic plane, possessing effective elastic properties and known solutions for sandwich composites.

The effect of the loading direction for a crack in the periodically layered plane is examined analytically. The energy release rate and the phase shift angle appear to be functions of the loading angle, except for some specific parameter combinations. The energy release is found to have an extremum corresponding to pure normal loading. This extremum is maximum for most material combinations when the crack is sufficiently long.

In addition to the delamination problems, a closed form solution is obtained for a perfectly bonded periodically layered strip. Such a solution can be employed for the prediction of crack nucleation. Comparisons with approximate laminated plate theory are carried out, limitations of which are emphasized.

Contents

Abstract	I
List of figures	IV
Nomenclature	VI
0.1 Preface	1
1 Introduction	2
1.1 Periodic Composites	2
1.1.1 Repetitive structures	2
1.1.2 Periodic multilayers	3
1.2 Failure	5
1.2.1 Delamination as a type of failure	5
1.2.2 The effect of delamination	6
1.3 Quasi-periodic problems	7
1.4 Literature survey	8
1.4.1 Methods of analysis of symmetric elastic systems	8
1.4.2 Fracture analysis of multilayers	11
Analysis of perfectly bonded multilayers without cracks	11
Delamination models. Fracture mechanics of multilayers.	13
1.4.3 Cracks in a periodically layered bi-material composite	16
1.5 Scope of the research	18
2 Methodology	22
2.1 An interface crack in a periodically layered bi-material strip.	22
2.2 Application of the dislocation approach.	25
2.2.1 An equivalent quasi-periodic problem.	26
2.2.2 The representative cell.	28
2.3 The integral equation.	33
3 Perfectly bonded periodically layered bi-material strip	36
3.1 Closed form solution	36
3.2 Three point bending	39
3.3 Strip on a rigid foundation	41
3.4 Conclusions	42
4 Preliminary analysis of a delamination crack in a periodically layered space	44
4.1 Main definitions	45
4.2 Effect of the loading direction	48
4.3 Energy release rate for a semi-infinite crack	51

5	Interface crack in a periodically layered plane	55
5.1	Derivation of the integral equation	55
5.2	Solution of the singular integral equation	59
5.3	Numerical results	60
5.3.1	Influence of the material mismatch	60
5.3.2	Fineness of the layering	64
5.3.3	Influence of the geometry and the loading direction	65
5.4	Conclusions	68
6	Non-interface delamination crack in the periodically layered plane	70
6.1	Statement of the problem	71
6.2	Numerical Results	75
6.2.1	Influence of the materials mismatch	75
6.2.2	Fineness of the layering	77
6.2.3	Mode I crack locations	80
6.2.4	Thickness ratio of the layers.	81
6.3	Conclusions	82
7	Strip with an interface debonding	84
7.1	Delamination crack in a strip on a rigid foundation	84
7.2	Tractions-free crack in the strip subjected to point forces at the edges . .	87
7.3	Conclusions	89
8	Conclusions	91
	Bibliography	93
A		103
	Appendix	103
A.1	Matrix M	103
A.2	Matrix S for the stress boundary conditions	103
A.3	Fredholm kernels. Interface debonding	105
A.4	Fredholm kernels. Intra-layer delamination	106

List of Figures

2.1	Finite thickness periodically layered strip.	23
2.2	The equivalent cyclic problem for a periodically layered space containing dislocations and loaded by the virtual tractions defined via the stress jumps $\Delta_j(x)$	26
2.3	Problem for the representative cell with the Born-Von Karman type boundary conditions.	28
2.4	Choice of inverse Laplace integration contour Γ and associated coordinate system (x, y)	30
3.1	Periodically layered perfectly bonded strip.	37
3.2	Three point bending strip. Bending stress σ_{XX} in the cross section $X_0/H = 3$ distant from the load application points.	39
3.3	Bending stress σ_{XX} in the cross section $X_0/H = 1$ including the force line.	39
3.4	Longitudinal distribution of the bending stress $\sigma_{XX}(X, H - h_1 - 0)$ along the interface closest to the bottom within the stiffer layer.	40
3.5	Normal stress $\sigma_{YY}(X, H)$ along the fixed bottom of the strip a) and its maximal value b) for different volume fractions of the composite constituents.	42
4.1	Periodically layered plane containing a delamination crack subjected to the uniform traction at angle φ with axis y	45
4.2	Replacement of the periodically layered plane by the homogenized continuum.	52
4.3	Regions in (α, β) -plane, corresponding to the different types of the ERR dependence upon the loading angle for semi-infinite cracks.	54
5.1	Interface crack in periodically layered space.	56
5.2	Energy release rate (a) and phase shift angle (b) vs. elastic mismatch parameter α for $a/h_2 = 100$ and $\beta = 0$	61
5.3	Normalized absolute value of the SIF vs. elastic mismatch parameter α for $a/h_2 = 50$ and $\beta = \alpha/4$	63
5.4	Normalized ERR and phase shift ω vs. normalized crack length parameter h_m/a ($h_m = \min[h_1, h_2]$) for normal loading $\varphi = 0$. Elastic mismatch is specified by $\alpha = 0.8$ and $\beta = 0.2$. The curve numbers are the values of the thickness ratio h_2/h_1	64
5.5	ERR vs. relative crack length $\min\{h_1, h_2\}/a$ and loading angle φ for the sandwich with a compliant layer a), sandwich with a stiff layer b) and the periodic composite c).	65

5.6	Normalized ERR vs. relative crack length h_2/a and loading angle φ , for thickness ratio $h_2/h_1 = 0.2$ and elastic mismatch $\alpha = 0.8$ with $\beta = 0$ a) and $\beta = 0.2$ b).	66
5.7	Real phase angle vs. relative crack length h_m/a and applied loading angle φ for the sandwich composite with elastic mismatch $\alpha = 0.8$, $\beta = 0$.	67
5.8	Real phase angle vs. relative crack length h_m/a and loading angle φ for the periodically layered composite with thickness ratio $h_2/h_1 = 1$ and elastic mismatch $\alpha = 0.8$, $\beta = 0$.	67
5.9	Energy release rate (a) and real phase angle (b) vs. volume fraction h_2/h for short cracks with $h/a = 2$.	67
5.10	Energy release rate vs. volume fraction h_2/h for the long cracks with $h/a = 0.5$.	68
6.1	Periodically layered space with non-interface delamination crack.	71
6.2	SIF K_I and K_{II} vs. stiffness ratio $\mu = \mu_2/\mu_1$ for the crack of relative length $h_1/a = 0.5$ located in the compliant layer of thickness h_1 . Poisson ratios are $\nu_1 = \nu_2 = 0.3$	75
6.3	SIF K_I and K_{II} vs. normalized crack length h_1/a with the elastic mismatch specified by $\alpha = 0.8$ and $\beta = 0.2$. Crack is located in the compliant layer of thickness h_1 .	77
6.4	Dependence of the stress intensity factors \hat{K}_I and \hat{K}_{II} upon the crack location for the case of thin stiff non-cracked layers.	80
6.5	Crack location c^*/H corresponding to $\hat{K}_{II} = 0$ vs. crack length for different material mismatch with $\beta = \alpha/4$. The stiffer layers are thin $h_1/h_2 = 100$.	80
6.6	Dependence of the stress intensity factors \hat{K}_I and \hat{K}_{II} upon the outer layers thickness for different material combinations with $\beta = \alpha/4$.	81
7.1	Clamped base strip with an interface crack under the internal uniform pressure.	84
7.2	Clamped base strip with an interface crack under the internal pressure. Normalized ERR \hat{G} upon the relative crack length.	86
7.3	The absolute value of the SIF upon the crack length parameter h_2/a for different material combinations with $\beta = 0$ and various shear modulus ratio $\mu = \mu_2/\mu_1$.	88
7.4	Normalized absolute value SIF upon elastic mismatch parameter α for the case $\beta = \alpha/4$ a) and $\beta = 0$ b) and the crack length $a/h = 2$, when the strip is loaded by two point forces.	89

Nomenclature

A_j	– coefficients in the Laplace transforms (2.38)–(2.41)
\mathbf{A}	– a column-vector with elements $\{A_j\}$
a	– half the crack length
a^0	– coefficient in the singular terms in the integral equations
a_{ij}	– multipliers of the singular terms in the integral equations
a_j	– functions of the mismatch parameters and thickness ratio of the layers
\mathbf{B}	– the 12×12 matrix in equation (6.13) for derivation of A_j
\mathbf{b}^0	– vector of the Laplace transformed tractions at the strip edges
$\mathbf{b}^1, \mathbf{b}^2$	– vectors at the right hand side of the equation (2.44)
b_{ij}	– elements of the compliance matrix for orthotropic material
C	– right hand side term in integral equation (2.55)
c	– distance c above the layer midline defining the intra-layer crack location
c_n	– coefficients in Jacobi polynomial expansion (5.21) of the dislocation density
c_{ij}	– elements of the stiffness matrix
c_{ij}^*	– effective elastic moduli (elements of the stiffness matrix)
$\mathbf{D}^j(x)$	– discontinuity vector containing the stress jumps in j -th cell
d_j	– coefficients in the denominator of k_{lm} ($j = 0, 1, 2$)
d_{kn}^j	– coefficients of the system of algebraic equations (5.27) in terms of c_n
ERR	– energy release rate
$\mathbf{F}(t)$	– vector of the discontinuities across the crack line
$\hat{F}_i(t)$	– normalized dislocation densities
DFT	– Discrete Fourier Transform
FDFT	– Finite Discrete Fourier Transform
$f_1(t), f_2(t)$	– amplitudes of the dislocation at point $x = t$
$\underline{f}(t)$	$= f_1(t) + i f_2(t)$
$\overline{f}(t)$	– a complex conjugate of $f(t)$
G	– energy release rate
\hat{G}	– normalized energy release rate
G_b	– ERR for an interface crack between two dissimilar half planes
G_{hom}	– ERR for a crack in a homogeneous plane
G^{rem}	– ERR derived through the remote field
$g^*(x, y, \phi_m)$	– Discrete Fourier Transform of $g^k(x, y)$
H	– strip thickness
$H(x)$	– the Heaviside step function
h_r	– r -th layer thickness
h	$= h_1 + h_2$ – cell thickness
h_m	$= \min\{h_1, h_2\}$
\hat{h}	$= h_2/h_1$ – ratio of the layers thicknesses
K	– complex stress intensity factor
K_I, K_{II}	– the mode I and the mode II stress intensity factors
K_1, K_2	– components of the complex SIF for an interface crack
K^{hom}	– SIF for a crack under uniform loading in a homogeneous plane
K_b	– complex SIF for an interface crack between two dissimilar half planes
K_φ	– SIF corresponding to the loading angle φ
\hat{K}	– normalized stress intensity factor

$K_j(t, x)$	– kernels of the complex singular integral equation ($j = 1, 2$)
K_{ij}	– coefficients in the singular integral equations ($i, j = 1, 2$)
k_{lm}	– coefficients in the singular integral equations ($l, m = 1, 2$)
\mathcal{L}	– operator corresponding to Lamé field equations
L	$= l_1 + l_2$ – distance between the simple supports
\hat{L}	$= \min[h_1, h_2, 2a]$ – normalization length parameter
l_1, l_2	– distances between the point force line and the simple supports
\mathbf{M}	– the 8×8 matrix of the system (2.42) with respect to A_j
$M^{(ij)}$	– (i, j)-th algebraic complement of matrix \mathbf{M}
m_{ij}	– elements of matrix \mathbf{M}
m	– integer parameter of the FDFT
N	– number of cells in the strip
P	– number of cells in the cycle
$P(\varphi)$	– absolute value of normalized SIF \hat{K}
$P_n^{\eta, \zeta}(x)$	– the Jacobi polynomials
p	– right hand side term in integral equation (2.55)
Q	– normal point force applied at the top edge of the strip
Q_1, Q_2	– functions of the mismatch parameters and the thickness ratio
q	– amplitude of the tractions applied to the crack faces
r	– index denoting the layers
\mathbf{R}	– right side vector of the system (2.42)
\mathbf{S}	– 4×4 matrix of equations (2.44);(3.6) for the stress edge conditions
\mathbf{S}^C	– matrix of equation (7.6) for the clamped base strip
s	– real parameter of the Laplace or Fourier transform with respect to x
s_{ij}	– elements of the square matrix \mathbf{S}
SIF	– stress intensity factor
T	– tangential shear point force applied at the top strip edge
t	– dislocation point
$\mathbf{U}_r^k(x, y)$	– vector of the elastic field in the r -th layer of the k -th cell
$\hat{\mathbf{U}}_r^k(x, y)$	– vector of the elastic field of a perfectly bonded strip
$\check{\mathbf{U}}_r^k(x, y, t)$	– Green's function vector for a single dislocation
$\tilde{\mathbf{U}}_r^k(x, y, t)$	– solution of the auxiliary problem on a strip with a dislocation
$\tilde{\mathbf{U}}_r^*(x, y)$	$\equiv \tilde{\mathbf{U}}_r^*(x, y, t, \phi_m)$ – Fourier transformed elastic field in the representative cell
$\bar{\mathbf{U}}(z)$	– the Laplace transform of function $\mathbf{U}(x)$
u_r^k, v_r^k	– displacements in x and y directions respectively in r -th layer of k -th cell
$w(x)$	– the weight function of the Jacobi polynomials
x, y	– local Cartesian coordinates associated with the cells
X, Y	– global Cartesian coordinates associated with the strip
X_{lk}	– coefficients of the Jacobi polynomial expansion of kernels $K_j(t, x)$
z	– complex parameter of the Laplace transform
α, β	– Dundurs' mismatch parameters
Γ	– Laplace transform integration contour in z plane
$\Gamma(x)$	– the Gamma function
γ_m	$= e^{-i\phi_m}$
$\Delta_j(x)$	– the virtual stress jumps in the auxiliary problem
$\bar{\Delta}$	$= \bar{\Delta}_j(z)$ – vector of the Laplace transformed stress jumps

$\bar{\Delta}^0$	– transformed stress jump vector induced by the edge loading
$\bar{\Delta}^j$	– vector of the transformed stress jumps induced by dislocation $f_j(t)$
δ_{kn}	– the Kronecker symbol
$\delta(x)$	– the delta function
δ	$= c_{11}c_{22} - (c_{12})^2$
ϵ	– constant defining the oscillation of the crack tip stress field
ε	– real constant determining the location of contour Γ
ζ	$= -0.5 - i\epsilon$
η	$= -0.5 + i\epsilon$
$\theta_k(\eta, \zeta)$	– norm function of the Jacobi polynomials
κ_r	$= 3 - 4\nu_r$
$\mu = \mu_2/\mu_1$	– ratio of the shear moduli of the composite constituents
μ_r	– shear modulus of the r -th type layer
ν_r	– Poisson ratio of the r -th type layer
σ_r^k, τ_r^k	– stresses σ_{yy} and σ_{yx} in the r -th layer of the k -th cell
ρ	– real multiplier of the normalized ERR in (4.38)
$\sigma^u(x), \tau^u(x)$	– normal and tangent tractions on the upper edge of the strip
$\sigma^b(x), \tau^b(x)$	– normal and tangent tractions on the bottom edge of the strip
σ, τ	– uniform normal and tangent tractions applied to the crack faces
$\sigma(x), \tau(x)$	– tractions applied to the crack faces
ϕ, ϕ_m	– parameters of the DFT and FDFT respectively
φ	– angle between axis y and the direction of the crack face tractions
ψ	– real phase angle
ψ_φ	– real phase angle corresponding to loading angle φ
Ω_k	–repetitive bi-material cell
Ω	–periodically layered composite
Ω^*	–the representative cell in the DFT transformed space
ω	– phase shift angle

0.1 Preface

Man was ever intrigued by mysteries. One of them is symmetry striking the eye by the identity of recurring patterns. One pillar is grasped as nonsense while a row of columns is regarded to be aesthetic, may be, since the symmetry is a most vivid example of the order in the world. The symmetry is visible in most artificial and natural objects and constitutes internal structural arrangement of many materials. The spatial recurrence in a structure generally reduces the designing time and production costs. Moreover, when the element distribution is near-periodic or even random, the periodic model may serve as an approximation to the original one. Significant simplification, arising here from the symmetry, impels the researcher to examine periodic models.

Another mystery is an inherent ability of any solid thing to undergo fracture. Children break things to see how the fracture is happening. An engineer investigates the same question mostly for preventing failure. One could say that the fracture behavior is one of the most important characteristics of any material or structure.

Occasionally, symmetry and fracture are closely related. Failure usually originates from initial defect, which is commonly considered as a discontinuity or a dislocation, but in the framework of symmetry is viewed as perturbation. On the other hand, the certain kind of symmetry stipulates the corresponding possible type of failure. For example, one of the most frequently encountered forms of damage in layered materials is delamination. The present work is dedicated to this very phenomenon.

Chapter 1

Introduction

1.1 Periodic Composites

1.1.1 Repetitive structures

A structure is said to be repetitive if it consists of a number of identical structural units which are connected together in a regular pattern. Repetitive structures may be categorized as consisting of a finite or infinite number of repetitive units. Repetitive trusses and periodically stiffened shells, widely used in construction, aeronautic engineering and shipbuilding, have repetitive geometric form. The material recurrence is commonly encountered in the field of composite materials.

The symmetry properties of the repetitive structures are systematically treated in the symmetry group theory. The symmetric structure, accordingly, is defined as one invariant to a symmetry operation. The basic spatial symmetry operations are reflections, rotations, translations and dilatations. An infinite beam, for example, consisting of periodically alternating fragments of different material is said to possess the translational symmetry. The rotation symmetry appears also in finite structures such as gear wheels. While the more thorough classification of the spatial symmetry groups can be found, for example in the manual of Lax (1974), only translations are relevant in the framework of the present study. The elastic characteristics of the structures, possessing the above kinds of symmetry can be described mathematically with the help of periodic functions of spatial arguments. Such structures therefore will be referred to as periodic.

Strictly speaking, structures finite in the translation direction do not possess the

translational symmetry, since any translation will shift the structure beyond its boundary and thereby will not leave it invariant. The mathematical term "periodic", accordingly, may not be applied to finite domains. In the present research, however, a multilayered finite composite is referred to as a "periodic multilayer", if it consists of a finite number of identical sub-layers ¹.

1.1.2 Periodic multilayers

Periodically layered materials are widely used in the modern engineering practice due to their structural properties and relatively low manufacturing cost. They can be found in electronics, optics, microelectromechanical systems (MEMS), machining tool industry and other fields. Protective coatings, multilayer capacitors and stacked actuators, printed circuit boards, thin-film coated optics, mechanical filters for high-frequency dynamic isolation and reaction product layers contains periodically alternating layers. On the other hand, periodic multilayers belong to a wider class of multilayered composite laminates, used in many fields of engineering, especially in construction, aircraft industry and shipbuilding.

A high impact and corrosion resistance of multilayered materials was pointed out by Vaamonde (1993), who proposed to use multilayered steel-zinc sheets in the transport vehicle construction. The effect of structural layering and thermal residual stresses on dynamic impact resistance of alumina/aluminum laminated structures was studied experimentally by Roeder and Sun (2001).

The tribological performance of cutting tools covered with multilayered protective coatings substantially improves as a result of the residual stress reduction, the crack arrest or deflection by multiple interfaces, and the shear in the compliant layers, which prevents yielding of more brittle layers during bending. Holleck and Schier (1995) reported the doubled wear reduction of TiC and TiN multilayer coated tools, compared to a single layer coating. Improvements in hardness, indentation toughness, adhesion, and wear performance of TiC/TiB₂ coating under optimized layers thicknesses conditions were observed by Holleck *et al.* (1990).

Attenuation of the stress wave propagation in periodically layered composites is em-

¹with, may be, one additional non-complete external sub-layer

ployed in mechanical filters for vibration isolation. Such filters consist of a periodically layered stack of alternating materials with strong elastic and density mismatch. Due to the shock wave dissipation and dispersion induced by the interface scattering, periodically layered composites have an increased shock viscosity and, consequently, an improved vibration resistance (Sackman *et al.* 1989, Zhuang *et al.* 2003).

In MEMS and integrated circuit applications, multilayers are usually exploited for their structural functioning, while their mechanical properties may be a critical problem. For example, coating of optical components is often composed of thin films deposited at high temperatures. Significant interfacial residual shear stresses, which develop during the cooling-down, may cause delamination (Klein, 2001, Schreiber, *et al.* 2002). The appropriate selection of design parameters can considerably improve the mechanical reliability of multilayers. Yang *et al.* (2000) points out that with a proper parametric set, a polysilicon film composed of alternating tensile and compressive polysilicon layers can be deposited with a near-zero residual stress. Rather low electrical resistance is observed in magnetic periodic multilayers, subjected to a magnetic field. At the same time, Lu *et al.* (2001) report that a Fe-N/Ti-N periodic multilayer has better mechanical properties than a single-layered Fe-N film while retaining excellent magnetic characteristics.

Stacked multilayer actuators generally consist of piezoelectric thin layers alternating with metal electrodes. The abrupt end of an internal electrode concentrates the electric field, inducing stresses in the ceramic and, consequently, nucleation and growth of cracks. Fracture analysis of multilayer actuators (Hao *et al.* 1996) revealed that a critical layering parameter exists, below which the actuator does not crack around the electrode edges. Discussion of durability, fatigue and material composition of multilayer actuators can be found in Pritchard *et al.* (2001).

Multilayered laminates have higher damage tolerance and reliability combined with reduced weight with respect to monolithic systems. It must be noted here that laminates generally are not composed of alternating homogeneous layers. Some laminates are periodically layered, others are not, but in most cases they contain composite laminae, such as fiber reinforced plies.

Yet, the periodic multilayer can be employed as a model for analysis of laminates for two main reasons. First, the basic trends in the fracture behavior of both laminates and periodic multilayers are expected to be similar. Consequently, the parametric study can

be easily carried out, revealing qualitative effects which hold true for multilayered composites with a more complex and even non-periodic structure. Second, it is worthwhile, because when laminate consists of a large number of layers, its analysis is extremely difficult. In approximate models, laminae are usually replaced by homogenized orthotropic layers with effective elastic properties. But, even with this assumption, the problem remains very complicated. Approximate theories and numeric simulations, available for analysis, require to be tested with exact solutions. Study of periodic multilayers is motivated, therefore, by their plain structure which is convenient for analysis. The simplest periodic multilayer has alternating layers of two dissimilar materials.

As can be seen, multilayers demonstrate a wide range of mechanical properties from the high reliability and damage tolerance to the absence of those. The latter happens usually when the layered structure is chosen by reasons irrelevant to mechanical reliability. In most cases, examining of the multilayer stress bearing capability is of primary importance.

1.2 Failure

1.2.1 Delamination as a type of failure

Reliability and damage tolerance have become the main requirements for modern materials. Damage resistance of multilayers is determined by the competition between several failure mechanisms, such as yielding and cracking, multiplex microcracking and a single macrocrack, intra-layer cracking and interface debonding. The macrocrack can propagate across the layers or parallel to the planes of bonding. If in the last case the crack surface does not cross the interfaces, then this type of failure is referred to as delamination. Delamination is the most intrinsic damage of layered materials, because their through-thickness strength is generally several times less than the in-plane one.

In composite materials delamination cracks arise typically from the impact damage (Lin and Lee, 1990, Melin and Schon, 2001) or from initial imperfections such as gap, inclusion, initial crack, etc. Delamination is induced by tensile and tangent stresses acting on the area element, parallel to the layering. These stresses can be caused by external loading, thermal stresses, moisture absorption and residual stresses created by moisture

or temperature gradient. Extensive discussion on origin and effects of delamination can be found in the paper by Garg (1988).

Delamination of multilayers occurs as intra-layer cracks propagation in the direction of the layering, or as debonding of interfaces. The propagation path of delamination cracks sometimes appears to be wavy and lies partly within the layer and partly along the interface (Fleck *et al.* 1991, Chai 1987, Hutchinson and Suo 1991).

The concurrence between interface and sub-interface cracking has been treated by Hutchinson *et al.* (1987). Vast experiments reported in the literature indicate that interface debonding prevails over intra-layer delamination (Williams *et al.* 1986, Garg 1988, Cao and Evans 1989, etc.), especially under mixed mode loading. Yet, in certain cases, the opposite happens. Thus, a strong tendency of the cracks in the films subjected to residual tension to kink into brittle substrates and to propagate parallel to the interfaces was observed by Thouless *et al.* (1987), Hu *et al.* (1988), Drory *et al.* (1988), and by McNaney *et al.* (1994). Under a certain loading, the crack propagation has been observed (Cao and Evans 1989, Wang and Suo 1990) within the layer with fracture energy several times higher than the corresponding interfacial one. This contradiction has been explained by Fleck *et al.* (1991). A rather complete review of the subject and additional references can be found in the paper by Hutchinson and Suo (1991) .

1.2.2 The effect of delamination

Depending on structural loading, delamination can be the critical failure mode, but more frequently it results in stiffness loss, contributing thereby to overall failure. Under compressive in-plane loading, delamination allows out-of-plane displacement of plies to occur more easily, contributing thereby to local instability. Consequently, it causes reduction of compressive strength and leads to out-of-plane buckling (Bolotin 1996, Gaudenzi 1997, Melin and Schon 2001, Nilsson *et al.* 1993, Short *et al.* 2002).

On the other hand, fracture resistance of multilayers can be much higher than that of corresponding bulk homogeneous bodies. Dispersion of the damage in laminates by multiple cracking increases energy dissipation and hence the effective fracture energy (Arata *et al.* 2001). But the main contribution is made by arresting, trapping and deflecting the cracks at the interfaces (Holleck *et al.* 1990, Holleck and Schier 1995,

Sbaizero and Evans 1986, Li 2000, Kriven and Lee 2001). Tests of iron-aluminum (Loader *et al.* 1996), and ultra-high carbon steel–brass (Ohashi *et al.* 1992) multilayers indicate that the crack tip blunting in a more ductile layer and the crack deflection accompanied by delamination are factors preventing the total failure.

It was also revealed (Markaki and Clyne, 2002, Howard *et al.* 1998), that effective toughness of the metal/ceramic laminates can be significantly enhanced by the certain degree of interfacial weakening due to the energy dissipation in multiple debonding. Four-point bending tests (O’Brien *et al.* 2000) confirm the crucial role of the interface toughness in maximizing the fracture work by crack deflection. Kovar *et al.* (1998) pointed out that delamination cracks absorb high energy when propagating a sufficiently long distance, which, in turn, depends on bonding conditions.

Summarizing, delamination should be pointed out as an important damage mode which is capable of reducing strength, stiffness and reliability of layered composites. On the other hand, when the transverse cracking is predominant failure mode, delamination improves overall fracture resistance. The analysis of delamination problems carried out in the present study should be used in combination with experimental data for choosing the optimal composite design parameters.

1.3 Quasi-periodic problems

Consider a structure possessing translational symmetry², subjected to general loading. Three types of problems for the periodic structure can be indicated here. The problem is said to be periodic when both the structure and the loading are periodic with identical periods. Consequently, the stress-strain state is also periodic. This problem can be reduced to analysis of a representative volume element hereafter referred to as the repetitive cell.

The loading can be spatially periodic but may have a period different from that of the structure. We refer to the periodic loading as cyclic in order to distinguish the symmetry of the stress state from that of the structure. If periods of both the loading and the structure have common multiple then the stress field of the structure is periodic. Such a problem is said to be cyclic.

²concepts introduced in this section can be defined also for other types of symmetry e.g. rotation

Finally, the stress state of an infinite periodic structure can possess no translational symmetry whatever, in which case the problem is said to be quasi-periodic. Note, that the cyclic problem can be considered as a special case of the quasi-periodic one.

The subject of present research is delamination of periodically layered structures caused by interface debonding or intra-layer splitting. Accordingly, analysis of the infinite structures with a single crack requires the solution of corresponding quasi-periodic problems. Another objective is a closed form stress field of the strip composed of a large number of layers. Finally, the problem on a delamination crack in such strip is of the interest. In all the cases the initial problem will be reduced to a quasi-periodic one.

1.4 Literature survey

1.4.1 Methods of analysis of symmetric elastic systems

Methods that take advantage of the repetitive nature of a system deal with the repetitive properties rather than with the type of the system. Therefore, approaches to analysis of quasi-periodic problems arising in different fields of mechanics are reviewed here.

A method that does not take advantage of the spatial recurrence is commonly referred to as direct. When such method is used, an extension of the considered domain by adding repetitive cells inevitably results in multiple increase of the analysis complexity. On the other hand, there are a number of approaches that allow the simplification of the analysis by utilizing the benefits of the system symmetry.

Among such approaches, the continuum substitution may be named the most radical. The repetitive system or its part is replaced by the periodic continuum with effective properties obtained by some smearing procedure. Noor (1988) classified methods applicable to the discrete periodic structures, such as lattices and trusses, and expounded the advantages of continuum modelling. However, the pertinence of such substitution often becomes a weak point, as has been pointed out by Renton (1996) who applied the generalized beam theory to the finite-difference analysis of regular trusses. In the mechanics of composites, an inhomogeneous continuum is often replaced by a homogenized one. This procedure smears interfaces eliminating thereby the very possibility of analyzing the interface debonding. Nevertheless, when local effects do not govern the global behavior,

the equivalence to the original model can be reached on macro level. In these cases, the above method produces accurate results, and it is worthwhile to employ it because of a simple form of the solutions being obtained.

Initially, exploiting symmetry properties of periodic structures was carried out for dynamic problems. In the solid state physics the dispersion relation for harmonic wave propagation through a periodic medium can be derived by employing Bloch's theorem (Brillouin, 1946), which states that the change in the wave amplitude across a period does not depend upon the location of the period within the system. Consequently, the dynamic analysis of a non-periodic state of stress in periodic structures may be performed by solving problems defined over a single cell. The wave propagation in multi-connection repetitive chains was examined by Zhong and Williams (1995) via the stiffness matrix formulation. Response of beam grillages to a harmonic load was examined by Langley *et al.* (1997).

Different formulations of the transfer matrix technique are most efficient for the characteristic spectrum analysis. Calculating the propagation constants by the use of the transfer matrix and the eigenvector expansion, Vorovich *et al.* (1992, 1994) have obtained the pass-bands of periodic waveguides. A special representation related to the transfer matrix in combination with asymptotic homogenization has been exploited by Langley (1999) for analysis of inhomogeneous wave guides. Longitudinal waves perpendicular to the layers of a disordered near-periodically laminated media were examined by Li and Benaroya (1996). The methods of analysis of the wave propagation in continuous periodic structures have been reviewed by Mead (1996).

The functional characteristic spectrum of the static response to the point force allows examination of stress decay in the structure. This research was conducted by Karpov *et al.* (2002a) for a beam truss under end loading. Static problems for periodic structures were considered by Dean (1976), Renton (1964,1996) and Wah and Calcote (1970) via finite difference analysis of the stiffness matrix of a representative substructure. Application of the finite difference approaches to regular lattices was reviewed by Gutkowski (1974).

The boundary-value problems for repetitive structures are more difficult for analysis by means of the transfer matrices since the size of incorporated global matrix is proportional to the total number of cells. The advantage of symmetry can be utilized, however,

through some block-diagonalization procedure (Bossavit, 1986, Healey and Treacy, 1991, Dinkevich, 1991), which is actually equivalent to decomposing of the quasi-periodic problem into a series of periodic ones.

For a structure with the mirror symmetry, any loading can be split into symmetric and skew symmetric components, and then the corresponding problems can be analyzed separately. A similar technique was exploited by Kucherov and Chebakov (1991). The elastic response of the ring subjected to the system of four dies has been found as a superposition of corresponding solutions of symmetric and skew-symmetric cyclic problems. A more systematic approach to the analysis of symmetric systems based on the group theory has been suggested by Buryshkin (1978). The method is based on expansion of the load by the irreducible symmetry group representations.

The Discrete Fourier Transform (DFT) is proved to be the most effective tool for analysis of periodic structures, although few applications can be found in the literature. In dynamics, DFT have been introduced explicitly by Eatwell and Willis (1982) in a study of fluid-solid interaction and by Slepyan (1974, 1988) for the fracture analysis.

Bolotin and Novitchkov (1980) applied the DFT to the static problem on a periodically layered half-space with the layers orthogonal to the surface and one layer subjected to the edge tractions. An infinite periodically riveted sheet-stringer system was examined by Budiansky and Wu (1961). Cyclic problems with circulant stiffness matrices for structures possessing rotation and translational symmetry were treated by Samartin (1988) with the help of the finite DFT (FDFT). Kangwai *et al.* (1999) have employed DFT for block-diagonalization of the stiffness matrix, and emphasized that this method is a special case of the group representation approach to analysis of periodic structures. A mathematical similarity between formal DFT and the Bloch's waves was pointed out by Fuchs and Ryvkin (2002), who examined infinite periodic grids of orthogonal beams.

In the present work, the representative cell method suggested by Nuller and Ryvkin (1980) for analysis of infinite periodic elastic domains is employed. It provides a very convenient framework for applying DFT to the analysis of the quasi-periodic problems. This method hinges on reducing the initial boundary value problem to that for a single repetitive module (representative cell) subjected to the Born-Von Karman type boundary conditions. The method does not impose any certain analysis technique for the cell problem, and the solution can be obtained by the analytical methods (Nakhmein *et al.*

1981, Kamysheva *et al.* 1982, Nuller and Ryvkin, 1983, Ryvkin *et al.* 1999), as well as by the numerical ones (Moses *et al.* 2001, Ryvkin and Nuller, 1997).

As was mentioned earlier, finite structures do not possess the translation symmetry. It turns out, however, that the problem for a finite object consisting of repetitive units can be addressed by using a modified representative cell method. The initial domain is completed to an infinite periodically layered space directly, or is included into some larger one and then the periodic space is composed cyclically of these larger domains. Here the quasi-periodic problem arises. This technique has been employed by Nuller (1981) for analysis of periodically layered plates, the general approach was outlined by Ryvkin and Nuller (1987). Using similar ideas, Karpov *et al.* (2002b) have developed the FDFT based method for analysis of finite lattice structures. Ryvkin (1996) has implemented this approach for analysis of a semi-infinite mode III crack in a periodically layered medium not possessing the translational symmetry.

1.4.2 Fracture analysis of multilayers

In order to examine failure resistance of a periodically layered composite of finite thickness, the analysis of the stress field of the non-cracked composite is to be performed first. As was previously noticed, periodic multilayers may be considered as a rather wide, yet special case of multilayered laminates. Accordingly, methods and models designed for analysis of laminates are commonly used for the periodic multilayers also. In the following subsection, a brief review of approaches to analysis of the stress-strain field of multilayered composites will be presented.

Analysis of perfectly bonded multilayers without cracks

The transverse discontinuity of mechanical properties of layered composites with strong elastic mismatch entails a zigzag form of the displacement field exhibiting rapid changes and different slopes with respect to interfaces (Pagano, 1978). High gradients of shear and transverse stresses and discontinuity of in-plane tensile stresses are also involved. These complicating effects make it difficult to use numeric methods for accurate analysis of a large multilayered domain. In order to achieve solutions within reasonable computational time, special techniques are required. Consequently, numerous simplified approaches have

been developed, such as continuum substitute models and axiomatic plate theories based on classical, advanced and mixed formulations (Whitney, 1987), etc.

A homogenization procedure for periodic multilayer laminates was developed by Buefler (1998, 2000). One period, consisting of two or more different transversely isotropic homogeneous layers, was analyzed exactly by means of integral transforms and transfer matrices.

A refined higher-order shear deformation theory and displacement-based finite elements (FE) developed by Kant and Kommineni (1994) predicts warping of the cross-section, unlike the first-order shear deformation theory. FE models based on advanced smeared laminate plate theory was developed by Soldatos and Shu (2002). Results were compared with the elasticity solutions of Vel and Batra (2000) for laminated plate subjected to the bending edge conditions. A complete and detailed overview of the numerous plate theories dedicated to the layered systems and of the corresponding numeric techniques can be found in the papers by Carrera and Demasi (2002).

In order to obtain more precise results without additional computing, the global–local techniques (Voleti *et al.*, 1996) are often exploited, when the more accurate description is used in certain zones of the structure, whereas in the remaining parts, simpler modelling is employed. Babuska *et al.* (1992) performed so-called hierarchy FE analysis of laminated strips. A method based on the boundary integral formulation was employed by Davi and Milazzo (1999), who have computed the elastic response of a composite laminate under bending loads with the help of the boundary elements.

Wang *et al.* (2000) applied a combination of the elasticity and the plate theory for the analysis of the free edge stress decay in a laminate under uniform extension. The stress field exponentially decaying with the distance from the edge is derived as the elastic eigensolution by satisfying the interfacial and the traction-free top and bottom boundary conditions with the help of the transfer matrix. The interior stress field matching the top and bottom boundary conditions is obtained via the classical laminate theory. The complete stress field in the laminate is obtained as a superposition of these two solutions by satisfying numerically the edge boundary conditions.

An elasticity solution for a bending plate consisting of three homogeneous orthotropic laminae of different thicknesses was performed by Vel and Batra (2000), by the use of the Eshelby-Stroh formalism. The boundary and interface continuity conditions were

satisfied approximately in the sense of the truncated Fourier series. Clearly, it is difficult to perform within the referred model an effective parametric investigation including variation in the number of the layers. In fact, adding one more lamina evokes extension and partial rebuilding of the corresponding algebraic system. Such investigation, however, can be carried out for a simpler model of the periodic laminate. In this connection, one of the goals of the present study is to obtain an exact solution for a periodically layered composite, consisting of an arbitrarily large number of isotropic layers.

Delamination models. Fracture mechanics of multilayers.

When the initial flaw is small enough, the fracture analysis predicts the crack initiation load higher than that indicated by some strength criterion, which, consequently, should be used (Davies *et al.* 1997, Chai, 2003). In the strength criteria context, the delamination initiation is normally related to the material strength or to some interfacial fracture law, defined by the corresponding constitutive equations. However, when the initial cracks are long, the strength-based criteria cannot be applied to the stress state directly. Consequently, use of some delamination model should be made. Basically, any such model must be consistent with the concept of Griffith surface fracture energy (Griffith, 1924).

A number of cohesive or damage zone delamination models since works of Dugdale (1960), and Barenblatt (1962) exists, which incorporate a concept of fracture resistance based on some relation between the tractions and the relative displacements of the crack faces. The area beneath the traction–displacement curve is actually equal to the Griffith energy. In order to take into account the contribution of multiple delaminations to the global response of a layered composite, various continuum damage models (Allix *et al.* 1995, Mi *et al.* 1998, Corigliano and Ricci, 2001) have been developed. One or several damage parameters are usually used in such models, e.g. area of micro-cracks in a representative volume (Zou *et al.* 2003). Delamination also can be considered in the framework of the refined layer-wise plate theories (Barbero and Reddy, 1991, Liu *et al.* 1994, Williams and Addessio, 1997), where an approximate transverse distribution of displacements or stresses is adopted on the layer level.

Theoretical studies of the crack initiation are based mainly on the fracture mechanics

analysis of the singular stress field in the vicinity of the crack tip. The power expansion of the stress field near the tip of the crack in a homogeneous continuum has been obtained by Williams (1957) and by Irwin (1957). The singular stresses ahead of the crack tip in the plane problem of elasticity can be expressed via the stress intensity factors (SIFs) K_I , K_{II} .

$$\sigma_{yy}(x, 0) = \frac{K_I}{\sqrt{2\pi x}}; \quad \sigma_{xy}(x, 0) = \frac{K_{II}}{\sqrt{2\pi x}}; \quad (1.1)$$

where the Cartesian coordinates x, y are associated with the crack tip. For brittle elastic homogeneous materials, the delamination initiation is governed by the critical value G_C of the energy release rate (ERR) or, alternatively, by some combination of critical values K_{IC} , K_{IIC} of the SIFs. At the same time, the crack propagation may be characterized only by K_{IC} , in view of condition $K_{II} = 0$ (Fleck *et al.* 1991).

When dealing with interfacial cracks, the material mismatch across the interface almost always results in coupled fracture modes. The stresses at the interface directly ahead of the crack tip (Williams, 1959) can be expressed via the complex SIF $K = K_1 + iK_2$

$$\sigma_{yy}(x, 0) + i\tau_{xy}(x, 0) = \frac{K}{\sqrt{2\pi x}} x^{i\epsilon}. \quad (1.2)$$

where

$$\epsilon = \frac{1}{2\pi} \ln \frac{1 - \beta}{1 + \beta}. \quad (1.3)$$

with β denoting the corresponding Dundurs' elastic mismatch parameter. Consequently, the near crack tip stresses, as well as the relative displacements of the crack surfaces, are characterized (England, 1965) by the oscillating singularity. This leads to the physically inadmissible interpenetration of crack surfaces near the crack tip. The problem was discussed by Rice (1988). In this case, the condition for crack initiation is usually defined by the use of the critical interface energy G_C , which has been found to be a function of the phase angle of the local mode mix (Evans *et al.* 1990).

Thus the SIFs or, alternatively, the ERR and the phase angle are the parameters, assessment of which together with corresponding critical values is crucial in fracture analysis. The energy release can be calculated by using the virtual crack closure technique (Irwin, 1957). Classical beam theory has been used by Suo and Hutchinson (1990) in the case of a semi-infinite interface crack in a bi-material strip under edge loadings. The phase angle of the mode mix ratio has been calculated numerically.

A plate theory based methods for calculating ERR and its mode I and mode II components from the local values of bending moments and loads in a cracked laminate was suggested by Williams (1988) and by Sheinman and Kardomateas (1997). In the last work, the ERR was calculated through the J-integral and subsequent separation of the individual modes was carried out by means of an auxiliary asymptotic problem for homogeneous orthotropic plate with smeared characteristics.

The ERR for delamination in a pre-notched periodically layered (cross-ply) symmetric laminated beam has been approximated with the help of the laminate theory by Charalambides (1991). An approach, based on Reissner's variational principle, was suggested by Schoeppner and Pagano (1998), where elastic stress fields and ERRs for free-edge delamination and transverse cracking in four-layered laminates were presented. The model of a large radius axisymmetric hollow layered cylinder was exploited to represent a flat composite.

Computational expenses of using the standard FE technique for analysis of multilayers have given rise to a vast number of publications dedicated to development of various enhanced finite elements. SIFs for delaminations in composite laminates were evaluated by Zou *et al.* (2001) via the virtual crack closure by applying a laminate theory based FE analysis. A model of the laminate comprised of two sub-laminates in the delaminated region and a single intact laminate in the rest of the domain has been adopted. Classical beam theory based FE analysis was carried out by Toya *et al.* (1997) for a three-point bending layered beam with an interface crack. In order to achieve better accuracy with fewer elements, an eigenfunction expansion have been employed by Her (2000) in formulation of a global-local FE method for analysis of an interface crack between two anisotropic materials.

An exact analysis of the stress field in multilayers being far from easy in the absence of cracks (see p.1.4.2), becomes even more complicated in application to the fracture. Nevertheless, a number of solutions for particular cases can be found in the literature. Chatterjee (1987) obtained ERR and SIF for a circular and 2D intra-layer cracks in $((0_4/\pm 45_2)_s)_4$ and $((30_4/(75/-15)_2)_s)_4$ laminated plates. Normal or shear tractions were prescribed on the crack faces. Global stiffness matrix formulation was employed to derive integral equations on the crack line in terms of unknown displacement discontinuities. An interface crack in the symmetric $[0/45/90]_s$ laminate was examined by Shen *et al.*

(1999). With the help of the dislocation approach and the stiffness matrix formulation, the problem was reduced to a system of singular integral equations.

The list of the cited works is neither complete nor extensive. It emphasizes, that an exact analysis of multilayered structures is a challenging task, consequently, there is a lack of parametric investigation in the field. Approximate models provide an opportunity of a more complete investigation, but verification of the results, in turn, becomes a problem. Therefore, in order to examine fundamental mechanisms of splitting in multilayered composites, some basic problems on delamination cracks should be considered. A periodically layered bi-material strip, consisting of an arbitrary number of layers and containing a delamination crack at an interface or within a layer is a promising model, analysis of which is one of the goals of present study.

1.4.3 Cracks in a periodically layered bi-material composite

A rigorous mathematical model of a crack in a periodically layered bi-material strip is developed in this thesis. The analysis of this model is difficult, and for particular parameter combinations, there is an opportunity to use some short-cuts by considering simplified layered configurations. If the crack size and the characteristic layer thickness is small with respect to the distance from the outer boundaries, then the crack tip stress field can be obtained by using the model of a crack in a periodically layered infinite plane.

When the interface crack is also sufficiently small, being compared to the layer thicknesses, the layered structure of a composite is irrelevant, and the solution of Rice and Sih (1965) for the crack at the interface between two dissimilar half-spaces can be employed. If, in addition, the intra-layer crack is small relative to the distance from the nearest interface, the solution approaches that for the crack in a homogeneous plane. This approach corresponds to the dilute model in the theory of composites. Approximate models of higher orders, when the influence of several interfaces is taken into consideration, also can be used. Thus, for example, Chen and Sih (1971) considered antiplane deformation of a four layered structure containing a crack between two layers of equal thickness, under assumption that two outer layers of infinite thickness simulate the properties of a multilayered continuum. The ERR for an interface crack was found to be always less than the corresponding value for a crack between two dissimilar half-spaces.

When the thickness of the layers of one type significantly exceeds that of the second type, the sandwich model with a layer bonded to two similar half-spaces can be employed. The results for a crack in such a three-material sandwich have been obtained by Erdogan and Gupta (1971a,b) for the intra-layer as well as the interface crack. The dislocation approach has been introduced, by use of which the problem is reduced to the singular integral Fredholm equations. The limiting cases of a sandwich containing a semi-infinite crack lying along or at the interface have been treated by Suo and Hutchinson (1989a, 1989b).

All the above models are based on a concept of a medium composed of different homogeneous layers. According to another approach, the periodically layered medium is considered as a continuum with a smooth periodic variation of elastic parameters. A penny-shaped crack in a half-space, elastic parameters of which are harmonic functions of the axial variable, was examined by Selvadurai and Lan (1998). The equilibrium equations in terms of displacements were reduced to ordinary differential equations, numerical solutions of which were used to evaluate the kernel of the integral equation.

A non-standard homogenization procedure with microlocal parameters has been developed by Kaczyński and Matysiak (1988, 1989, 1995) for analysis of interface cracks in the periodically layered space and by Kaczyński *et al.* (1994) for the crack in the periodically layered strip. The layered material in this model is replaced by the one with a smooth variation of elastic parameters, and some assumptions are made concerning the displacement field.

Homogenized continuum replacement provides another opportunity to estimate the delamination parameters in a periodically layered composite, when the crack is long with respect to the thickness of the layers. In this case the remote field approaches that of the homogenized anisotropic material. Under this condition, the ERR, which can be calculated through the local as well as remote field (Ryvkin *et al.* 1995), can be assessed via a solution for the anisotropic strip with effective elastic properties. The corresponding problem for a finite centerline crack in the transversely isotropic strip has been examined by Konishi and Atsumi (1973) and the edge crack in the orthotropic layer has been analyzed by Suo (1990). When, in addition, the crack is short compared to the distance from the boundaries, the solution by Sih *et al.* (1965) for the crack in an anisotropic plane can be employed.

The SIFs for a long crack located in the middle of a layer in a bi-material composite have been obtained in terms of applied³ remote K-field by Jha and Charalambides (1998) through an asymptotic homogenization and the complex elastic potentials. In the exploited asymptotic expansion of the displacements, the first term has been retained, which corresponds to the solution for the crack in an anisotropic continuum. However, in order to designate the mode mix for the non-midline crack and, consequently, to assess the effect of the crack location, a refined FE formulation for a boundary value problem on a cut-out layered region around the crack tip has been used.

A closed form solution for a specific case of the anti-plane deformation of a laminated medium with a semi-infinite crack parallel to the interfaces has been obtained by Ryvkin (1996), who employed the representative cell and the Wiener-Hopf methods.

A recently developed technique (Ryvkin, 1998) for exact analysis of the delamination crack in a periodically layered medium is based on combined use of the representative cell method (Nuller and Ryvkin, 1980, Ryvkin and Nuller, 1997) and the dislocation approach (Erdogan and Gupta, 1971a,b). This technique provides an attractive opportunity of examining the crack near-tip stress field without any simplifying assumptions. Parametric investigation for the mode III finite crack in a periodically layered plane has been presented by Ryvkin (1998). The problem was reduced to a singular Fredholm integral equation of the first kind. The same technique has been used by Ryvkin (1999) for the case of a Mode I crack located in the midplane of a layer in a periodic composite. A simple analytic expression for SIF has been derived in the limiting case of a semi-infinite crack via the homogenization procedure. The case of a delamination crack arbitrarily located in the periodically layered space has been considered in the papers by Ryvkin and Kucherov (2000, 2001) and by Kucherov and Ryvkin (2002), the contents of which are a part of the present thesis.

1.5 Scope of the research

Composite consisting of a large number of layers is a difficult object for the fracture analysis. The use of numerical methods for accurate analysis of a large multilayered

³Applied or apparent mode I and mode II SIFs associated with the corresponding problem for the crack in the homogeneous material have been introduced as loading by Suo and Hutchinson (1989b)

domain with a strong elastic mismatch is computationally expensive and, consequently, inefficient for parametric investigation. The validity of approximate plate theories and corresponding computational techniques must be ascertained by comparing the results with exact solutions. Closed form solutions produced by equivalent continuum methods are acceptable only in a certain range of problem parameters, and do not allow assessment of the local stress state. The phase angle of the mode mix for example, cannot be estimated in the framework of homogenized continuum. The asymptotic solutions based on various sandwich models can be adopted for a multilayered composite only under certain limiting conditions. On the other hand, when the number of layers increases, the use of any direct method becomes extremely cumbersome.

A new effective method for analysis of delamination in periodically layered composites will be developed. The linear elasticity model of periodically layered bi-material composite is adopted, although a developed solution scheme allows investigation for an arbitrary number of different layers in a period. The layers are supposed to be homogeneous and isotropic.

By using this method, a number of specific practically important problems for a periodically layered composite of finite and infinite thickness will be examined. The singular stress field at the tip of a delamination crack arbitrarily located in a periodically layered plane will be analyzed. To this end, two problems must be solved: the one for an interface crack and the other for an intra-layer crack parallel to the interfaces and located arbitrarily within a layer.

With reference to the above two problems, a functional dependence of the fracture parameters upon the loading direction will be derived analytically, which will allow establishment of the criterion defining the shape of these functions. For the special case of a long crack in a periodically layered plane, an asymptotic formula for the ERR will be derived and regions of elastic parameters defining the form of the ERR as a function of the loading direction will be specified.

Delamination in a finite thickness composite will be examined. The problem of a periodically layered strip with a single interface debonding will be solved for a set of different boundary conditions on the strip edges and on the crack faces. In addition, closed form solutions will be obtained for the stress field of a perfectly bonded periodically layered strip.

Obtained solutions will be used for examining the influence of the design parameters on the fracture characteristics and on the stress distribution in the periodically layered composites. The stress intensity factors, the ERR and the phase angle shift will be presented as functions of the problem parameters.

In Chapter 2 the general solution scheme for the problems on a periodically layered bi-material finite thickness composite containing a delamination crack is presented. The case of an interface crack with the stress boundary conditions at the strip edges are considered in detail.

In Chapter 3 an infinite perfectly bonded periodically layered strip with arbitrary boundary conditions is examined by using the scheme presented in Chapter 2. The solution is obtained in a closed form in quadratures and is illustrated by two problems for a strip with boundary conditions of different types. Comparison with the plate theory and the parametric investigation are carried out.

In Chapter 4, analytical investigation of the stress field near the tip of a delamination crack located in a periodically layered plane is carried out. The dependence of the fracture characteristics upon the loading angle is examined and an expression for the ERR in front of a semi-infinite crack in the periodically layered space is obtained by the use of the homogenization procedure.

In Chapter 5 the problem on a periodically layered plane with an interface crack is solved. The Green's function for a single dislocation is obtained in a closed form by means of the representative cell method. Then a singular integral equation is derived and solved by using the Jacobi polynomials expansion. Parametric investigation of the fracture characteristics as functions of applied loading, material mismatch and problem geometry is performed.

In Chapter 6 the intra-layer delamination crack is considered. The system of two singular integral equations of the first kind is derived with the help of the closed form Green's function for a single dislocation, obtained by means of the representative cell method. The system is solved by the use of the Gauss-Chebyshev integration formula. The influence of the crack location within the layer and of the other problem parameters on the SIFs is studied.

In Chapter 7 the suggested technique is employed for analysis of an interface debonding in a layered finite thickness strip. Two different sets of boundary conditions are

considered: In the first set, one edge of the strip is clamped and the other one is free. The crack is loaded by uniform normal tractions. In the second set, both sides of the strip are subjected to collinear equilibrated point forces while the crack faces are tractions-free. Comparisons with known results for limiting cases are made.

Chapter 2

Methodology

In this chapter the general scheme of analysis of a delamination crack in a periodically layered infinite strip with arbitrary boundary conditions is presented. For the sake of lucidity and in order to avoid redundant nomenclature the scheme is expounded as applied to a particular case of an interface crack in a bi-material strip composed of alternating layers and subjected to arbitrary edge tractions. On the crack faces arbitrary opening tractions are specified. A solution for a perfectly bonded strip can be obtained in the framework of the presented scheme as a special case.

2.1 An interface crack in a periodically layered bi-material strip.

Consider an infinite composite bi-material strip Ω of thickness H . The strip consists of isotropic elastic layers of two different types ($r = 1, 2$) arranged periodically (Fig. 2.1a). The thickness, shear modulus and Poisson ratio of the layers of r -th type are denoted as h_r , μ_r and ν_r respectively. The perfect bonding of the layers is violated by a delamination crack of length $2a$ located at the inner interface in the cell number n . The strip is subjected to arbitrary edge tractions while on both crack faces some equal opposite opening tractions are prescribed. The stress-strain state in the strip and specifically the singular crack tip stress field is sought.

Note, that under the simultaneous action of the strip edge loading and the crack face tractions, the crack should be open excluding perhaps some negligibly small region near

the crack tips, where the linear elasticity theory predicts (England, 1965) interpenetration of the crack faces. The size of this region is assumed to be small enough (Rice, 1988) so that the use of the present interface crack model could be made in the framework of the linear elasticity theory.

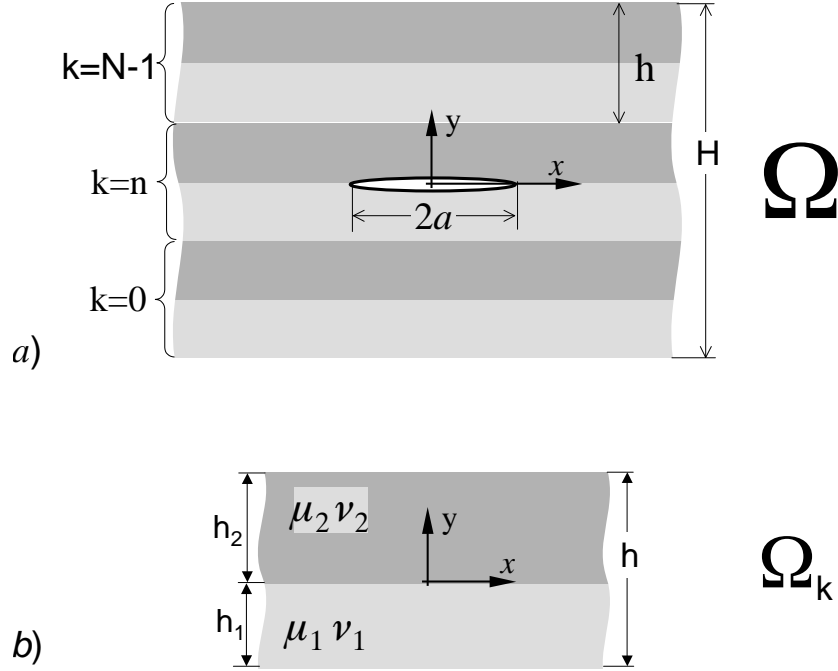


Figure 2.1: Finite thickness periodically layered strip.

If the total number of layers is even, then the strip without the crack may be viewed as an assemblage of N bonded identical cells Ω_k , $k = 0, \dots, N - 1$ of thickness $h = h_1 + h_2$. The typical cell Ω_k consisting of two dissimilar layers is depicted in Fig. 2.1b. In accordance with the representative cell approach, systems of local Cartesian coordinates are introduced in all cells in an identical manner. Axis x of coordinate systems x, y with origins corresponding to the crack center coincides with the interface in each cell, as it is shown in the figure. It is convenient to introduce a vector of elastic field defined by the stress and by the displacement fields in the r -th layer of the k -th cell

$$\mathbf{U}_r^k(x, y) = \{u_r^k, v_r^k, \sigma_r^k, \tau_r^k\}, \quad (2.1)$$

where $u_r^k \equiv u_r^k(x, y)$ and $v_r^k \equiv v_r^k(x, y)$ are the displacements in the x - and y -directions respectively, and $\sigma_r^k \equiv \sigma_{yy}^{kr}(x, y)$ and $\tau_r^k \equiv \sigma_{yx}^{kr}(x, y)$ are the normal and shear stresses at

the planes parallel to the interfaces. The boundary value problem for the strip in the case of the prescribed tractions at the upper and the lower edges and on the crack faces is defined by the Lamé field equations

$$\begin{aligned} \mu_r \nabla^2 u_r^k + (\lambda_r + \mu_r) \frac{\partial}{\partial x} \left(\frac{\partial u_r^k}{\partial x} + \frac{\partial v_r^k}{\partial y} \right) &= 0, \\ \mu_r \nabla^2 v_r^k + (\lambda_r + \mu_r) \frac{\partial}{\partial y} \left(\frac{\partial u_r^k}{\partial x} + \frac{\partial v_r^k}{\partial y} \right) &= 0, \quad k = 0, \dots, N-1; \quad r = 1, 2; \end{aligned} \quad (2.2)$$

where λ_r is the Lamé elastic constant, and the following system of boundary equations (the adopted cells numbering is upwards from the bottom)

$$\mathbf{U}_1^k(x, -h_1) - \mathbf{U}_2^{k-1}(x, h_2) = 0, \quad k = 1, \dots, N-1 \quad (2.3)$$

$$\mathbf{U}_2^k(x, 0) - \mathbf{U}_1^k(x, 0) = 0, \quad k = 0, \dots, N-1, \quad k \neq n \quad (2.4)$$

$$\mathbf{U}_2^n(x, 0) - \mathbf{U}_1^n(x, 0) = 0, \quad |x| \geq a \quad (2.5)$$

$$\sigma_r^n(x, 0) + i\tau_r^n(x, 0) = -\sigma(x) - i\tau(x), \quad |x| < a \quad r = 1, 2. \quad (2.6)$$

$$\sigma_2^{N-1}(x, h_2) + i\tau_2^{N-1}(x, h_2) = \sigma^u(x) + i\tau^u(x), \quad (2.7)$$

$$\sigma_1^0(x, -h_1) + i\tau_1^0(x, -h_1) = \sigma^b(x) + i\tau^b(x). \quad (2.8)$$

Here relations (2.3)–(2.5) provide the perfect bonding conditions at the interfaces between the layers; loading conditions at the crack faces are stipulated by equations (2.6); functions $\sigma^u(x)$, $\tau^u(x)$ and $\sigma^b(x)$, $\tau^b(x)$ in the right hand sides of equations (2.7) and (2.8) are the known stresses at the upper (u) and bottom (b) edges of the strip respectively. Conditions (2.6)–(2.8) are presented in the complex form with i denoting the imaginary unit.

The solution scheme follows. First, the crack is presented by superposition of distributed dislocations with unknown amplitudes. Consequently, the solution is obtained as a superposition of the solution corresponding to the perfectly bonded strip subjected to the given external tractions, and the integral sum of the Green's functions. The Green's function is the elastic field vector generated by a single dislocation in the strip with homogeneous external boundary conditions.

In order to derive the Green's function and the solution for the perfectly bonded strip, an auxiliary problem is formulated for the strip with a single dislocation and boundary conditions (2.7)–(2.8). The auxiliary problem is replaced by an equivalent

quasi-periodic problem for a periodically layered plane. The response equivalence between these problems is maintained by introducing additional loads in the form of stress jumps at the interfaces, corresponding to the edges of the strip. By applying DFT to the formulated quasi-periodic problem the solution of the auxiliary problem is derived in terms of the unknown stress jumps and dislocation amplitudes. The stress jumps are determined from the edge boundary conditions (2.7) and (2.8) of the initial problem.

2.2 Application of the dislocation approach.

Following Erdogan and Gupta (1971b) the crack in the n -th cell is considered as an assemblage of distributed dislocations with unknown amplitudes¹ $f_1(t), f_2(t)$

$$u_2^n(x, 0) - u_1^n(x, 0) = f_1(t)H(x - t), \quad (2.9)$$

$$v_2^n(x, 0) - v_1^n(x, 0) = f_2(t)H(x - t), \quad |t| \leq a \quad (2.10)$$

where $H(x)$ is the Heaviside step function. An additional restriction

$$\int_{-a}^a f_j(t) dt = 0, \quad j = 1, 2. \quad (2.11)$$

must be imposed on the dislocation amplitudes in order to ensure the crack faces closure at the crack tips.

The solution for the non-cracked strip with a single dislocation, defined by the elastic field vector $\tilde{\mathbf{U}}_r^k(x, y)$, is sought as a superposition of two fields:

$$\tilde{\mathbf{U}}_r^k(x, y, t) = \check{\mathbf{U}}_r^k(x, y, t) + \hat{\mathbf{U}}_r^k(x, y) \quad (2.12)$$

The first one $\check{\mathbf{U}}_r^k(x, y, t)$, referred to as the Green's function, is the stress state of the strip with the homogeneous boundary conditions

$$\sigma_2^{N-1}(x, h_2) = \tau_2^{N-1}(x, h_2) = \sigma_1^0(x, -h_1) = \tau_1^0(x, -h_1) = 0, \quad (2.13)$$

perturbed by the interface dislocation at the point $x = t, y = 0$ in the cell number n . The second one $\hat{\mathbf{U}}_r^k(x, y, t)$ is the field of the perfectly bonded strip subjected to the given boundary conditions (2.7)-(2.8).

¹Erdogan and Gupta (1971a) have defined dislocation in terms of the partial derivative $\partial/\partial x$ of the displacement jumps across the crack line with the help of the delta function. Here the dislocation is defined equivalently by means of the step-function.

The elastic field for the initial problem is then

$$\mathbf{U}_r^k(x, y) = \int_{-a}^a \check{\mathbf{U}}_r^k(x, y, t) dt + \hat{\mathbf{U}}_r^k(x, y). \quad (2.14)$$

Consequently, the stress condition (2.6) on the crack faces is expressed via the corresponding components of the Green's function $\check{\sigma}_r^n(x, 0, t)$, $\check{\tau}_r^n(x, 0, t)$ and by the stresses $\hat{\sigma}_r^n(x, 0)$, $\hat{\tau}_r^n(x, 0)$ at the crack line in the perfectly bonded strip under the external loading.

$$\hat{\sigma}_r^n(x, 0) + i\hat{\tau}_r^n(x, 0) + \int_{-a}^a [\check{\sigma}_r^n(x, 0, t) + i\check{\tau}_r^n(x, 0, t)] dt = -\sigma(x) - i\tau(x), \quad r = 1, 2. \quad (2.15)$$

After solving the auxiliary problem and defining vector $\check{\mathbf{U}}_r^k(x, y, t)$, the corresponding superposition terms $\check{\mathbf{U}}_r^k(x, 0, t)$ and $\hat{\mathbf{U}}_r^k(x, 0)$, proportional to dislocation amplitudes $f_1(t)$, $f_2(t)$ and to edge tractions $\sigma^u(x)$, $\tau^u(x)$, $\sigma^b(x)$, $\tau^b(x)$ respectively, must be separated. Then, by satisfying (2.15), a system of two singular integral equations for deriving the unknown dislocation densities $f_j(t)$, $j = 1, 2$ is obtained.

Vector $\mathbf{F}(t) = \{f_1(t), f_2(t), 0, 0\}$ is introduced, which defines the displacement jumps and the continuity of the stresses across the interface $y = 0$ in the cell number n with the dislocation at the point $x = t$. The auxiliary boundary value problem for the strip containing a single dislocation is specified by the following set of equations

$$\mathcal{L}_r[\check{u}_r^k(x, y, t), \check{v}_r^k(x, y, t)] = 0, \quad k = 0, \dots, N-1; \quad r = 1, 2 \quad (2.16)$$

$$\check{\mathbf{U}}_1^k(x, -h_1, t) - \check{\mathbf{U}}_2^{k-1}(x, h_2, t) = 0, \quad k = 1, \dots, N-1 \quad (2.17)$$

$$\check{\mathbf{U}}_2^k(x, 0, t) - \check{\mathbf{U}}_1^k(x, 0, t) = \mathbf{F}(t)H(x-t)\delta_{kn}, \quad k = 0, \dots, N-1 \quad (2.18)$$

$$\check{\sigma}_2^{N-1}(x, h_2, t) + i\check{\tau}_2^{N-1}(x, h_2, t) = \sigma^u(x) + i\tau^u(x), \quad (2.19)$$

$$\check{\sigma}_1^0(x, -h_1, t) + i\check{\tau}_1^0(x, -h_1, t) = \sigma^b(x) + i\tau^b(x), \quad (2.20)$$

where operator \mathcal{L}_r corresponds to the field equations (2.2) and δ_{kn} is the Kronecker delta. Symbol " \sim " is added to all the components of the elastic field in order to distinguish this problem from the initial one, in which conditions (2.4)–(2.6) are replaced by (2.18).

2.2.1 An equivalent quasi-periodic problem.

The considered strip, in spite of its repetitive structure, does not possess translational symmetry with reference to the repetition direction. The elastic field in such a strip can

be derived by using the method suggested by Nuller (1981). According to this method, the problem for a finite thickness periodic composite is replaced by an equivalent quasi-periodic problem for a periodically layered plane. A similar technique was employed recently by Karpov *et al.* (2002b) in the analysis of finite periodic structures.

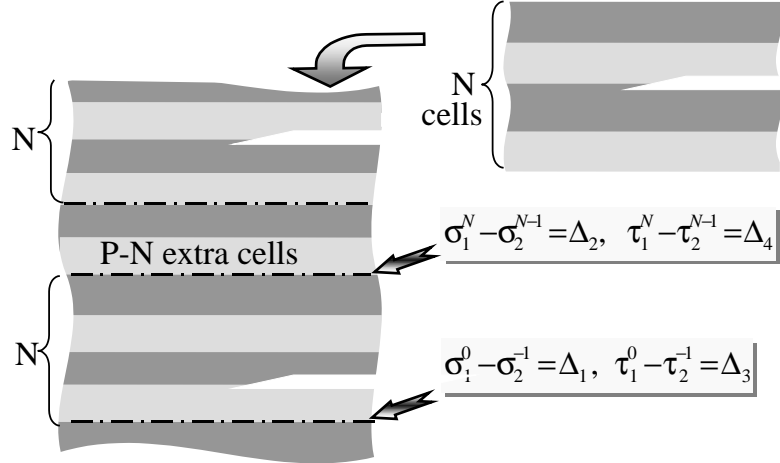


Figure 2.2: The equivalent cyclic problem for a periodically layered space containing dislocations and loaded by the virtual tractions defined via the stress jumps $\Delta_j(x)$.

The strip is extended with additional cells Ω_k , $k = -\infty..-1, N.. \infty$ to a periodically layered plane (Fig.2.2) loaded by the dislocation (2.18) in a cyclic manner, so that the elastic field in the plane is cyclic with a period containing $P > N$ cells. Namely,

$$\tilde{\mathbf{U}}_r^{k+jP}(x, y) = \tilde{\mathbf{U}}_r^k(x, y), \quad r = 1, 2; \quad k = 0, \dots, P-1; \quad j = 0, \pm 1, \pm 2 \dots \quad (2.21)$$

In order that the stress state in the N-strip be equivalent to that in the initial problem, some unknown virtual forces are introduced in each P - strip somewhere in the region occupied by the $P - N$ additional cells. These forces appear as the stress jumps, compensating the effect of the continuum adjacent to the N-layered domains. It is convenient to apply them² at the interfaces corresponding to the bottom and the top edges of the original N-strip:

$$\tilde{\sigma}_1^{jP}(x, -h_1) - \tilde{\sigma}_2^{jP-1}(x, h_2) = \Delta_1(x), \quad (2.22)$$

$$\tilde{\tau}_1^{jP}(x, -h_1) - \tilde{\tau}_2^{jP-1}(x, h_2) = \Delta_3(x), \quad (2.23)$$

$$\tilde{\sigma}_1^{N+jP}(x, -h_1) - \tilde{\sigma}_2^{N-1+jP}(x, h_2) = \Delta_2(x), \quad (2.24)$$

²The stress jumps being applied at the same lines, where the edge conditions should be satisfied, have the minimal amplitudes.

$$\tilde{\tau}_1^{N+jP}(x, -h_1) - \tilde{\tau}_2^{N-1+jP}(x, h_2) = \Delta_4(x), \quad j = 0, \pm 1, \pm 2 \dots \quad (2.25)$$

The unknown functions $\Delta_i(x)$ are to be adjusted in order to provide the fulfillment of the conditions (2.7)–(2.8) at the boundaries of the N - strip.

Since the dislocation, in fact, represents an additional loading and enters only the right hand side of the bonding conditions, the constructed layered plane possesses the translational symmetry. Therefore, the problem is reduced to the cyclic quasi-periodic one. The period of the structure consists of two layers and that of the stress state contains P cells³. The boundary conditions for the first cycle $j = 0$ have the form

$$\tilde{\mathbf{U}}_1^k(x, -h_1) - \tilde{\mathbf{U}}_2^{k-1}(x, h_2) = \mathbf{D}^0(x) \delta_{k0} + \mathbf{D}^N(x) \delta_{kN} \quad (2.26)$$

$$\tilde{\mathbf{U}}_2^k(x, 0) - \tilde{\mathbf{U}}_1^k(x, 0) = \mathbf{F}(t) H(x - t) \delta_{kn}, \quad k = 0, 1 \dots P - 1 \quad (2.27)$$

$$\tilde{\mathbf{U}}_2^P(x, -h_1) = \tilde{\mathbf{U}}_1^0(x, -h_1). \quad (2.28)$$

Here vectors $\mathbf{D}^0(x) = \{0, 0, \Delta_1(x), \Delta_3(x)\}$ and $\mathbf{D}^N(x) = \{0, 0, \Delta_2(x), \Delta_4(x)\}$, are defined by the four unknown stress jumps.

It should be pointed out that number P of the cells in the cycle is arbitrary, as far as it is greater than N . The last reservation is essential in order that boundary conditions (2.19) and (2.20) be consistent. Note also that there is some freedom in the choice of the jump location and origin. For example, the jumps in the displacements may be considered. The interested reader can find more information on this subject in the paper by Nuller (1981).

2.2.2 The representative cell.

The cyclic quasi-periodic problem specified with (2.26)–(2.28) for a single cycle is reduced to analysis of the repetitive module i.e., the cell consisting of two layers by means of the representative cell technique (Nuller and Ryvkin, 1980), based on the Finite Discrete Fourier Transform (FDFT):

$$g^*(x, y, \phi_m) = \sum_{k=0}^{P-1} g^k(x, y) e^{-ik\phi_m}, \quad \phi_m = 2\pi m/P, \quad m = 0, 1, \dots, P - 1, \quad (2.29)$$

³In fact, the stated problem is periodic with period P , but it is hardly simpler than the initial one for the N -strip if it is not considered as a quasi-periodic one with the single cell period.

application of which to equations (2.27)-(2.28) yields the boundary value problem for the representative cell Ω^* ($-h_1 < y < h_2$, $-\infty < x < \infty$) depicted in Fig. 2.3.

$$\mathcal{L}_r[\tilde{u}_r^*(x, y), \tilde{v}_r^*(x, y)] = 0, \quad (x, y) \in \Omega^* \quad (2.30)$$

$$\tilde{\mathbf{U}}_1^*(x, -h_1) - \gamma_m \tilde{\mathbf{U}}_2^*(x, h_2) = \mathbf{D}^0(x) + \mathbf{D}^N(x)\gamma_m^N \quad (2.31)$$

$$\tilde{\mathbf{U}}_2^*(x, 0) - \tilde{\mathbf{U}}_1^*(x, 0) = \mathbf{F}(t)H(x-t)\gamma_m^n. \quad (2.32)$$

where $\tilde{\mathbf{U}}_r^*(x, y) \equiv \tilde{\mathbf{U}}_r^*(x, y, t, \phi_m)$ are composed of the corresponding FDFT transforms of the displacements and the stresses and $\gamma_m = e^{-i\phi_m}$. All the stress and displacement components here depend upon the transform parameter m due to equation (2.31) relating the opposite sides of the representative cell and sometimes referred to as Born - Von Karman type boundary conditions. It should be emphasized that the representative cell

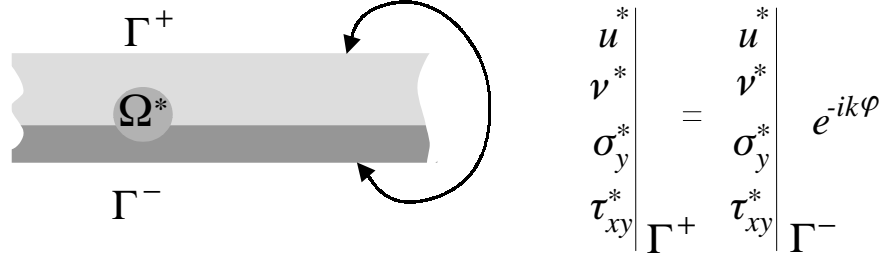


Figure 2.3: Problem for the representative cell with the Born-Von Karman type boundary conditions.

Ω^* is not one of the bi-layered physical cells but a domain in Fourier transformed space.

After deriving $\tilde{\mathbf{U}}_r^*(x, y)$, functions $\tilde{\mathbf{U}}_r^k(x, y)$ are obtained by means of the inverse FDFT

$$g_r^k(x, y) = \frac{1}{P} \sum_{m=0}^{P-1} g_r^*(x, y, \phi_m) e^{ik\phi_m}, \quad k = 0, \dots, P-1. \quad (2.33)$$

Periodicity condition (2.21) is thereby satisfied automatically.

Note. In those cases when the infinite number P of the layers in the cycle is chosen, or the periodically layered space ($N = \infty$) is considered from the very beginning, the quasi-periodic problem corresponding to (2.26)–(2.28) has no cyclic symmetry. Then FDFT (2.29), (2.33) should be replaced with the (infinite) DFT:

$$g^*(\phi) = \sum_{k=-\infty}^{\infty} g^k e^{ik\phi}, \quad -\pi < \phi < \pi. \quad (2.34)$$

$$g^{(k)} = \frac{1}{2\pi} \int_{-\pi}^{\pi} g^*(\phi) e^{-ik\phi} d\phi, \quad k = 0, \pm 1, \pm 2, \dots \quad (2.35)$$

Here relation (2.35) represents the inverse DFT.

The solution of problem (2.30)–(2.32) for the representative cell is obtained by applying the two-sided Laplace transform

$$\bar{\bar{\mathbf{U}}}_r^*(z, y, t, \phi_m) = \frac{1}{2\pi} \int_{-\infty}^{\infty} \tilde{\mathbf{U}}_r^*(x, y, t, \phi_m) e^{-zx} dx . \quad (2.36)$$

The real part of the transform parameter $z = i s + \varepsilon$ must be chosen for each specific set of boundary conditions (2.7)–(2.8) from the physical considerations, in order to ensure convergence of the integral in (2.36). Use of $\varepsilon > 0$ enables to consider the stress and displacement fields which do not vanish at $x \rightarrow \infty$ but decay exponentially for $x \rightarrow -\infty$. Hence, tractions that equal zero outside some finite interval on the x -axis can be considered by the use of such transform, even if they are balanced by a force moment at $x \rightarrow \infty$. In the case of three point bending to be considered in Chapter 3, choosing $\varepsilon > 0$ corresponds to zero displacements for $x \rightarrow -\infty$ and linear growing ones for $x \rightarrow +\infty$ (Fig. 2.4).

The field equations (2.30) are satisfied by the Papkovitch-Neuber elastic solution representation (e.g. Uflyand, 1968), taken in the form of the inverse Laplace integrals

$$\tilde{\mathbf{U}}_r^*(x, y, t, \phi_m) = \frac{1}{2\pi} \int_{\Gamma} \bar{\bar{\mathbf{U}}}_r^*(z, y, t, \phi_m) e^{zx} dz , \quad (2.37)$$

where vector $\bar{\bar{\mathbf{U}}}_r^*(z, y, t, \phi_m)$ is composed of the corresponding displacement and stress transforms

$$\bar{\bar{u}}_r^*(z, y, t, \phi_m) = \mu_r^{-1} [(A_{4r-3} + yzA_{4r-1}) \cos zy + (A_{4r-2} + yzA_{4r}) \sin zy] , \quad (2.38)$$

$$\begin{aligned} \bar{\bar{v}}_r^*(z, y, t, \phi_m) &= \mu_r^{-1} [A_{4r-2} - \kappa_r A_{4r-1} + yzA_{4r}] \cos zy \\ &\quad - (yzA_{4r-1} + \kappa_r A_{4r} + A_{4r-3}) \sin zy , \end{aligned} \quad (2.39)$$

$$\begin{aligned} \bar{\bar{\sigma}}_r^*(z, y, t, \phi_m) &= 2z [(2(1 - \nu_r)A_{4r-1} - yzA_{4r} - A_{4r-2}) \sin zy \\ &\quad - (yzA_{4r-1} + 2(1 - \nu_r)A_{4r} + A_{4r-3}) \cos zy] , \end{aligned} \quad (2.40)$$

$$\begin{aligned} \bar{\bar{\tau}}_r^*(z, y, t, \phi_m) &= 2z [(yzA_{4r-1} + (1 - 2\nu_r)A_{4r} + A_{4r-3}) \sin zy \\ &\quad + ((1 - 2\nu_r)A_{4r-1} - yzA_{4r} - A_{4r-2}) \cos zy] . \end{aligned} \quad (2.41)$$

$$\kappa_r = 3 - 4\nu_r , \quad r = 1, 2.$$

Contour Γ in (2.37) is a line $\text{Re}(z) = \varepsilon$ located in accordance with the above considerations in the plane of complex variable z .

Note, that each dislocation (2.9)-(2.10) cyclically introduced into the periodic plane as shown in Fig. 2.2 induces the stress jumps and, consequently, the stresses in the representative cell, which do not vanish at $x \rightarrow +\infty$. Therefore, Γ should be taken to the right from the imaginary axis. However, stresses produced by the dislocation superposition modelling the crack in the initial problem vanish at $x \rightarrow \infty$. Hence, if the edge tractions in the initial problem are self-balanced, the Laplace transforms of the stresses do not possess singularities on the line $\text{Re}(z) = 0$ and, therefore, after changing

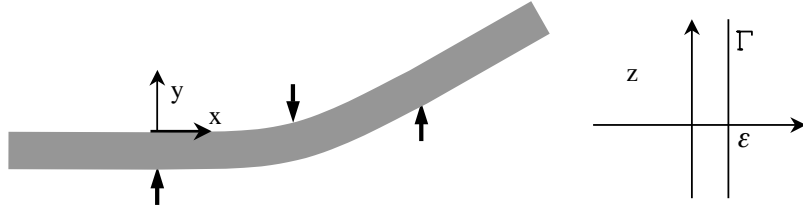


Figure 2.4: Choice of inverse Laplace integration contour Γ and associated coordinate system (x, y) .

the integration order, the contour can be shifted to the imaginary axis. In this particular case, the Laplace integrals become the Fourier ones, and this simplifies the calculations. The displacements, however, can increase at infinity even under the action of the localized self-balanced load, as it is shown on Fig. 2.4.

Thus, the solution of the representative cell problem (2.30)-(2.32) is expressed through the eight unknown coefficients $A_j \equiv A_j(z, t, \phi_m)$, $j = 1, \dots, 8$. Substitution of expressions (2.37)-(2.41) to the Laplace transformed boundary conditions (2.31), (2.32) yields after some manipulation⁴ the system of eight linear algebraic equations with respect to A_j

$$\mathbf{MA} = \mathbf{R}, \quad (2.42)$$

$$\mathbf{R} = \{0, 0, \bar{\Delta}_1(z) + \gamma_m^N \bar{\Delta}_2(z), \bar{\Delta}_3(z) + \gamma_m^N \bar{\Delta}_4(z), \mu_2 f_1(t) \gamma_m^n e^{-zt}, \mu_2 f_2(t) \gamma_m^n e^{-zt}, 0, 0, 0\}^T.$$

Here \mathbf{A} is a column-vector with elements A_j , and \mathbf{M} is a 8×8 matrix presented in the Appendix A.1. Consequently, functions A_j are expressed by the linear combinations of the Laplace transformed stress jumps $\bar{\Delta}_j(z)$ and dislocation amplitudes $f_1(t)$, $f_2(t)$.

$$A_j = \{ M^{(3j)} [\bar{\Delta}_1(z) + \gamma_m^N \bar{\Delta}_2(z)] + M^{(4j)} [\bar{\Delta}_3(z) + \gamma_m^N \bar{\Delta}_4(z)]$$

⁴The only way to carry out lengthy manipulations required by the present analysis technique is to use symbolic computation. In the present research program MAPLE was exploited.

$$+ \gamma_m^n e^{-zt} [M^{(5j)} f_1(t) + M^{(6j)} f_2(t)] \} [\det(\mathbf{M})]^{-1}, \quad j = 1, 2, \dots, 8, \quad (2.43)$$

where $\det(\mathbf{M})$ is the determinant of matrix \mathbf{M} and $M^{(ij)}$ is the algebraic cofactor of the corresponding element.

Four unknown functions $\bar{\Delta}_j(z)$ are to be determined from boundary conditions (2.7), (2.8). The Laplace transformed stresses in any cell Ω_k , ($k = 0, 1 \dots P-1$) of the P -strip can be found from the solution for the representative cell by applying the inverse FDFT (2.33) to expressions (2.40)–(2.41) with A_j substituted from (2.43). By calculating, in this manner, the stress transforms at the lines corresponding to the initial strip edges and employing the Laplace transformed boundary conditions (2.7)–(2.8), the 4-th order linear algebraic system for determining the stress jumps transforms is obtained

$$\mathbf{S} \bar{\Delta} = \mathbf{b}^0 + e^{-zt} [f_1(t) \mathbf{b}^1 + f_2(t) \mathbf{b}^2], \quad (2.44)$$

where $\mathbf{b}^0 = \{ \bar{\sigma}^b(z), \bar{\tau}^b(z), \bar{\sigma}^u(z), \bar{\tau}^u(z) \}^T$ and $\bar{\Delta} = \{ \bar{\Delta}_1(z), \bar{\Delta}_3(z), \bar{\Delta}_2(z), \bar{\Delta}_4(z), \}^T$ are vector-columns of the Laplace transforms of the edge tractions and the stress jumps, respectively. Vectors \mathbf{b}^1 and \mathbf{b}^2 are known functions. The structure of matrix \mathbf{S} is clarified in the next chapter and in Appendix A.2. Note, that the elements of matrix \mathbf{S} and of vectors \mathbf{b}^0 , \mathbf{b}^1 , \mathbf{b}^2 involve the inverse FDFT sums.

As consistent with the right hand side of the above equation the stress jump vector can be presented as follows

$$\bar{\Delta} = \bar{\Delta}^0 + e^{-zt} (f_1(t) \bar{\Delta}^1 + f_2(t) \bar{\Delta}^2), \quad (2.45)$$

$$\bar{\Delta}^k = \mathbf{S}^{-1} \mathbf{b}^k, \quad k = 0, 1, 2. \quad (2.46)$$

Then expression (2.43) for functions $A_j(z, t, \phi_m)$, $j = 1, \dots, 8$ takes on the following form

$$A_j = \left\{ a_j^0 + e^{-zt} [f_1(t)(a_j^1 + \gamma_m^n M^{(5j)}) + f_2(t)(a_j^2 + \gamma_m^n M^{(6j)})] \right\} \det(\mathbf{M})^{-1}, \quad (2.47)$$

$$a_j^k = d_1^k M^{(3j)} + d_3^k M^{(4j)}, \quad d_i^k = [\bar{\Delta}_i^k + \gamma_m^N \bar{\Delta}_{i+1}^k], \quad i = 1, 3; \quad k = 0, 1, 2.$$

where $\bar{\Delta}_i^k$ are the elements of the corresponding vectors $\bar{\Delta}^k$.

Substitution of A_j to (2.38)–(2.41) yields the solution $\bar{\mathbf{U}}_r^*(z, y, t, \phi_m)$ of the representative cell problem. By using inverse transforms (2.37) and (2.33) the elastic field of the P -strip (quasi-periodic problem) and, consequently, the field of the N -strip with a single dislocation (auxiliary problem) is provided by

$$\tilde{\mathbf{U}}_r^k(x, y, t) = \frac{1}{2\pi P} \int_{\Gamma} \sum_{m=0}^{P-1} \bar{\mathbf{U}}_r^*(z, y, t, \phi_m) e^{ik\phi_m} e^{zx} dz, \quad (2.48)$$

where $\bar{\mathbf{U}}_r^*(z, y, t, \phi_m)$ is given by (2.38)–(2.41) and (2.47).

By retaining term a_j^0 in the numerator of the right hand side of (2.47), the elastic field $\hat{\mathbf{U}}_r^k(x, y, t)$ in the perfectly bonded strip is provided by (2.48). On the other hand, putting a_j^0 to zero yields the Green's function $\check{\mathbf{U}}_r^k(x, y, t)$ for a single dislocation in the strip with homogeneous boundary conditions (2.19)–(2.20). These closed form solutions are of importance, since they allow formulating different interface crack problems for a bi-material periodically layered strip in terms of the integral equations.

Note 1. The case of the strip with an odd number of layers (symmetric laminate) also can be addressed by the use of the employed technique without difficulty. Suppose both the top and the bottom layers are of the same type (say, type two), then boundary condition (2.8) must be replaced by relation

$$\sigma_2^0(x, 0) + i\tau_2^0(x, 0) = \sigma^b(x) + i\tau^b(x) \quad (2.49)$$

and value $k = 0$ must be excluded in (2.4). Construction of the corresponding quasi-periodic problem slightly differs in this case. First, an incomplete cell is supplemented with the missing layer, and then the strip is extended with additional cells Ω_k , $k = -\infty \dots, -1, N, \dots \infty$ to a periodically layered plane as depicted in Fig.2.2. Accordingly, the stress jumps defined by (2.22)–(2.23) are translated to the corresponding interface and the following relations

$$\tilde{\sigma}_2^{jP}(x, 0) - \tilde{\sigma}_1^{jP}(x, 0) = \Delta_1(x), \quad (2.50)$$

$$\tilde{\tau}_2^{jP}(x, 0) - \tilde{\tau}_1^{jP}(x, 0) = \Delta_3(x), \quad j = 0, \pm 1, \pm 2 \dots \quad (2.51)$$

are used instead of (2.22)–(2.23).

Note 2. The solution scheme can be easily adjusted to the case of boundary conditions of other types. In fact, the quasi-periodic problem for the layered space is formulated in terms of the dislocation amplitudes and of the stress jumps. Hence, the Green's function and the solution for the perfectly bonded strip with corresponding homogeneous boundary edge conditions will have the same form in terms of the stress jumps. Consequently, the same way as in the previous symmetric laminate case, in the present scheme only composition of the vector equation of the type (2.44) undergoes modification.

2.3 The integral equation.

Solution of the initial problem for the crack in the periodically layered strip is derived in terms of dislocation amplitudes $f_1(t)$ and $f_2(t)$ by the use of (2.14) after detaching constituents $\hat{\mathbf{U}}_r^k(x, y, t)$ and $\check{\mathbf{U}}_r^k(x, y, t)$ in solution (2.48) of the auxiliary problem. Dislocation distribution $f_1(t)$, $f_2(t)$ along the crack line will be determined from conditions (2.15) on the crack faces, in accordance with the general procedure developed by Erdogan and Gupta (1971a,b).

The stresses on the opposite crack faces are equal, therefore, for satisfying conditions (2.15) presented via the corresponding stress components $\hat{\sigma}_r^n(x, 0)$, $\hat{\tau}_r^n(x, 0)$ and $\check{\sigma}_r^n(x, 0, t)$, $\check{\tau}_r^n(x, 0, t)$ of the elastic field, knowledge of only four functions A_j , $j = 1, 2, 3, 4$ is sufficient. By setting $y = 0$ and $r = 1$ in expressions (2.40)–(2.41) with A_j defined by (2.47), the stress transforms at the crack line take the form

$$\begin{aligned}\bar{\sigma}_1^*(z, 0, t, \phi_m) &= S_0^1 + e^{-zt}[f_1(t)(S_1^1 + \gamma_m^n K_5^1) + f_2(t)(S_2^1 + \gamma_m^n K_6^1)], \\ \bar{\tau}_1^*(z, 0, t, \phi_m) &= S_0^2 + e^{-zt}[f_1(t)(S_1^2 + \gamma_m^n K_5^2) + f_2(t)(S_2^2 + \gamma_m^n K_6^2)],\end{aligned}\quad (2.52)$$

$$K_i^1 = [2(1 - \nu_1)M^{(i4)} + M^{(i1)}] \det(\mathbf{M})^{-1}, \quad K_i^2 = [(1 - 2\nu_1)M^{(i3)} - M^{(i2)}] \det(\mathbf{M})^{-1},$$

$$S_k^r = d_1^k K_3^r + d_3^k K_4^r, \quad k = 0, 1, 2; \quad r = 1, 2; \quad i = 3, 4, 5, 6.$$

Terms S_0^r are actually the transformed stresses at the crack line in the perfectly bonded strip under the external loading. Terms with S_k^r , $k = 1, 2$ define the influence of the external boundaries on the dislocation induced stresses. Finally, singular terms K_5^i and K_6^i define the direct influence of the dislocation on the stresses at the crack line. After extracting the singular, non decaying for $z \rightarrow \pm i\infty$ parts from K_5^i and K_6^i , applying the inverse Laplace transform to (2.52) and finally changing the order of integration and summation, the stresses at the crack line in the cell number n of the auxiliary problem are obtained as follows

$$\begin{aligned}\tilde{\sigma}_1^n(x, 0, t) &= C_0^1 + \frac{1}{2\pi} \int_{-\infty}^{\infty} e^{is(x-t)} [f_1(t)a_{11} + f_2(t)a_{12} - f_1(t)K_{11} - f_2(t)K_{12}] ds \\ \tilde{\tau}_1^n(x, 0, t) &= C_0^2 + \frac{1}{2\pi} \int_{-\infty}^{\infty} e^{is(x-t)} [f_1(t)a_{12} - f_2(t)a_{11} - f_1(t)K_{21} - f_2(t)K_{22}] ds,\end{aligned}\quad (2.53)$$

where

$$K_{rk} = \frac{-i}{P} \sum_{m=0}^{P-1} [\gamma_m^{-n} S_k^r + K_{4+k}^r + a_{rk}], \quad r, k = 1, 2; \quad (2.54)$$

$$C_0^r = \frac{i}{2\pi P} \int_{-\infty}^{\infty} \sum_{m=0}^{P-1} S_0^r e^{isx} ds, \quad r = 1, 2.$$

$$a_{11} = -a_{22} = \mu_2 \frac{\lambda_2 - \lambda_1}{\lambda_1 \lambda_2}, \quad a_{12} = a_{21} = ia^0 \text{sign}(s),$$

$$a^0 = \mu_2 \frac{\lambda_1 + \lambda_2}{\lambda_1 \lambda_2}, \quad \lambda_1 = \mu + \kappa_2, \quad \lambda_2 = 1 + \mu \kappa_1, \quad \mu = \frac{\mu_2}{\mu_1}.$$

Note, that the first terms in the right hand side of (2.53) are the stresses at the crack line in the perfectly bonded strip $C_0^1 = \hat{\sigma}_1^n(x, 0)$; $C_0^2 = \hat{\tau}_1^n(x, 0)$. Substitution of (2.53) into the stress conditions on the crack faces (2.15) leads to a system of two singular integral equations in terms of unknown dislocation densities $f_1(t)$, $f_2(t)$. Making use of identities

$$\frac{1}{2\pi i} \int_{-\infty}^{\infty} e^{is(x-t)} ds = \delta(x-t), \quad \int_{-\infty}^{\infty} \text{sign}(s) e^{is(x-t)} ds = -2 \int_0^{\infty} \sin s(x-t) ds,$$

$$\int_1^1 f_r(t) dt \int_0^{\infty} \sin s(x-t) ds = \int_1^1 \frac{f_r(t)}{x-t} dt,$$

after some manipulations, the two integral equations are presented (Erdogan and Gupta, 1971b) as one complex integral equation with respect to complex dislocation amplitude $f(t) = f_1(t) + if_2(t)$

$$\frac{1}{\pi i} \int_{-1}^1 \frac{f(t) dt}{t-x} - \beta f(x) + \int_{-1}^1 [f(t) K_1(t, x) dt + \overline{f(t)} K_2(t, x)] dt = p + C, \quad (2.55)$$

$$p = \frac{i\sigma(x) - \tau(x)}{a^0}, \quad C = \frac{iC_0^1 - C_0^2}{a^0}.$$

Here all the length quantities are normalized by the half of the crack length a , and $\overline{f(t)}$ is a complex conjugate of $f(t)$. As can be seen, the tractions on the crack faces enters explicitly the right-hand side of the integral equation, while the strip edge loading results in term C . The kernels in (2.55) are given by

$$K_1(t, x) = \frac{1}{2\pi a^0} \int_{-\infty}^{\infty} e^{is(x-t)} [K_{11} - K_{22} + i(K_{12} + K_{21})] ds, \quad (2.56)$$

$$K_2(t, x) = \frac{1}{2\pi a^0} \int_{-\infty}^{\infty} e^{is(x-t)} [-K_{11} - K_{22} + i(K_{12} - K_{21})] ds.$$

The explicit expression for the functions $K_r(t, x)$, being rather cumbersome, have been obtained with the help of program of symbolic computations MAPLE, and are not presented here.

The solution method for integral equations of the considered type is a well developed procedure (Erdogan and Gupta, 1971b, Erdogan, 1969, and Karpenko, 1966). It will be outlined in Chapter 5 when considering the similar integral equation in the problem of an interface crack in a periodically layered plane.

Chapter 3

Perfectly bonded periodically layered bi-material strip

The analysis of the perfectly bonded periodically layered strip without cracks, being a particular case of the problem considered in the previous chapter, is of practical importance in itself. For example, prediction of the crack nucleation can be made only on the basis of such analysis, usually performed in the framework of axiomatic or asymptotic theories and with the help of corresponding computational techniques. In the present chapter an exact closed form elastic solution will be derived, which can serve as a benchmark problem for approximate solutions.

After the principal solution steps will have been summarized for this problem, two particular sets of boundary conditions will be considered. The problem for a strip with the fixed base subjected to the point force at the top edge and the three point bending problem will be examined. The stress field will be obtained in quadratures, and the parametric investigation will be carried out. Comparisons of the obtained results will be made with the data obtained by using the classic theory of laminated plates.

3.1 Closed form solution

Consider an infinite periodically layered bi-material strip Ω of thickness H . The strip consists of perfectly bonded isotropic elastic layers of two different types ($r = 1, 2$) arranged periodically (Fig. 3.1). The thickness, shear modulus and Poisson ratio of the

layers of r -th type are denoted as h_r, μ_r and ν_r respectively.

The stress state for arbitrary boundary conditions at the strip edges is sought. This problem is a particular case of the auxiliary one considered in Section 2.2. Consequently, the closed form solution is derived by using the equivalent quasi-periodic problem (Noller, 1981).

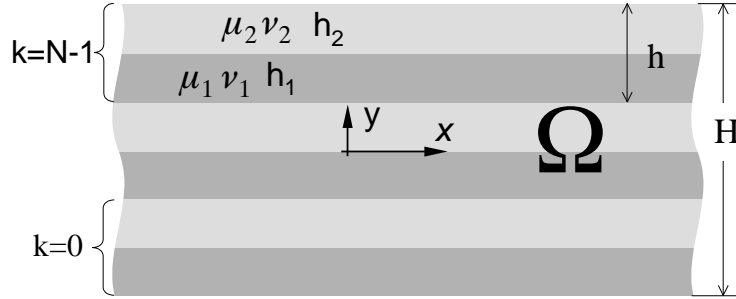


Figure 3.1: Periodically layered perfectly bonded strip.

Suppose for definiteness, that the total number of layers is even, then the strip may be viewed as an assemblage of bonded identical bi-layered cells Ω_k , $k = 0, \dots, N - 1$ of thickness $h = h_1 + h_2$. The elastic field vector $\mathbf{U}_r^k(x, y)$ is introduced with the help of (2.1). The boundary value problem for the strip in the case of prescribed tractions at its edges is defined by the following system of equations

$$\mathcal{L}_r[u_r^k(x, y), v_r^k(x, y)] = 0, \quad k = 0, 1, \dots, N - 1; \quad r = 1, 2; \quad (3.1)$$

$$\mathbf{U}_1^k(x, -h_1) - \mathbf{U}_2^{k-1}(x, h_2) = 0, \quad k = 1, \dots, N - 1 \quad (3.2)$$

$$\mathbf{U}_2^k(x, 0) - \mathbf{U}_1^k(x, 0) = 0, \quad k = 0, \dots, N - 1 \quad (3.3)$$

$$\sigma_2^{N-1}(x, h_2) + i\tau_2^{N-1}(x, h_2) = \sigma^u(x) + i\tau^u(x), \quad (3.4)$$

$$\sigma_1^0(x, -h_1) + i\tau_1^0(x, -h_1) = \sigma^b(x) + i\tau^b(x) \quad (3.5)$$

Here operator \mathcal{L}_r corresponds to the Lamé field equations (2.2). Recall that relations (3.2) and (3.3) provide the bonding conditions at the interfaces between the layers and the functions in the right hand sides of equations (3.4)-(3.5) denote the known stresses at the upper (u) and bottom (b) edges of the strip. It can be seen that the formulated problem is equivalent to that defined by (2.16),(2.20) with $\mathbf{F}(t) \equiv 0$.

Consequently, functions A_j are expressed by the linear combinations of the unknown stress jumps and are obtained from (2.43) with $f_1(t) = f_2(t) \equiv 0$. The solution for the

representative cell is obtained in terms of unknown jump transforms $\bar{\Delta}_j(z)$, $j = 1..4$ by substituting the obtained A_j into expressions (2.38–(2.41).

The Laplace transformed stresses $\bar{\sigma}_2^{N-1}, \bar{\tau}_2^{N-1}, \bar{\sigma}_1^0, \bar{\tau}_1^0$ are derived by applying the inverse FDFT (2.33) to the solution for the representative cell. Then, by employing boundary conditions (3.4)-(3.5), the 4-th order linear system for determining transformed stress jumps $\bar{\Delta}_i$ is formed

$$\left(\frac{1}{P} \sum_{m=0}^{P-1} \begin{bmatrix} s_{11} & \gamma_m^N s_{11} & s_{13} & \gamma_m^N s_{13} \\ s_{21} & \gamma_m^N s_{21} & s_{23} & \gamma_m^N s_{23} \\ \gamma_m^{-N} s_{11} & s_{11} - 1 & \gamma_m^{-N} s_{13} & s_{13} \\ \gamma_m^{-N} s_{21} & s_{21} & \gamma_m^{-N} s_{23} & s_{23} - 1 \end{bmatrix} \right) \begin{bmatrix} \bar{\Delta}_1(z) \\ \bar{\Delta}_2(z) \\ \bar{\Delta}_3(z) \\ \bar{\Delta}_4(z) \end{bmatrix} = \begin{bmatrix} \bar{\sigma}^b(z) \\ \bar{\tau}^b(z) \\ \bar{\sigma}^u(z) \\ \bar{\tau}^u(z) \end{bmatrix} \quad (3.6)$$

where the expressions for the elements s_{ij} being rather cumbersome are given in Appendix A.2. Note that these expressions depend upon the FDFT parameter m and the summation symbol is understood as being applied to all the elements of the matrix. Having derived the jump transforms from the latter system one obtains, in view of (2.38–2.41), (2.43) and (2.33), the closed form solution of the initial problem on a bi-material periodically layered strip of finite thickness.

Exchanging the order of summation and integration gives the solution in the form of the Laplace integrals of rather cumbersome expressions which, nevertheless, can be successfully handled by the use of symbolic computation. For example, stress $\sigma_{xx}^r(x, y)$ in the k -th cell can be presented in terms of obtained stress jump transforms as follows

$$\begin{aligned} \sigma_{xx}^r &= \frac{1}{2P\pi} \int_{\Gamma} e^{zx} \sum_{m=0}^{P-1} [-(A_{4r-2} + 2\nu_2 A_{4r-1} + yzA_{4r}) \sin zy \\ &\quad - (yzA_{4r-1} - 2\nu_2 A_{4r} + A_{4r-3}) \cos zy] z e^{ik\phi_m} dz, \\ A_j &= \{ M^{(3j)} [\bar{\Delta}_1(z) + \gamma_m^N \bar{\Delta}_2(z)] + M^{(4j)} [\bar{\Delta}_3(z) + \gamma_m^N \bar{\Delta}_4(z)] \} [\det(\mathbf{M})]^{-1}, \\ &\quad r = 1, 2; \quad j = 1, \dots, 8. \end{aligned} \quad (3.7)$$

When using this solution representation for boundary conditions of other types it is sufficient to recalculate only the stress jumps from the system of equations, similar to (3.6).

As it was noted in Subsection 2.2.2, in the case of localized self-equilibrated loading, the integrands for the stresses do not possess poles at the imaginary axis and the

inverse Laplace transform integration can be carried out along the line $\text{Re}(z) = 0$. The numerical evaluation of the integrals presents no special problems since the behavior of the integrands for large $|z|$ is defined by the relation

$$\bar{\sigma}_r^k(z, y) \sim O \left[\exp \left(-|z| \frac{l}{H} \right) \right], \quad z \rightarrow \infty \quad (3.8)$$

where l is the distance from the point of interest to the nearest outer boundary of the strip.

It is important to point out that when number N of the cells and, consequently, the number of terms in inverse FDFT (2.33) increases, the numerical efficiency of the obtained solution decreases. This inconvenience can be obviated by setting $P \rightarrow \infty$ and, consequently, by replacing FDFT (2.29), (2.33) with the infinite one (2.34). The interested reader can find the detailed description of such procedure in the paper by Kamysheva *et al.* (1982).

In order to illustrate the obtained solution for the stress field of a bi-material periodically layered strip of finite thickness, two particular sets of boundary conditions will be considered.

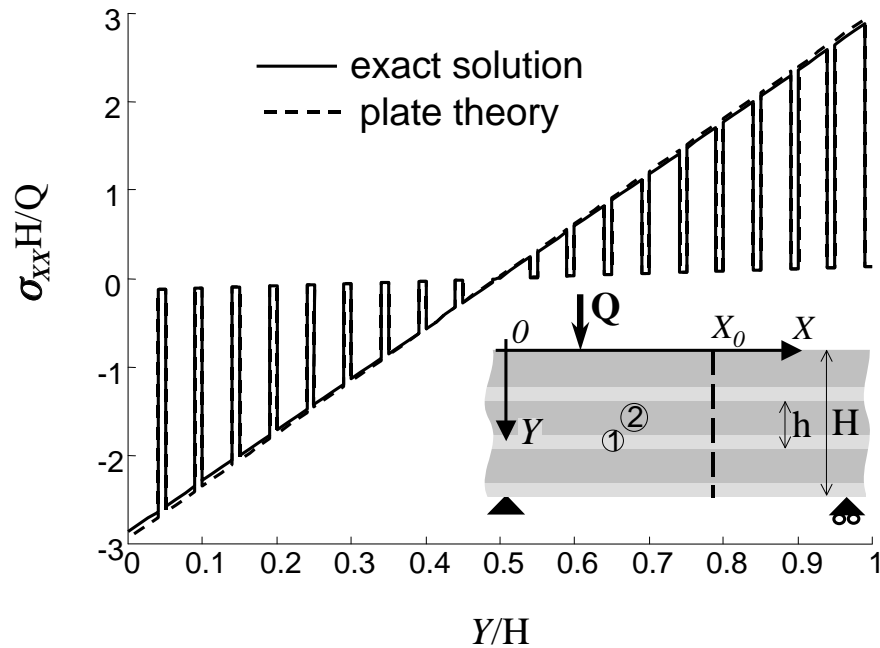


Figure 3.2: Three point bending strip. Bending stress σ_{XX} in the cross section $X_0/H = 3$ distant from the load application points.

3.2 Three point bending

Let us first consider a well known three point bending configuration represented by the insert in Fig. 3.3. An infinite strip consisting of twenty bi-layers ($N = H/h = 20$) is subjected to a normal point force Q applied between the simple supports in a non-symmetric manner $l_1/H = 1$, $l_2/H = 4$. Consequently, the distance $L = l_1 + l_2$ between supports is five times as long as the strip thickness H . The thinner layers are assumed

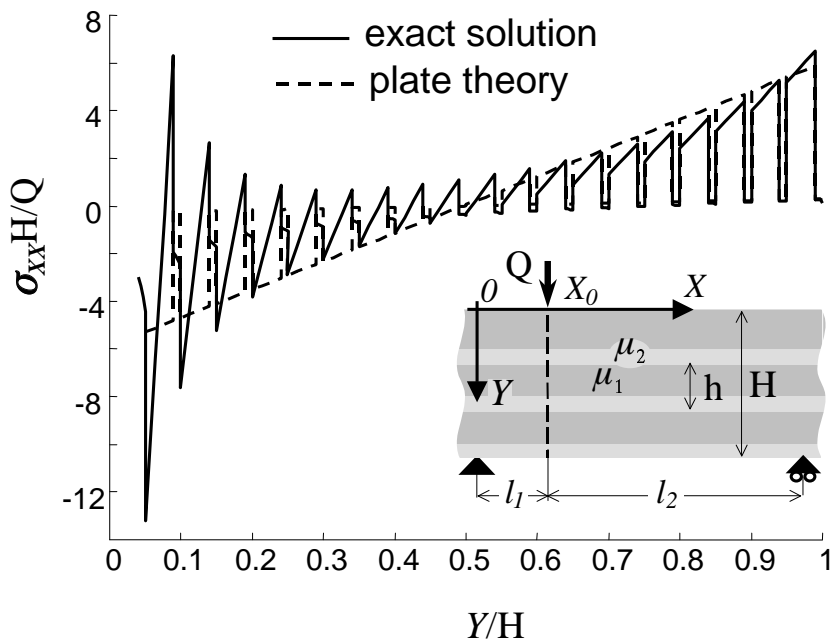


Figure 3.3: Bending stress σ_{XX} in the cross section $X_0/H = 1$ including the force line.

to be the more compliant ones $h_1/h = 0.2$, $\mu = \mu_2/\mu_1 = 20$ and the Poisson ratios of the materials are taken as $\nu_1 = 0.3$ and $\nu_2 = 0.35$.

The stresses at the strip edges, defining conditions (3.4)-(3.5), take on the following values

$$\sigma^u(x) = -Q \delta(x - l_1), \quad (3.9)$$

$$\sigma^b(x) = -Q \left[\frac{l_2}{L} \delta(x) + \frac{l_1}{L} \delta(x - L) \right], \quad (3.10)$$

$$\tau^u(x) = \tau^b(x) = 0. \quad (3.11)$$

where $\delta(x)$ is the delta function.

It was found that it is most efficient to carry out the calculations when the total thickness of the P -strip is about 5% larger than that of the N -one. Consequently, in the considered example, two additional bi-layers were added to the given domain.

The numerical results for the stress distribution are presented in the global Cartesian coordinate system (X, Y) shown in the inserts. In Fig. 3.2 and Fig. 3.3 the normalized bending stresses $\sigma_{xx}(X_0, Y)$ composed from the corresponding values of $\sigma_{xx}^{kr}(x, y)$ in each layer are shown in global coordinates. Two cross sections $X_0/H = 3$ and $X_0/H = 1$ are considered. Both graphs are discontinuous at the interfaces between the layers because of the jumps in the elastic properties. For the cross-section away from the point forces (Fig. 3.2), the stresses within each layer exhibit linear behavior and parts of the graph corresponding to the stiff and the compliant layers are located along two corresponding straight lines. Such behavior points out a linear bending strain distribution

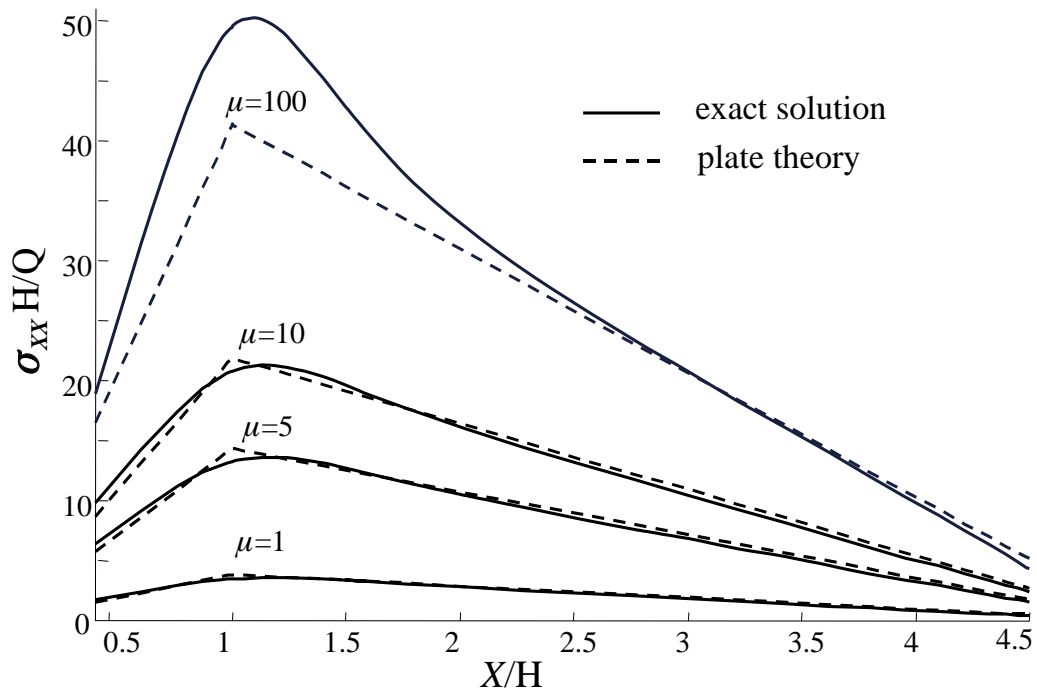


Figure 3.4: Longitudinal distribution of the bending stress $\sigma_{XX}(X, H - h_1 - 0)$ along the interface closest to the bottom within the stiffer layer.

in the N -strip which is in agreement with the plane cross sections hypothesis, adopted in the plate theory of composites. In fact, the stresses calculated by the use of this theory (dashed line) are found to be very close to the exact values.

On the other hand, in the applied force cross-section plane the plate theory, as expected, does not produce satisfactory results (Fig. 3.3). The stress distribution within each layer is found to be linear as in the previous case. This may be explained by a relatively large difference in the elastic moduli of the materials, when the thick stiff layers

behave like beams and the thin compliant ones like linear springs. At the same time, the angles defining the linear distribution within the layers of the specific type are different and the bending strain is a non-linear function of through-thickness coordinate Y . Another comparison of the obtained solution with the plate theory is presented in Fig. 3.4 where the longitudinal distribution of the bending stress $\sigma_{xx}(X, H - h_1 - 0) \equiv \sigma_{xx}^{02}(x, 0)$ in the stiff layer closest to the bottom is depicted. The results are presented for different materials mismatch. It is seen that for the considered geometry the difference between the plate theory solution and the exact one becomes significant only for the large elastic moduli ratio and decreases rapidly with the distance from the cross-section where the point force is applied.

3.3 Strip on a rigid foundation

In the next example a multilayered strip with boundary conditions of different types at the upper and bottom edges is considered. The strip is subjected to a tangential shear force T applied at the upper edge while the bottom is clamped (insert in Fig. 3.5). Therefore, the stress boundary conditions (3.4)-(3.5) should be replaced by the following ones

$$\sigma_2^{N-1}(x, h_2) + i \tau_2^{N-1}(x, h_2) = iT \delta(x), \quad (3.12)$$

$$u_1^0(x, -h_1) = v_1^0(x, -h_1) = 0. \quad (3.13)$$

The change in the type of boundary conditions does not preclude from employing, as previously, the stress jumps Δ_j as the adjusting factor. The matrix equation (2.42) remains unaltered. After adjusting the vector equation (3.6) in accordance with conditions (3.13), the closed form solution is derived, in which only the expressions for the stress jumps are altered compared to those in the problem with stress boundary conditions.

With the help of the obtained solution the stresses at the interface between the strip and the rigid substrate are examined. Calculations were carried out for the strip consisting of eight bi-layered cells with elastic moduli ratio $\mu = 9$ and identical Poisson ratios $\nu_1 = \nu_2 = 1/3$ for all the layers. Numerical results for normal stresses $\sigma_{YY}(X, H) \equiv \sigma_{yy}^{01}(x, -h_1)$ at the strip bottom are presented in Fig. 3.5a for different volume fractions of the constituents. The stress distribution is skew symmetric and, consequently, is shown

for $X > 0$.

The solution for the homogeneous strip, obtained by the standard Laplace transformation technique (e.g. Uflyand, 1968) is shown for comparison in the same figure by the dotted line. Note that in this solution the stress distribution is independent of shear modulus. Consequently, since the Poisson ratios in the considered composite are taken as equal, the limiting cases $h_1/h \rightarrow 0$ and $h_1/h \rightarrow 1$ produce the same result corresponding to the homogeneous strip.

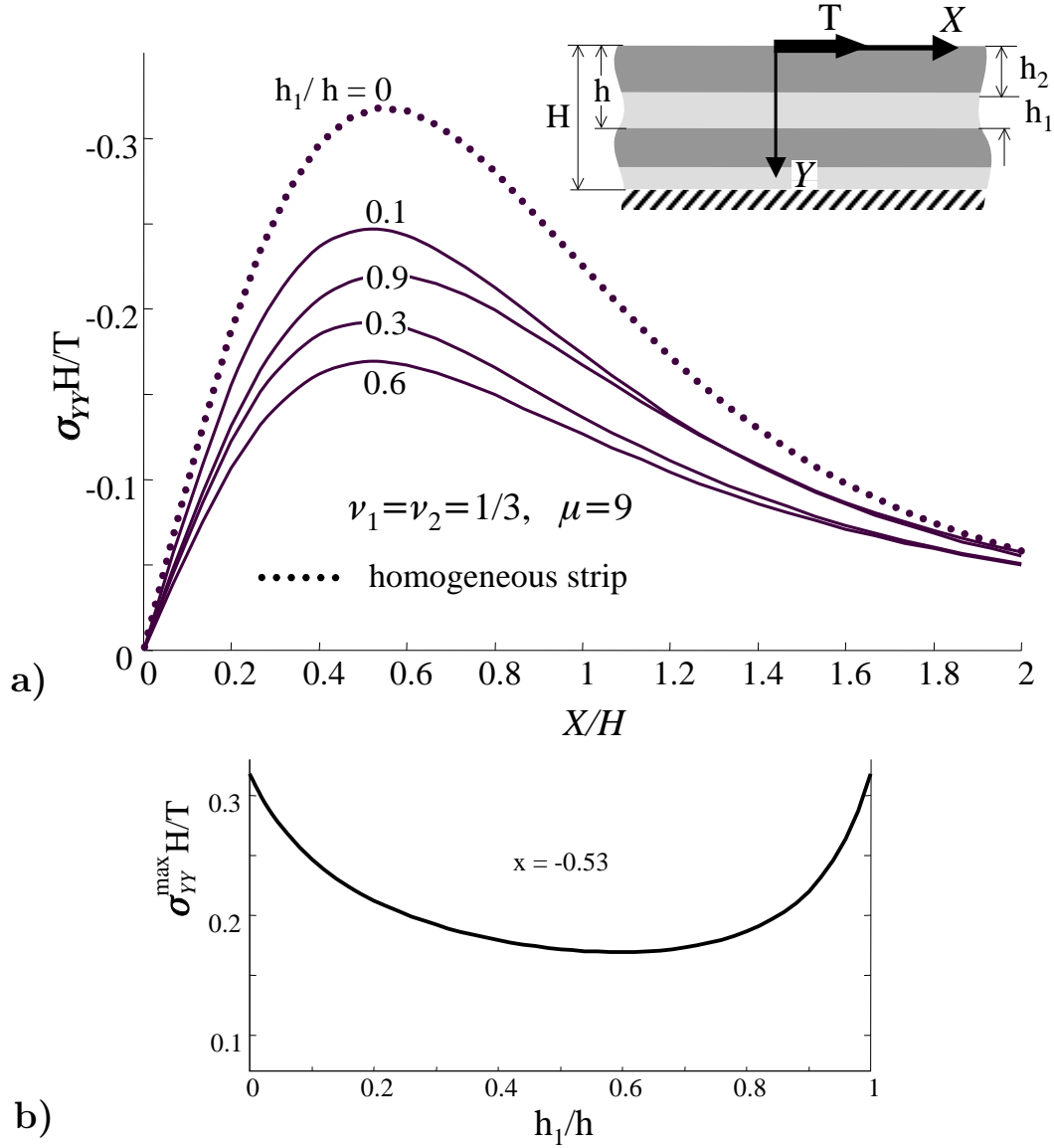


Figure 3.5: Normal stress $\sigma_{YY}(X, H)$ along the fixed bottom of the strip a) and its maximal value b) for different volume fractions of the composite constituents.

The stress distribution is characterized by a single maximum, depending upon the

volume fraction h_1/h . The obtained results reveal an interesting phenomenon: for sufficiently thin layers this maximum always decrease with increasing their thickness independently of the fact whether these layers are the stiffer or the more compliant ones. Consequently, the considered contact stresses at the bottom of the layered strip will be, as a rule, less than those for the strip made of the bulk material. Clearly, there is some optimum value of thickness ratio h_1/h minimizing the contact stresses. For the considered materials this value is found to be about 0.6 as it is seen from Fig. 3.5b where the dependence of the maximum normal stress upon the thickness ratio is presented.

Results for homogeneous strips made of materials with different Poisson ratios deviate from the presented ones. But the only qualitative difference is that the limiting cases $h_1/h \rightarrow 0$ and $h_1/h \rightarrow 1$ (Fig. 3.5b) result in different values of the corresponding stress $\sigma_{YY}(X, H)$. Consequently, the main conclusion of the above paragraph remains valid.

Calculations show that the similar phenomenon takes place in the conjugate problem, when the shear stresses at the clamped bottom of the strip are generated by a normal force applied at the upper edge. Namely, there is some optimal thickness ratio minimizing the shear stresses.

3.4 Conclusions

Employing the obtained closed form solution for analysis of the specific periodically layered composites revealed some interesting phenomena. Analysis of the periodically layered strip subjected to the three point bending has shown, as expected, that in the vicinity of the point forces the cross section of the strip does not remain plane after the deformation and, consequently, the approximate plate theory is not valid. On the other hand, it appeared that in the case of a large elastic mismatch between the materials, the strain distribution is linear in each individual layer, except the one nearest to the force application point. The investigation of the protective properties of the periodically layered strip bonded to the rigid substrate has shown that there is an optimal ratio between the layers thicknesses, providing the minimal normal (shear) contact stresses induced by the shear (normal) tractions at the top edge.

Chapter 4

Preliminary analysis of a delamination crack in a periodically layered space

Consider the problem of a delamination crack in a periodically layered strip. Assume the crack to be sufficiently short with respect to the overall strip thickness and to be located far from its boundaries. Then, the stress field perturbation caused by the crack is localized and, consequently, an approximate solution can be found by decomposing the problem into two separate ones. The first is the problem for the non-cracked strip examined in the previous chapter. The second is an asymptotic problem on the periodically layered plane containing the crack loaded by the tractions opposite to the stresses existing at the crack line in the first problem. The next consistent simplification is approximation of these tractions by uniformly distributed ones.

In this chapter some general mechanisms predetermining the behavior of the fracture characteristics for a delamination crack in a periodically layered space will be examined analytically. Namely, the effect of the loading direction is investigated and an expression for the energy release rate in front of the semi-infinite crack in the periodically layered space is obtained by the use of homogenization procedure. We recall that delamination crack can lie within the layer (intra-layer crack) or at the interface.

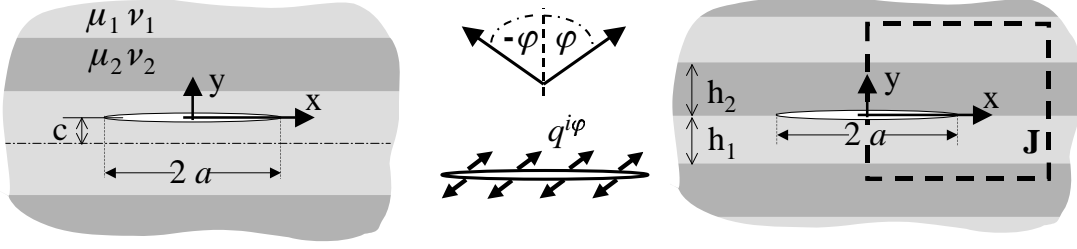


Figure 4.1: Periodically layered plane containing a delamination crack subjected to the uniform traction at angle φ with axis y .

4.1 Main definitions

Consider a composite bi-material plane consisting of isotropic elastic layers arranged periodically (Fig.4.1). The translational symmetry of the body is violated by a delamination crack of length $2a$, which can be located at an interface as well as within a layer. The layers have thickness h_r , where the index $r = 1, 2$ denotes the layer type. Hence the size of the repetitive cell is $h = h_1 + h_2$, and the ratio between the volumes of composite constituents is given by the non-dimensional parameter $\hat{h} = h_2/h_1$.

The elastic properties of the layers are defined by the shear modulus μ_r and Poisson ratio ν_r . The materials mismatch is characterized by Dundurs' parameters

$$\alpha = \frac{\mu(\kappa_1 + 1) - (\kappa_2 + 1)}{\mu(\kappa_1 + 1) + (\kappa_2 + 1)}, \quad \beta = \frac{\mu(\kappa_1 - 1) - (\kappa_2 - 1)}{\mu(\kappa_1 + 1) + (\kappa_2 + 1)} \quad (4.1)$$

with

$$\mu = \mu_2/\mu_1 \quad \text{and} \quad \kappa_r = 3 - 4\nu_r, \quad r = 1, 2. \quad (4.2)$$

The Cartesian coordinate system is introduced with the origin at the crack center and x axis parallel to the layering. The stress state is generated by the uniform opening tractions applied to the crack faces.

$$\sigma_{yy}(x, 0) + i\tau_{xy}(x, 0) = -\sigma - i\tau, \quad -a < x < a \quad (4.3)$$

Alternatively, it is convenient to characterize the loading by the traction amplitude q and the loading angle φ

$$q = \sqrt{\sigma^2 + \tau^2}, \quad \varphi = \tan^{-1}(\tau/\sigma). \quad (4.4)$$

Note that the singular stress field in the crack tip vicinity will be the same as in the case

when the external stresses are applied at infinity and the crack faces are free of tractions. This can be shown by the superposition procedure.

In order to make some preliminary remarks the fracture characteristics adopted in this study must be defined. The right hand crack tip will be considered hereafter for definiteness. We do not address the kinking phenomenon and consider only the straight-line cracks. Consequently, the subject of interest is the singular stresses directly ahead of the crack tip which in the case of the interface crack can be expressed by the complex stress intensity factor $K = K_1 + iK_2$:

$$\sigma_{yy}(x, 0) + i\tau_{xy}(x, 0) = \frac{K}{\sqrt{2\pi(x-a)}}(x-a)^{i\epsilon}, \quad (4.5)$$

$$\epsilon = \frac{1}{2\pi} \ln \frac{1-\beta}{1+\beta}, \quad (4.6)$$

and in the case of the non-interface crack, when the normal and tangential stresses are characterized by separate SIFs K_I and K_{II} , a complex SIF is introduced in the uniform manner.

$$K = K_I + iK_{II}, \quad \sigma_{yy}(x, 0) + i\tau_{xy}(x, 0) = \frac{K}{\sqrt{2\pi(x-a)}}, \quad (4.7)$$

Considering the above definitions, the non-interface crack SIF can be referred to as a special case, when constant ϵ equals zero.

The phase angle of the complex SIF K does not have clear physical meaning when ϵ is not zero, and it is convenient to define the real phase angle ψ (Rice, 1988, Suo and Hutchinson, 1989b)

$$\psi = \tan^{-1} \left[\frac{\text{Im}(K\hat{L}^{i\epsilon})}{\text{Re}(K\hat{L}^{i\epsilon})} \right], \quad (4.8)$$

where \hat{L} is some length parameter of the problem. Consequently, the SIF can be written in the following form

$$K = |K|\hat{L}^{-i\epsilon} e^{i\psi}, \quad (4.9)$$

where angle ψ defines the proportion between normal and tangential stresses at the distance \hat{L} from the crack tip. We choose \hat{L} as follows

$$\hat{L} = \min[h_1, h_2, 2a]. \quad (4.10)$$

In view of this definition, the magnitude of ψ may provide information about the relation between the fracture modes at a point apart from the region where the actual fracture

process takes place. In order to determine the stress state in the vicinity of some other point at a distance L_R from the crack tip one has to employ, as usual (e.g. Rice, 1988), the shifting relation

$$\psi_R = \psi + \epsilon \ln(L_R/\hat{L}) . \quad (4.11)$$

Note that for the non-interface cracks, ψ defined by (4.8) with $\epsilon = 0$ is the conventional phase angle of the mode mix.

In the present study, the complex SIF and its components for both types of delamination cracks are normalized with the help of the absolute value of the corresponding complex SIF K^{hom} for the crack in a homogeneous space:

$$\hat{K} = \frac{K\hat{L}^{i\epsilon}}{|K^{hom}|}, \quad |K^{hom}| = q\sqrt{\pi a} . \quad (4.12)$$

This value is independent of the loading mode and anisotropy in the material properties (Sih and Chen, 1981). The expression for the energy release rate through the complex SIF for the interface crack has been obtained by Malishev and Salganik (1965)

$$G = \frac{K\bar{K}}{16}(1 - \beta^2) \left(\frac{\kappa_1 + 1}{\mu_1} + \frac{\kappa_2 + 1}{\mu_2} \right) \quad (4.13)$$

where \bar{K} denotes the complex conjugate of K . It is convenient to normalize G by the known result for a crack at the interface between two dissimilar elastic half planes (Rice and Sih, 1965)

$$K_b = (1 + 2i\epsilon)(2a)^{-i\epsilon} q\sqrt{\pi a} e^{i\varphi} . \quad (4.14)$$

Denoting the corresponding ERR by G_b , we obtain the normalized one, in accordance with (4.13), as follows

$$\hat{G} = \frac{G}{G_b} = \frac{K\bar{K}}{\pi a q^2 (1 + 4\epsilon^2)} . \quad (4.15)$$

For the case of a non-interface crack, the energy release rate

$$G = \frac{1 - \nu_1}{2\mu_1} (K_I^2 + K_{II}^2), \quad (4.16)$$

is normalized with the help of the corresponding ERR for the homogeneous plane with the same elastic properties as those of the cracked layer.

$$\hat{G} = G/G_{hom}, \quad G_{hom} = \frac{1 - \nu_1}{2\mu_1} q^2 \pi a \quad (4.17)$$

The physical meaning of two above normalization types for the ERR is different. In fact, by assessing the normalized ERR (4.15) of the interface crack, the ERR for the crack in

the layered composite is compared with that for the limiting case of the crack between two very thick layers. At the same time, normalization (4.17) allows the discovery of how the ERR of the crack in the homogeneous material is influenced by the presence of the layers of another type. Actually, normalization (4.17) also could be applied to the interface ERR (4.13). Then the energy release for the interface crack could be related to that for the crack in the homogeneous continuum of first or second material type, which is not of much practical importance, because the interface fracture toughness usually differs from that of the bulk material.

Finally, it should be noted that for a special case of the material mismatch when β and, consequently, ϵ equal zero, both the normalized energy release rates for interface and intra-layer cracks are, actually, squared absolute values of the corresponding normalized stress intensity factors.

When examining the effect of the direction of the applied loading, it is convenient to introduce a phase shift angle representing the difference between the real phase angle and the applied loading angle

$$\omega = \psi - \varphi. \quad (4.18)$$

The question as to how the problem parameters influence the phase shift has received much consideration in fracture problems on layered composites (Fleck *et al.* 1991, Hutchinson *et al.* 1987, Jha and Charalambides, 1998, Suo and Hutchinson, 1989a,b). Some general trends characterizing dependence of the phase shift and the ERR upon the loading angle for a delamination crack in an arbitrary multilayered composite are in order.

4.2 Effect of the loading direction

In the cases of a semi-infinite crack in a composite consisting of two or three layers (Hutchinson *et al.* 1987, Suo and Hutchinson, 1989a,b, Fleck *et al.* 1991) or a finite length crack between two dissimilar half-spaces (Rice and Sih, 1965) the phase shift does not depend upon the applied loading direction, and

$$\frac{\partial \omega}{\partial \varphi} = 0. \quad (4.19)$$

On the other hand, for a semi-infinite non-interface crack in a periodically layered composite this dependence does not vanish, i.e. the above derivative is not zero as was found by Jha and Charalambides (1998) for the case of a long intra-layer crack in a periodically layered media. In order to address this issue in the case of a delamination crack of arbitrary length and location we will establish the general conditions for the validity of (4.19).

Let us compare the fracture characteristics for two marginal cases of pure normal and pure tangential loading $\varphi = 0$ and $\varphi = \pi/2$. The fact that the value $\varphi = \pi/2$ associated with pure shear loading on the crack faces may correspond to a not negligibly small physically senseless interpenetration zone, is not relevant in the present context since we are looking for *mathematical* conditions for the validity of (4.19). When employing the results of the numerical analysis presented in the subsequent chapters, only such values of φ which provide the desired bounds for this zone may be used (see Rice, 1988).

It will be shown now that alteration of the normal ($\varphi = 0$) and the tangent ($\varphi = \pi/2$) loading rotates the real phase angle by 90 degrees. With the subscript denoting the corresponding loading angle, it can be written in the following form

$$\psi_{\pi/2} = \psi_0 + \pi/2. \quad (4.20)$$

Therefore, in accordance with (4.18), the phase shifts for the normal and the tangent loading are equal:

$$\omega_{(\pi/2)} = \omega(0). \quad (4.21)$$

This follows directly from the symmetry of the problem. In fact, due to the problem linearity, the stress intensity factor corresponding to an arbitrary loading angle φ may be presented in the form

$$K_\varphi = K_0 \cos \varphi + K_{\pi/2} \sin \varphi. \quad (4.22)$$

where K_0 and $K_{\pi/2}$ are the complex SIFs corresponding to the pure normal and the pure shear loading respectively. Consequently, as consistent with (4.8), (4.9) and (4.15), the expression for the normalized energy release rate is given by

$$\hat{G} = \frac{|K_0|^2 \cos^2 \varphi + |K_{\pi/2}|^2 \sin^2 \varphi + |K_0 K_{\pi/2}| \sin 2\varphi \cos(\psi_0 - \psi_{\pi/2})}{\pi a q^2 (1 + 4\epsilon^2)}. \quad (4.23)$$

Consider now the J - integral taken round the contour containing the line $x = 0$ and closed by some contour located sufficiently far from the crack. Taking into account the

mirror symmetry of the elastic domain it may be concluded that

$$\hat{G}(\varphi) = \hat{G}(-\varphi) , \quad (4.24)$$

Therefore the odd part of expression (4.23) must vanish, which can occur only if

$$\cos(\psi_0 - \psi_{\pi/2}) = 0 , \quad (4.25)$$

i.e., if relation (4.20) is fulfilled. At the same time, by analyzing relation (4.23) in view of (4.25) a conclusion can be drawn concerning the shape of function $\hat{G}(\varphi)$, which appears to reach an extremum at $\varphi = 0, \pm\pi/2$. When $-\pi/2 < \varphi < 0$ or $0 < \varphi < \pi/2$, the ERR is a monotonic function of φ . The sign of the second derivative at $\varphi = 0$ is defined by that of expression $|K_0| - |K_{\pi/2}|$. Consequently, the normal traction produces a maximum or a minimum of the ERR depending on whether the above expression has positive or negative value.

Suppose now that the energy release rates corresponding to the considered marginal cases are equal, i.e.

$$\hat{G}(\pi/2) = \hat{G}(0) . \quad (4.26)$$

In accordance with (4.20) and (4.9) it follows that

$$K_{\pi/2} = K_0 \exp(i\frac{\pi}{2}) . \quad (4.27)$$

Then, employing the linearity of the problem it can be shown (by using (4.22)) that a similar relation is valid for an arbitrary angle φ

$$K_\varphi = K_0 \exp(i\varphi) , \quad 0 \leq \varphi \leq \pi/2 , \quad (4.28)$$

and, consequently, the derivative $\partial\omega/\partial\varphi$ vanishes. Hence the sought condition for the independence of the phase shift ω of the loading angle φ is the equality of the energy release rates for the normal and the tangential loading (4.26).

The above considerations can be reversed, and it may be shown that condition (4.26) is not only sufficient but also necessary for condition $\partial\omega/\partial\varphi = 0$ to be fulfilled. Indeed, as consistent with (4.9), (4.12) and (4.18) the normalized SIF can be presented in the form

$$\hat{K} = P(\varphi) e^{i[\omega(\varphi)+\varphi]} \quad (4.29)$$

where $P(\varphi)$ is a dimensionless real valued function of the loading and the composite parameters. By using the problem linearity (4.22) and condition $\omega(0) = \omega(\frac{\pi}{2}) = \omega^*$ stipulated by (4.19), the above expression can be rewritten as

$$\hat{K} = \left[P(0) \cos \varphi + i P\left(\frac{\pi}{2}\right) \sin \varphi \right] e^{i\omega^*}. \quad (4.30)$$

Comparing the two above expressions for \hat{K} (with $\omega(\varphi) = \omega^*$), the following equivalence is obtained

$$\varphi = \tan^{-1} \left(\frac{P(\frac{\pi}{2})}{P(0)} \tan \varphi \right), \quad (4.31)$$

which can hold true for any loading direction φ only if

$$P\left(\frac{\pi}{2}\right) = P(0), \quad (4.32)$$

and, consequently, (4.26) takes place.

Thus, conditions $\partial\omega/\partial\varphi = 0$ and $\hat{G}(\pi/2) = \hat{G}(0)$ are equivalent as applied to the considered case of a crack in a periodically layered plane. Moreover, if these conditions hold true, then from (4.27) it follows that the energy rate is likewise independent of the loading angle

$$\frac{\partial\hat{G}}{\partial\varphi} = 0. \quad (4.33)$$

Hence, the normalized ERR and the phase shift angle can be independent of the loading angle only simultaneously. The established condition (4.26) is fulfilled, for example, in the case of a crack in a homogeneous plane or an interface crack between two dissimilar half-planes, but not in the general case of a layered composite.

It must be pointed out here that in the considered case of the delamination crack in the periodically layered plane, the ERR G and the normalized ERR \hat{G} have identical behavior as functions of the loading angle φ .

4.3 Energy release rate for a semi-infinite crack

Consider the case of a very fine layering, when the ratio of the cell thickness to the crack length is small. The asymptotic problem relevant here is that for a semi-infinite crack in the periodically layered space loaded by the remote apparent SIF $K^{hom} = K_I^{hom} + iK_{II}^{hom}$

with the corresponding phase angle $\varphi = \tan^{-1}(K_{II}^{hom}/K_I^{hom})$. For such a self-similar configuration the ERR at the crack tip can be derived through the remote field

$$G = G^{rem} . \quad (4.34)$$

The value G^{rem} can be determined by substituting the periodically layered composite for a transversely isotropic one with effective elastic properties obtained with the help of homogenization. This procedure is schematically depicted on Fig. 4.2. The idea was

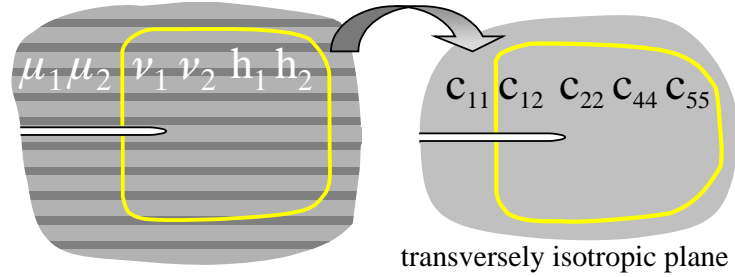


Figure 4.2: Replacement of the periodically layered plane by the homogenized continuum.

systematically employed by Ryvkin (1996, 1998, 1999), similar considerations can be found in Jha and Charalambides (1998).

The effective elastic moduli $c_{ij}^*(h_1, h_2, \mu_1, \mu_2, \nu_1, \nu_2)$, being the elements of the stiffness matrix for a transversely isotropic material can be obtained through the homogenization formulas of Postma (1955).

The fundamental results for a crack in an orthotropic homogeneous media have been obtained by Sih *et al.* (1965):

$$G = \begin{cases} (K_I^{hom})^2 \sqrt{\frac{b_{11}b_{22}}{2}} \left[\sqrt{\frac{b_{11}}{b_{22}}} + \frac{2b_{12} + b_{66}}{2b_{11}} \right]^{1/2} & \text{mode I,} \\ (K_{II}^{hom})^2 \frac{b_{11}}{\sqrt{2}} \left[\sqrt{\frac{b_{11}}{b_{22}}} + \frac{2b_{12} + b_{66}}{2b_{11}} \right]^{1/2} & \text{mode II,} \end{cases} \quad (4.35)$$

where $\{b_{ij}\}$ are the elements of the compliance matrix, which in the plane strain case are related to the elements c_{ij} of the stiffness matrix as follows

$$\begin{aligned} b_{11} &= \frac{c_{11}}{\delta}, & b_{22} &= \frac{c_{22}}{\delta}, & b_{12} &= -\frac{c_{12}}{\delta}, \\ b_{66} &= \frac{1}{c_{44}}, & \delta &= c_{11}c_{22} - (c_{12})^2. \end{aligned} \quad (4.36)$$

By substituting constants c_{ij} , for the effective elastic moduli $c_{ij}^*(h_1, h_2, \mu_1, \mu_2, \nu_1, \nu_2)$ and taking into consideration (4.15)–(4.17) and (4.34)–(4.36), the following explicit expression for the normalized energy release rate is obtained in terms of the layers parameters:

$$\hat{G} = \rho [Q_1 \cos^2 \varphi + Q_2 \sin^2 \varphi] , \quad (4.37)$$

where

$$\rho = \begin{cases} \frac{1 + \alpha}{(1 - \beta^2)(1 + 4\epsilon^2)} & \text{for interface cracks} \\ 1 & \text{for intra-layer cracks} \end{cases} \quad (4.38)$$

$$Q_1 = \left(\frac{a_1}{a_2}\right)^{1/2} \left[\left(\frac{a_1}{a_3}\right)^{1/2} + \frac{a_4}{a_3} \right]^{1/2}, \quad Q_2 = \frac{a_0}{\sqrt{2}} \left[\left(\frac{a_1}{a_3}\right)^{1/2} + \frac{a_4}{a_3} \right]^{1/2},$$

$$a_0 = (1 + \hat{h})(1 - \alpha)[1 - \alpha + \hat{h}(1 + \alpha)]^{-1}, \quad a_1 = 16\hat{h}\beta(\alpha - \beta) + a_3,$$

$$a_2 = 2(1 + \alpha)(1 - \alpha + \hat{h}(1 + \alpha))^2(1 - \alpha)^{-1}, \quad a_3 = (1 - \alpha^2)(1 + \hat{h})^2,$$

$$a_4 = 4\hat{h}\alpha^2 - \alpha^2(1 - \hat{h})^2 + (1 + \hat{h})^2 - 8\hat{h}\alpha.$$

Recall that \hat{h} is the layers thickness ratio.

Let us now apply the general relations obtained in the previous section to the considered case of semi-infinite crack. As it was noted, in the general case the ERR and the phase shift angle ω depend upon loading angle φ . Nevertheless, in order to point out those parameter combinations when ω and ERR are independent of φ , we will examine condition (4.26) as applied to (4.37). Obviously, it can be maintained only when

$$Q_1 = Q_2 . \quad (4.39)$$

Then the energy release rate becomes independent of the applied loading angle

$$\hat{G} = \rho Q_1 . \quad (4.40)$$

Inspection of formulas (4.38) indicates several cases when (4.39) and, consequently, (4.19) and (4.33) hold true. These are $\hat{h} = 0$; $\hat{h} = \infty$; $\alpha = \beta$ and $\beta = 0$. In the first two cases, the periodically layered composite degenerates to a sandwich. For $\hat{h} = 0$ one obtains

$$\hat{G} = \rho . \quad (4.41)$$

This result meets the asymptotic formula derived by Suo and Hutchinson (1989b) which relates the local and the remote stress intensity factors for a semi-infinite interface crack in a sandwich composite.

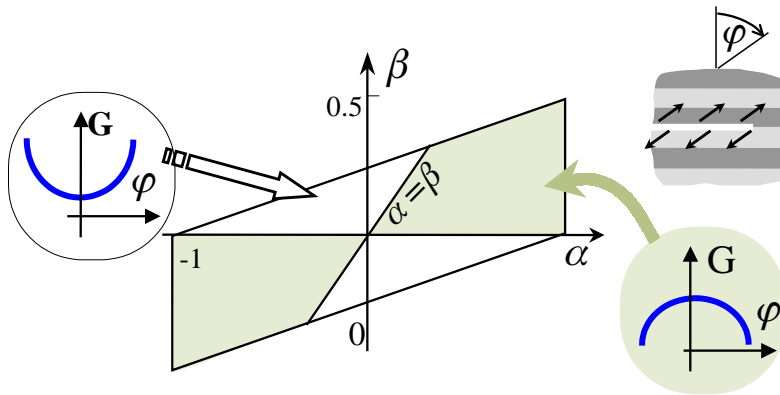


Figure 4.3: Regions in (α, β) -plane, corresponding to the different types of the ERR dependence upon the loading angle for semi-infinite cracks.

The ERR G and the normalized ERR \hat{G} have identical behavior as functions of the loading angle φ for cracks in a periodically layered plane but not in a transversely isotropic one. In the latter case, the mode I and the mode II stress intensity factors are equal, but the corresponding ERR is generally a function of φ because the ERR/SIF relation here (that can be derived from (4.35)), unlike (4.13) and (4.16), is φ -dependent. We examine here the case of periodically layered plane, consequently, all conclusions made in the previous and the present sections may be reformulated in terms of G .

By using formula (4.37) the $G(\varphi)$ -behavior for other parameter combinations can be predicted. Clearly, $\varphi = 0$ produces maximal \hat{G} if and only if $Q_1 > Q_2$ or

$$\frac{Q_1}{Q_2} = \sqrt{1 + \frac{16h\beta(\alpha - \beta)}{(1 - \alpha^2)(1 + h)^2}} > 1. \quad (4.42)$$

The latter inequality is equivalent to the simple condition $\alpha/\beta > 1$. Since it is obeyed for most known material combinations (Suga *et al.* 1988), the normal loading of long cracks in periodic composites usually corresponds to the maximum value of the ERR. Otherwise, when $\alpha/\beta < 1$, the normal loading, accordingly, produces the minimum of G . The corresponding domains in the (α, β) -plane are shown in Fig.4.3.

It is worthwhile to point out also an essential qualitative difference between the cases $\beta = 0$ and $\beta \neq 0$. In the first case the energy release for a semi-infinite crack is independent of the loading angle. On the other hand, for $\beta \neq 0$ when $Q_1 \neq Q_2$ this dependence, as can be easily verified by (4.37), is significant. Therefore, in the considered case of a semi-infinite crack in a periodic composite, the results for the relatively simple specific case $\beta = 0$ cannot be used in order to predict the fracture behavior in a general situation.

In conclusion, it should be noted, that in the case of finite length cracks, the energy release rate and the phase shift angle generally depend upon the applied loading angle. The parametric study of this dependence for interface cracks is presented in Chapter 5.

Chapter 5

Interface crack in a periodically layered plane

In this chapter a plane strain problem for an interface finite length crack in a periodically layered bi-material space is considered. The crack faces are subjected to the uniform opening tractions. The problem is quasi-periodic, consequently the solution scheme presented in Chapter 2 can be employed in an abridged form. By applying the DFT, the Green's function for a single interface dislocation in a periodically layered space without cracks is derived analytically. Using this result, the problem is then reduced to the system of two singular integral Fredholm equations of the second kind, which are solved numerically.

An extensive parametric investigation is carried out, in which the characteristics of the crack tip stress field are examined upon geometric, material and loading parameters. Obtained results confirm those of the preliminary analysis. Comparisons with known solutions for some limiting cases are made.

5.1 Derivation of the integral equation

The problem of the interface delamination in a periodically layered bi-material space is formulated in terms of Chapter 2. The space (Fig. 5.1) is viewed as an assemblage of infinite number $k = 0, \pm 1, \pm 2, \dots$ of identical bi-layered cells. The cell number 0 contains a delamination crack of length $2a$ along the inner interface. The systems of local Cartesian

coordinates are introduced in each cell in an identical manner with the x axis directed along the interface, the origin of the coordinate system in the cell number zero coincides

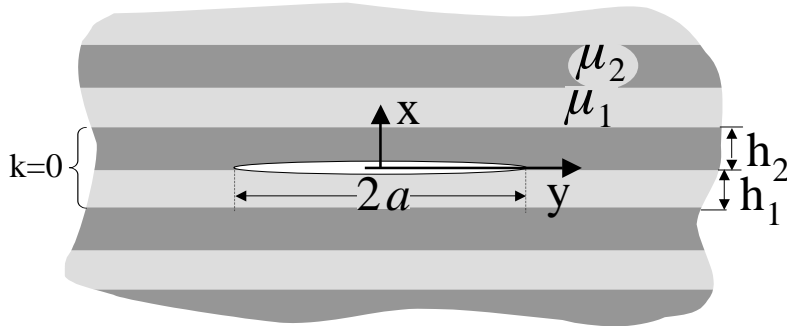


Figure 5.1: Interface crack in periodically layered space.

with the center of the crack. The displacements in the x and y directions are denoted as u_r^k and v_r^k respectively (recall that the subscript $r = 1, 2$ defines the type of the layer). The stress state is generated by the uniform opening tractions

$$\sigma_{yy}(x, 0) + i\tau_{xy}(x, 0) = -\sigma - i\tau, \quad -a < x < a \quad (5.1)$$

applied to the crack faces. The stress components are assumed to vanish at infinity. Besides the elasticity field equations (2.2) within the layers, the formulation of the considered problem includes the bonding conditions between the cells and between the layers composing a cell.

$$\mathbf{U}_1^{k+1}(x, -h_1) - \mathbf{U}_2^k(x, h_2) = 0, \quad k = 0, \pm 1, \pm 2, \dots, \quad (5.2)$$

$$\mathbf{U}_2^k(x, 0) - \mathbf{U}_1^k(x, 0) = 0, \quad k = \pm 1, \pm 2, \dots \quad (5.3)$$

$$\mathbf{U}_2^0(x, 0) - \mathbf{U}_1^0(x, 0) = 0, \quad |x| \geq a \quad (5.4)$$

$$\sigma_r^0(x, 0) + i\tau_r^0(x, 0) = -\sigma - i\tau, \quad |x| < a \quad r = 1, 2. \quad (5.5)$$

The solution of the formulated problem is obtained by following the scheme expanded in Chapter 2 with some simplifications. In order to reduce the problem to a singular integral equation, the Green's function presenting the solution of a problem for the layered non-cracked plane "loaded" by the point dislocation is sought. The boundary conditions for the corresponding problem have the following form

$$\check{\mathbf{U}}_1^{k+1}(x, -h_1, t) - \check{\mathbf{U}}_2^k(x, h_2, t) = 0, \quad (5.6)$$

$$\check{\mathbf{U}}_2^k(x, 0, t) - \check{\mathbf{U}}_1^k(x, 0, t) = \mathbf{F}(t)H(x - t)\delta_{k0}, \quad k = 0, \pm 1, \pm 2, \dots \quad (5.7)$$

Recall that $H(x)$ is the Heaviside step function and vector $\mathbf{F}(t) = \{f_1(t), f_2(t), 0, 0\}$ defines the displacement jumps across the interface with the dislocation at the point $x = t$, symbol " \smile " denotes the Green's function solution, and f_1, f_2 are the dislocation amplitudes. The stress state of this problem is not cyclic. It can be considered as a limiting case of the cyclic state with the number of cells in the cycle tending to infinity. Consequently, instead of the FDFT, the DFT (2.34) should be applied to the Green's function boundary value problem, converting it thereby into the problem for the bi-layered representative cell Ω^* (Fig. 2.3)

$$\check{\mathbf{U}}_1^*(x, -h_1, t) - e^{i\phi} \check{\mathbf{U}}_2^*(x, h_2, t) = 0, \quad (x, y) \in \Omega^* \quad (5.8)$$

$$\check{\mathbf{U}}_2^*(x, 0, t) - \check{\mathbf{U}}_1^*(x, 0, t) = \mathbf{F}(t)H(x - t). \quad (5.9)$$

All the components of the elastic field depend here upon the transform parameter ϕ because of non-standard boundary condition (5.8). The mirror symmetry of the elastic domain in the initial problem with respect to the $x = 0$ axis can be taken into account,

$$u_r^{(k)}(0, y) = 0, \quad \frac{\partial v_r^{(k)}(0, y)}{\partial x} = 0, \quad r = 1, 2, 3; \quad k = 0, \pm 1, \pm 2, \dots, \quad (5.10)$$

hence, the cases of the symmetric and the skew symmetric loading can be treated separately. In both cases the same integral equation is obtained due to the linearity of the problem, although the corresponding Green's functions differ. We introduce dislocation (2.9)-(2.10) with even normal and odd shear components

$$f_1(t) = -f_1(-t), \quad \text{and} \quad f_2(t) = f_2(-t), \quad (5.11)$$

so that the stress field corresponding to the symmetric normal and the skew-symmetric shear loading can be obtained. Consequently, the components of the stress strain state in each layer may be expressed by either sin or cos Fourier integrals satisfying the elasticity equations and including four unknown constants. In the case of the normal loading the displacements in the r -th layer, in view of the symmetry, are taken in the form

$$\begin{aligned} \check{u}_r^*(x, y, t, \phi) &= \frac{2}{\pi} \int_0^\infty \{ [A_{4r-3} + yzA_{4r-2}]e^{-yz} + [A_{4r-1} + yzA_{4r}]e^{yz} \} \sin xz \, dz, \quad (5.12) \\ \check{v}_r^*(x, y, t, \phi) &= \frac{2}{\pi} \int_0^\infty \{ [A_{4r-3} + (\kappa_r + yz)A_{4r-2}]e^{-yz} + [(\kappa_r - yz)A_{4r} - A_{4r-1}]e^{yz} \} \cos xz \, dz, \end{aligned}$$

where $\kappa_r = 3 - 4\nu_r$ and $r = 1, 2$.

By satisfying boundary conditions (5.8)-(5.9) the linear system (2.42) with right hand side vector $\mathbf{R} = \{0, 0, 0, 0, 0, 0, 0, 0, f_1(t) \cos zt, f_2(t) \sin zt, 0, 0\}$ is obtained, from which constants $A_j = A_j(z, t, \phi)$, $j = 1, 2 \dots 8$ are derived. Applying then the inverse discrete Fourier transform

$$g^{(k)} = \frac{1}{2\pi} \int_{-\pi}^{\pi} g^*(\phi) e^{-ik\phi} d\phi, \quad k = 0, \pm 1, \pm 2, \dots; \quad (5.13)$$

the expression for the Green's function is obtained in closed form as

$$\check{\mathbf{U}}_r^k(x, y, t) = \frac{1}{2\pi} \int_0^\infty \frac{1}{2\pi} \int_{-\pi}^{\pi} \check{\mathbf{U}}_r^*(z, y, t, m) e^{ik\phi_m} e^{zx} d\phi dz. \quad (5.14)$$

Note that the components of function $\check{\mathbf{U}}_r^*(z, y, t, m)$ are expressed by the linear combination of terms proportional to the dislocation amplitudes $f_1(t)$ and $f_2(t)$. In the present context, the normal and the tangential stresses $\sigma_1^0(x, 0)$ and $\tau_1^0(x, 0)$ at the interface in the cell number zero at the line corresponding to the crack are of interest. Using these stresses we will seek the dislocation distribution in the region $-a < t < a$ providing the stress boundary conditions (5.4), at the crack faces

$$\int_{-a}^a [\check{\sigma}_1^0(x, 0, t) + i\check{\tau}_1^0(x, 0, t)] dt = -\sigma - i\tau. \quad (5.15)$$

where $\check{\sigma}_1^0(x, 0, t) \equiv \check{\sigma}_1^0(x, 0)$ and $\check{\tau}_1^0(x, 0, t) \equiv \check{\tau}_1^0(x, 0)$ are the obtained stress components of the Green's function. After extracting singular parts of these equations and some identical transformations expounded by Erdogan and Gupta (1971b), two singular integral equations of the second kind are obtained. These equations are to be used simultaneously with restriction (2.11) for determining the dislocation amplitudes $f_i(t)$. In the same way as in Chapter 2, they are combined into one complex integral equation in terms of the unknown dislocation density $f(t) = f_1(t) + if_2(t)$

$$\frac{1}{\pi i} \int_{-1}^1 \frac{f(t) dt}{t-x} - \beta f(x) + \int_{-1}^1 [f(t) K_1(t, x) + \overline{f(t)} K_2(t, x)] dt = p, \quad (5.16)$$

where

$$K_l(t, x) = \int_0^\infty [k_{l1} \cos z(t-x) + ik_{l2} \sin z(t-x)] dz, \quad (5.17)$$

$$k_{lm} = \frac{1}{\pi} \int_0^\pi \frac{e_{lm}^0 + e_{lm}^1 \cos \phi + e_{lm}^2 \cos 2\phi}{d_0 + d_1 \cos \phi + d_2 \cos 2\phi} d\phi, \quad k_{21} \equiv 0, \quad (5.18)$$

$$p = \frac{(\mu_2 - \mu_1)(1 - \beta^2)}{2\mu_1\mu_2(\alpha - \beta)} (i\sigma - \tau), \quad l = 1, 2; \quad m = 1, 2 \quad (5.19)$$

Expressions for the coefficients e_{lm}^j, d_j are presented in Appendix A.3. The integration in (5.18) has been carried out analytically, but the final expressions are not exhibited for the sake of brevity. In the limiting case $h_2 \rightarrow \infty$ when the periodically layered composite turns into the three layered sandwich, the obtained integral equation coincides with the equation derived for the latter problem by Erdogan and Gupta (1971b).

5.2 Solution of the singular integral equation

The solution method for the integral equations of the considered type is a well developed procedure (Erdogan and Gupta, 1971b; Erdogan, 1969; and Karpenko, 1966). The fundamental solution of the dominant homogeneous part of integral equation¹ (5.16) is given to within a constant multiplier by function $w(x)$

$$w(x) = (1-x)^\eta(1+x)^\zeta, \quad \eta = -0.5 + i\epsilon, \quad \zeta = -0.5 - i\epsilon, \quad (5.20)$$

which is the weight function of the Jacobi polynomials $P_n^{\eta, \zeta}(x)$. Consequently, the complex dislocation density is sought in the form of the Jacobi polynomial series expansion

$$f(t) = \sum_{n=0}^{\infty} c_n w(t) P_n^{\eta, \zeta}(t), \quad (5.21)$$

with the first coefficient put to zero ($c_0 \equiv 0$), in order to satisfy stipulation (2.11). After substituting series expansion (5.21) of $f(t)$ into the integral equation (5.16), the integration of the singular term is carried out by the use of relation (Karpenko, 1966)

$$\frac{1}{2\pi} \int_{-1}^1 w(t) P_n^{\eta, \zeta}(t) \frac{dt}{t-x} - \beta w(x) P_n^{\eta, \zeta}(x) = \frac{\sqrt{1-\beta^2}}{2i} P_{n-1}^{-\eta, -\zeta}(x), \quad |x| < 1, \quad (5.22)$$

The integral equation, therefore, takes the form

$$\begin{aligned} \sum_{n=1}^{\infty} \left[c_n \frac{\sqrt{1-\beta^2}}{2i} P_{n-1}^{-\eta, -\zeta}(x) + \int_{-1}^1 [c_n w(t) P_n^{\eta, \zeta}(t) K_1(t, x) + \overline{c_n w(t) P_n^{\eta, \zeta}(t)} K_2(t, x)] dt \right] \\ = p, \quad |x| \leq 1, \end{aligned} \quad (5.23)$$

where the upper bar denotes the complex conjugation. Expansion of the kernels into the series of Jacobi polynomials

$$K_l(t, x) = \sum_{k=0}^{\infty} X_{lk} P_k^{-\eta, -\zeta}(x), \quad l = 1, 2 \quad (5.24)$$

$$X_{lk} = \frac{1}{\theta_k(-\eta, -\zeta)} \int_{-1}^1 K_l(t, x) w(x)^{-1} P_k^{-\eta, -\zeta}(x) dx \quad (5.25)$$

¹the dominant homogeneous part of (5.16) is obtained by setting K_1, K_2 and p equal zero.

with $\theta_k(\eta, \zeta)$ defined by

$$\theta_k(\eta, \zeta) = \int_{-1}^1 w(x) \left(P_k^{\eta, \zeta}(x) \right)^2 dx = \frac{2^{\eta+\zeta+1}}{2k + \eta + \zeta + 1} \frac{\Gamma(k + \eta + 1)\Gamma(k + \zeta + 1)}{k!\Gamma(k + \eta + \zeta + 1)}; \quad (5.26)$$

where $\Gamma(x)$ is the Gamma function, yields an infinite system of linear algebraic equations in terms of the unknown expansion coefficients c_n . By truncating the series, the following system of N^* algebraic equations is obtained

$$\frac{\sqrt{1 - \beta^2}}{2i} \theta_k(-\eta, -\zeta) c_{k+1} + \sum_{n=1}^{N^*} d_{kn}^1 c_n + \sum_{n=1}^{N^*} d_{kn}^2 \bar{c}_n = p \theta_0(-\eta, -\zeta) \delta_{k0}, \quad (5.27)$$

$$k = 0 \dots N^* - 1.$$

Function $\theta_k(-\eta, -\zeta)$ can be calculated by the following recurrent formula

$$\theta_k(-\eta, -\zeta) = \frac{2\Gamma(k + 1.5 - i\epsilon)\Gamma(k + 1.5 + i\epsilon)}{((k + 1)!)^2} = \frac{2\pi(\frac{1}{4} + \epsilon^2) \dots (k(k + 1) + \frac{1}{4} + \epsilon^2)}{((k + 1)!)^2 \cosh \epsilon\pi}. \quad (5.28)$$

and coefficients d_{kn}^j , $j = 1, 2$ are given by

$$d_{kn}^1 = \int_{-1}^1 w(x)^{-1} P_k^{-\eta, -\zeta}(x) \int_{-1}^1 w(t) P_n^{\eta, \zeta}(t) K_1(t, x) dt dx$$

$$d_{kn}^2 = \int_{-1}^1 w(x)^{-1} P_k^{-\eta, -\zeta}(x) \int_{-1}^1 \overline{w(t) P_n^{\eta, \zeta}(t)} K_2(t, x) dt dx \quad (5.29)$$

Having determined the dislocation distribution one can find all the components of the stress-strain state using the Green's functions. The complex stress intensity factor defined by (4.5) is expressed in terms of coefficients c_n of the dislocation density expansion as follows (Erdogan and Gupta, 1971b):

$$K = 2^{-i\epsilon} i p^{-1} \sqrt{\pi(1 - \beta^2)} \sum_{n=1}^N c_n P_n^{\eta, \zeta}(1). \quad (5.30)$$

5.3 Numerical results

The analytical expressions for the kernels are rather cumbersome but since they are decreasing exponentially in z the obtained solution is convenient for numerical evaluation and parametric study. Convergence problems appear only when ratio h_m/a , where $h_m = \min\{h_1, h_2\}$, defining the speed of decrease of the integrands becomes very small.

5.3.1 Influence of the material mismatch

The issue to be considered first is the dependence of the considered fracture characteristics upon the material properties of the composite constituents. For the considered case of bi-material composite with the stress boundary conditions, as is well known, this dependency is completely defined by the two Dundurs' elastic mismatch parameters. In the paper of Suo and Hutchinson (1989b), it was noted that parameter α is a more important characteristic of the material dissimilarity than β . Therefore, the normalized ERR \hat{G} as a function of α is investigated.

The $\hat{G}(\alpha)$ graphs for different ratios $h_2/h_1 = 1, 0.5, 0.1, 0.02$ are presented in Fig.5.2a. Values $\alpha < 0$ correspond to the case when the thinner layers are the soft ones, except for the symmetric case of equal thicknesses. Pure normal loading $\varphi = 0$ with $\beta = 0$ and $a/h_2 = 100$ is considered. In the limiting case $h_2/h_1 \rightarrow 0$, the periodic composite becomes a three layered one with two similar layers of infinite thickness. If, in addition, the crack length far exceeds the thickness of the middle layer i.e. $h_1/a \ll 1$, the case of the sandwich with a semi-infinite interface crack emerges. For this case, in view of $\beta = 0$, it follows from (4.41) and (4.38) that $\hat{G}(\alpha) = 1 + \alpha$. The corresponding graph (dashed line) is presented in Fig. 5.2a for comparison. Recall, that in accordance with the accepted normalization (4.15) the normalized ERR, in the considered case $\beta = 0$, equals the squared absolute value of the normalized SIF: $\hat{G} = |\hat{K}|^2$.

Before discussing these results let us recall the influence of the materials mismatch on the fracture characteristics in Mode III. Chen and Sih (1971) considered the antiplane deformation of a four layered composite consisting of two half-spaces and two layers. In the case of an interface crack located at the midplane of the symmetric bi-material composite they found that for any shear modulus ratio, the SIF for the interface crack is always less than the corresponding value for the crack in a bulk material (note that the stress intensity factors for Mode III cracks in a bulk material and at the interface between two dissimilar half spaces are equal). This led the authors to the general conclusion that layered composites help to reduce singular stresses near the crack tip. However, for the case of the Mode III interface crack in a periodically layered composite (Ryvkin, 1998), it appeared that this is true only for that specific case, when the layers of both types have the same thickness.

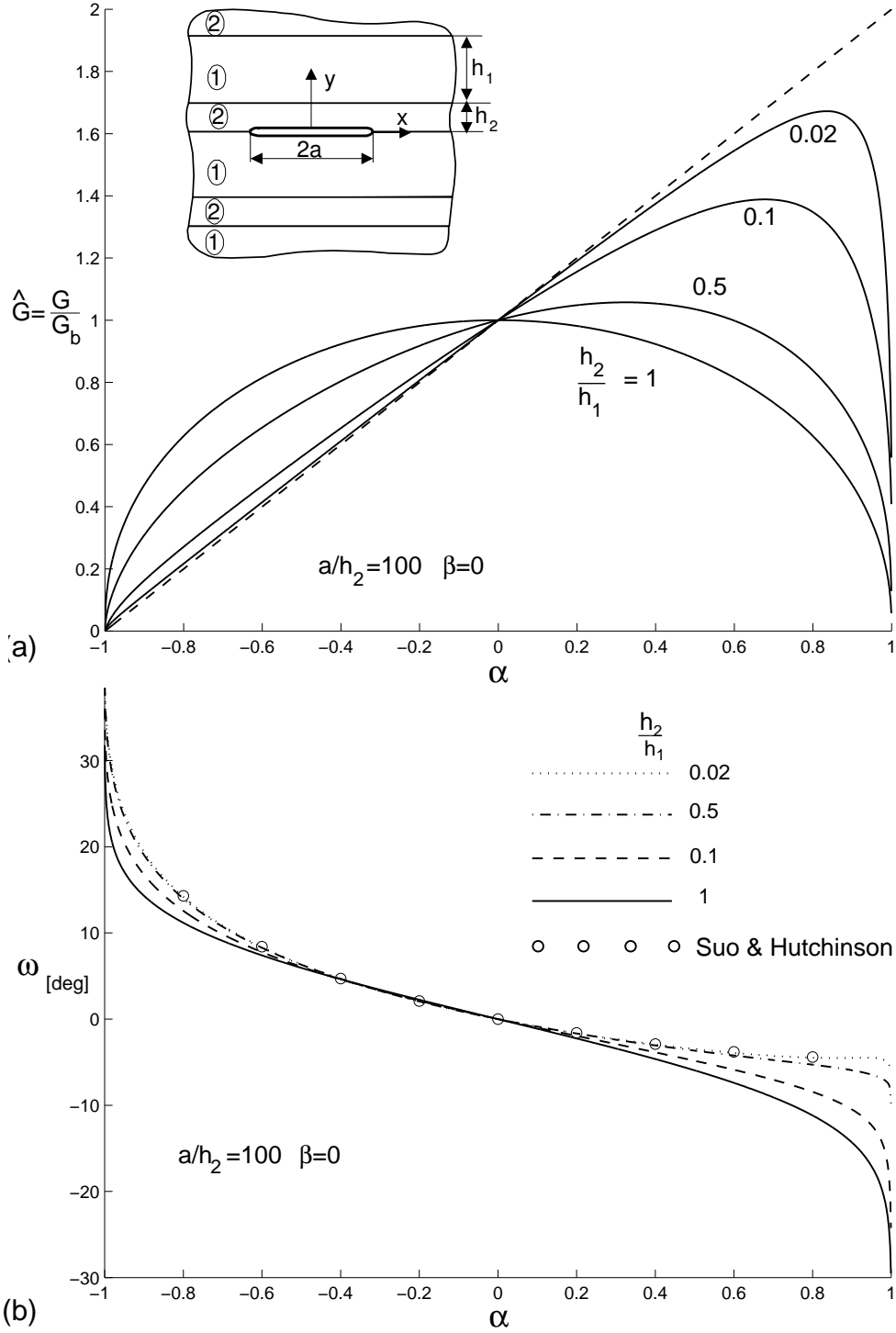


Figure 5.2: Energy release rate (a) and phase shift angle (b) vs. elastic mismatch parameter α for $a/h_2 = 100$ and $\beta = 0$.

The results presented in Fig. 5.2a are in complete agreement with the latter finding. Namely, only when $h_2/h_1 = 1$, the energy release for the interface crack in periodic composites is always less than G_b in the corresponding problem of the same crack between two dissimilar half planes. For all other thickness ratios the energy release is below G_b when the thin layers are the more compliant ones ($\alpha < 0$). In the opposite situation, when the thin layers are stiffer, the energy release can be higher or lower than G_b and behaves non-monotonically, approaching some maximum. This phenomenon will be analyzed here in details.

Increase of α corresponds to the stiffening of the thinner layers compared to the thicker ones. In the considered case the thinner layers are the more compliant ones when $-1 < \alpha < 0$ and the stiffer ones when $0 < \alpha < 1$. When $\alpha = 0$ the elastic properties of the composite constituents coincide and, consequently, $\hat{G} = 1$.

For negative α the general trend observed for periodic composites is the same as for the sandwich. Namely, the SIF monotonically increases with the rise of the thin layer stiffness while its value is less than unity as a result of the so-called elastic shielding effect (Fleck *et al.*, 1991). Clearly, for very thin compliant layers ($h_2/h_1 = 0.02$ and $\alpha < 0$) only the single layer near the interface is relevant, therefore the results are, in fact, the same as for the semi-infinite crack in the sandwich (dashed line).

When the thin layers are very stiff, as can be seen from the right part $\alpha > 0$ of Fig.5.2a, the deviation from the sandwich limit may be significant. The curve for the case of equal thicknesses $h_2/h_1 = 1$ is symmetric with respect to the axis $\alpha = 0$ owing to the symmetry of the problem. Therefore, the normalized ERR for an interface crack will always be less than that for the crack in a homogeneous material. On the other hand, for the sandwich composite, a monotonic enlargement of \hat{G} with increasing α , i.e. with increasing stiffness of the sandwiched layer is observed, which may be referred to as the inverse shielding effect. For layered composites this effect is interfered with an opposite trend induced by the restriction of the displacements due to the presence of stiff layers. For $\alpha = 1$ when the stiffness of these layers becomes infinite we obtain, as in case $\alpha = -1$, the problem for a strip with clamped edges. As a result, the behavior of \hat{G} (and, hence, $|\hat{K}|$) is found to be non-monotonic.

Thus, if we increase stiffness of the thinner layers in a periodic composite it may lead not only to increasing but also to decreasing of the singular stresses in front of the crack

tip. Consequently, for some parameter combination, the SIF reaches its maximum. For given materials, the magnitude of this maximum increases with the rise of the difference in layers thicknesses and can appreciably exceed the corresponding value for the crack in homogeneous material.

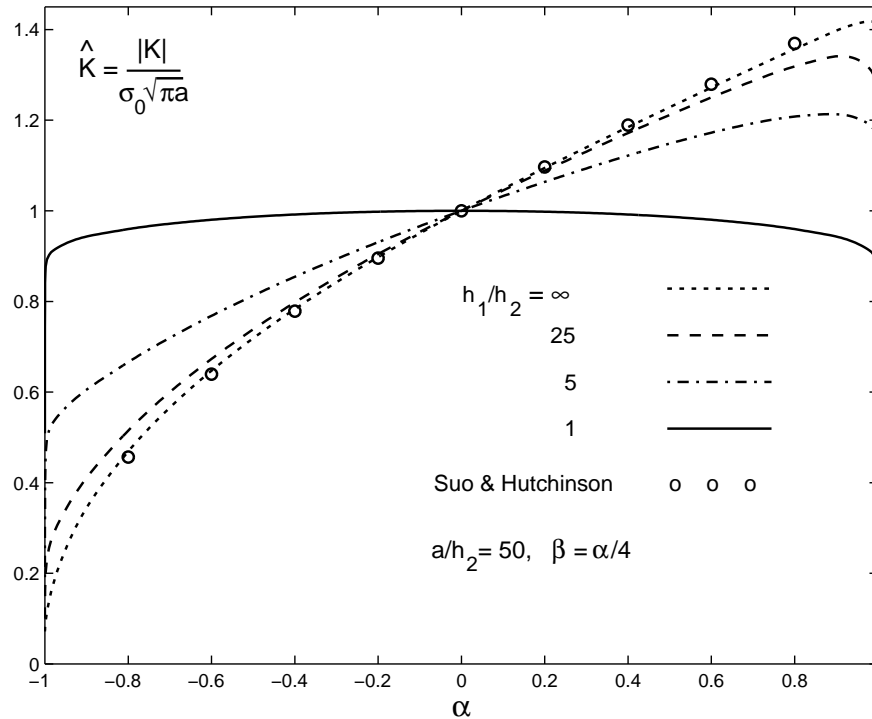


Figure 5.3: Normalized absolute value of the SIF vs. elastic mismatch parameter α for $a/h_2 = 50$ and $\beta = \alpha/4$

The dependence of the phase shift angle ω upon α is depicted in Fig. 5.2b. Note, that for the considered case of normal loading $\varphi = 0$ and elastic mismatch with $\beta = 0$, there is no oscillating singularity and $\omega = \psi = \tan^{-1}(K_2/K_1)$. The curve for the case of equal thicknesses $h_2/h_1 = 1$ is skew-symmetric in accordance with the symmetry of the problem. For other cases, it is seen that the influence of the thickness ratio on the absolute value of the shift angle for $\alpha < 0$ and $\alpha > 0$ is opposite. Namely, when the thinner layers are more compliant, then the decrease of their thickness leads to increasing $|\omega|$ and for the case of thin stiff layers $|\omega|$ diminishes. Consequently, the case of thin compliant layers is characterized usually by larger values of the phase shift angles in comparison to the case when the thinner layers are stiffer. A similar conclusion was reached by Suo and Hutchinson (1989b) for a semi-infinite crack in a sandwich composite. Their results are

presented in Fig. 5.2b for comparison. As will be demonstrated further in the case of non-zero loading angles φ , the mentioned features of the phase shift behavior are not present when the crack is not sufficiently long.

In order to clarify the influence of the elastic mismatch on the singular stress field in the case $\beta = \alpha/4$, which is a good approximation for many engineering materials (Fleck *et al.*, 1991), we examine the absolute value $|\hat{K}|^2$ of the normalized SIF (4.7). The dependence of $|\hat{K}|$ upon α is illustrated in Fig.5.3.

Three thickness ratios $h_1/h_2 = 1, 5, 25$ are considered, i.e. the layers of the first type are thicker than the layers of the second type. The curve corresponding to the sandwich composite ($h_1/h_2 = \infty$) is depicted for reference. The ratio of the crack length to the thinner layers thickness is now fixed and relatively large $a/h_2 = 50$. Therefore the results for the sandwich composite are very close to those obtained from the asymptotic formula for a semi-infinite crack derived by Suo and Hutchinson (1989b). In the limiting case $\alpha \rightarrow -1$ when the stiffness of the thick type 1 layers tends to infinity, their thickness becomes irrelevant, and we obtain the problem for the elastic strip of thickness h_2 with delamination crack along one of its clamped edges. Consequently, \hat{G} as well as $|\hat{K}|$ approaches the same minimum value for all thickness ratios. Comparing Fig.5.3 and Fig. 5.2a, one can see that all trends pertaining the case $\beta = 0$ are also actual in the present more common situation.

5.3.2 Fineness of the layering

In the problem on a crack in the periodically layered space, the relative crack length a/h may be considered as the fineness of the layering. In order to examine the dependence of the fracture characteristics upon parameter h_m/a , $h_m = \min[h_1, h_2]$, the layered space with significant elastic mismatch of the constituents, specified by $\alpha = 0.8$ and $\beta = 0.2$ is considered. The graphs for the normalized ERR \hat{G} and the phase shift ω (in view of normal loading $\omega = \psi$) upon the normalized crack length parameter h_m/a are presented in Fig. 5.4a and Fig. 5.4b, respectively. The results for periodically layered composites are exhibited in a broad range of the thickness ratio h_2/h_1 from thin stiff to thin compliant layers, including the limiting cases of corresponding sandwiches (the dashed lines). The results for a semi-infinite interface crack in the sandwich, obtained

by Suo and Hutchinson (1989b) and denoted by asterisks on the ordinates, match the

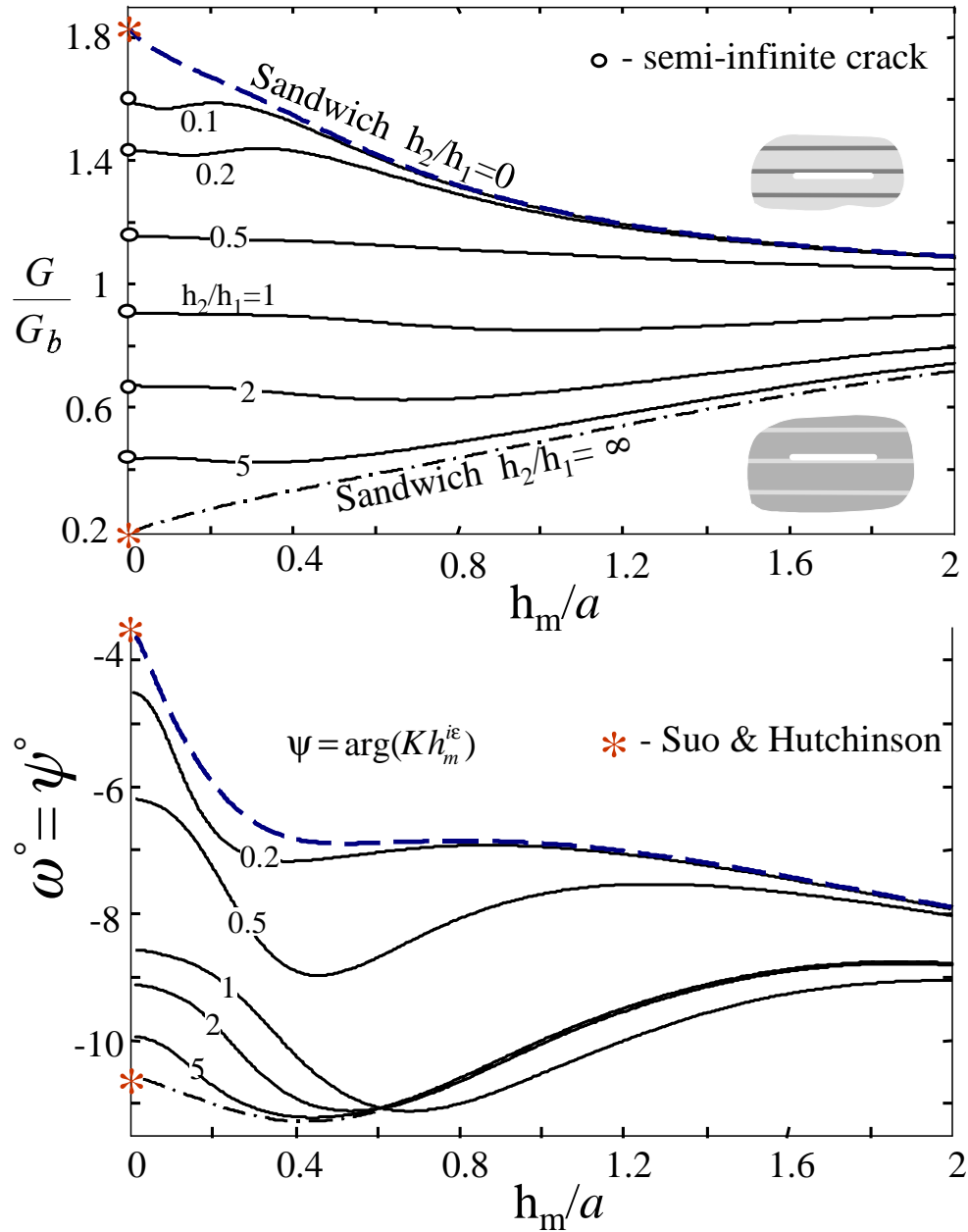


Figure 5.4: Normalized ERR and phase shift ω vs. normalized crack length parameter h_m/a ($h_m = \min[h_1, h_2]$) for normal loading $\varphi = 0$. Elastic mismatch is specified by $\alpha = 0.8$ and $\beta = 0.2$. The curve numbers are the values of the thickness ratio h_2/h_1 .

obtained numerical data. Asymptotic values for $h_m/a \rightarrow 0$ calculated by the use of the analytic formula for the semi-infinite crack (4.37) are denoted by circles.

It is seen from Fig. 5.4a that when different layers have thicknesses of the same order, the ERR is weakly affected by the crack length. When the thickness ratio varies in range $0.2 < h_2/h_1 < 5$, for long cracks ($h_m/a < 0.4$) accuracy of approximation by the semi-

infinite crack asymptote is better than 4%. On the other hand, for the thickness ratio $h_2/h_1 < 0.1$, the sandwich approximation can be employed with less than 1% error for the cases when $h_m/a > 0.4$. The same accuracy is achieved for combination $h_2/h_1 = 0.2$ and $h_m/a > 0.9$. An inverse sandwich (with compliant film) asymptotic produces some larger error for corresponding thickness ratios. Finally, it can be noted that for considered elastic mismatch there is an interval of the thickness ratio variation somewhere within $1 < h_2/h_1 < 0.5$, such that ERR can be approximated in the whole range of the crack length rather accurately by solution (4.14) (Rice and Sih, 1965) for the crack between two dissimilar half-planes. Corresponding asymptotic for normalized ERR is line $\hat{G} = 1$.

Study of the phase angle behavior (Fig. 5.4b) allows to draw similar conclusions regarding the sandwich approximations. The obtained results meet the short crack asymptotic $\omega = \tan^{-1}(2\epsilon)$ derived from the solution (4.14) of Rice and Sih (1965), which for $\beta = 0.2$ is found to be $\omega = -7.35^\circ$.

5.3.3 Influence of the geometry and the loading direction

The analysis performed in Section 4.2 helps to examine the effect of the loading angle φ and the geometry of the problem on the fracture characteristics. The results are visualized as 3D graphs $\hat{G}(\varphi, h_m/a)$ and $\omega(\varphi, h_m/a)$ (recall that $h_m = \min\{h_1, h_2\}$). The case of materials with a significant elastic mismatch, $\alpha = 0.8$ and $\beta = 0.2$ is considered.

It is worthwhile to present first the results for two sandwich composites with a compliant (Fig. 5.5a) and a stiff (Fig. 5.5b) middle layer. As it has been shown in Section 4.2, the ERR is an even function of the loading angle, hence the surfaces are symmetric with respect to the plane $\varphi = 0$. It is seen that for a given ratio h_m/a , this value always corresponds to the minimum energy release for the case of the compliant layer and to the maximum when the layer is stiff. For a sufficiently short crack $h_m/a \gg 1$ the case of two bonded half planes (Rice and Sih (1965)) is approached asymptotically, the dependence upon φ disappears and $\hat{G} \rightarrow 1$. In the opposite limiting case of a semi-infinite crack $h_m/a \rightarrow 0$ (Suo and Hutchinson, 1989b), the 3D surfaces for both sandwiches also approach a straight lines, as was predicted in Section 4. The limiting values of \hat{G} are derived from (4.41), (4.38) and found to be 0.205 and 1.844 for the cases of the compliant and the stiff layer, respectively.

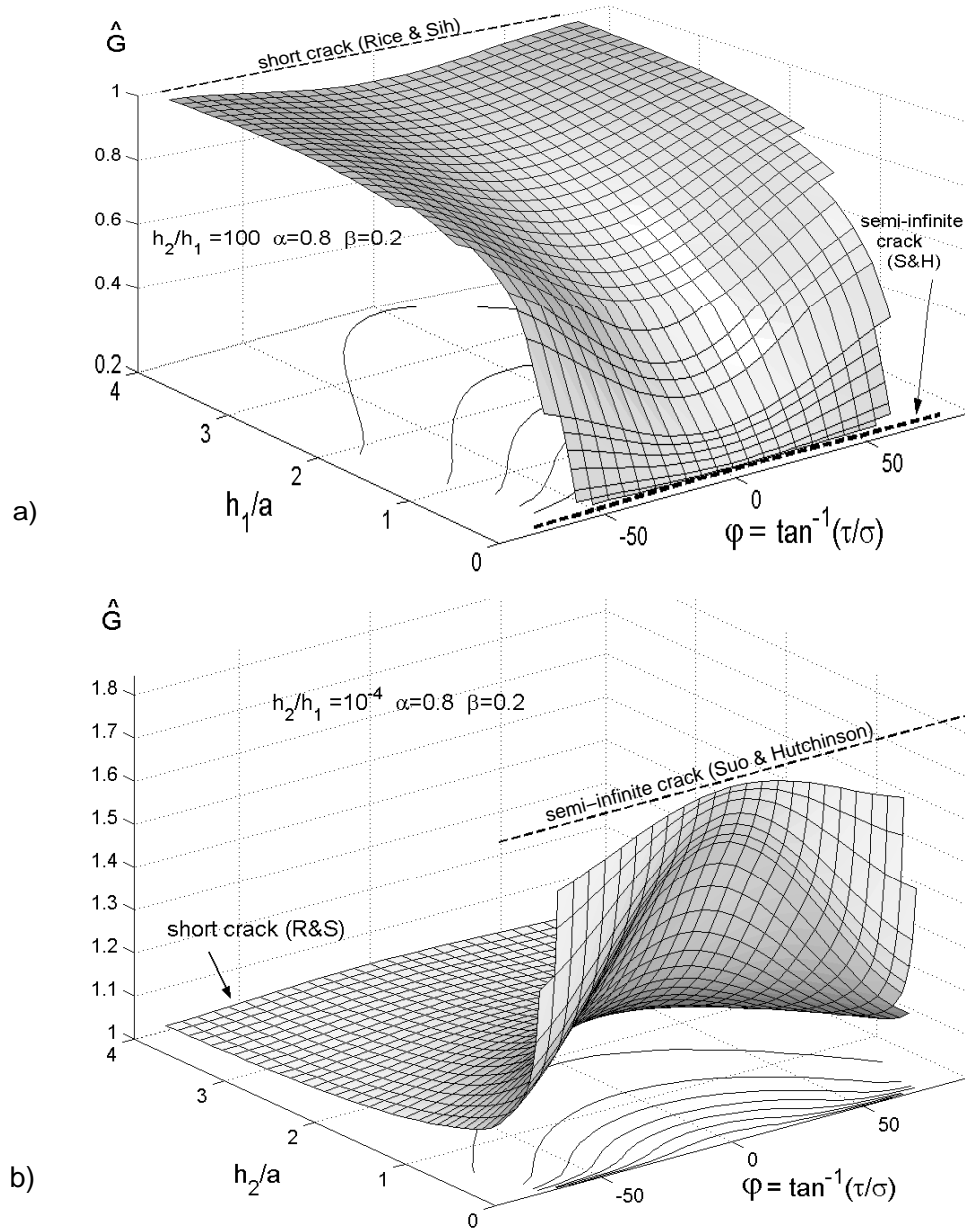


Figure 5.5: ERR vs. relative crack length $\min\{h_1, h_2\}/a$ and loading angle φ for the sandwich with a compliant layer a), sandwich with a stiff layer b) and the periodic composite c).

For periodically layered composites with $h_2/h_1 = 1$, ERR behavior significantly different from that in the sandwich cases is observed in Fig. 5.5c. For the short cracks ($h_1/a < 0.67$), the normal loading $\varphi = 0$ produces the minimum of the ERR, while for $h_1/a > 0.67$ it yields the maximum. The limit for the semi-infinite crack is not a straight line but a curve defined by (4.37). The relation $\alpha/\beta > 1$ takes place, accordingly, the curve is concave, and the observed behavior of the ERR is in complete agreement with the preliminary findings obtained analytically in Sections 4.2 and 4.3. It is seen also

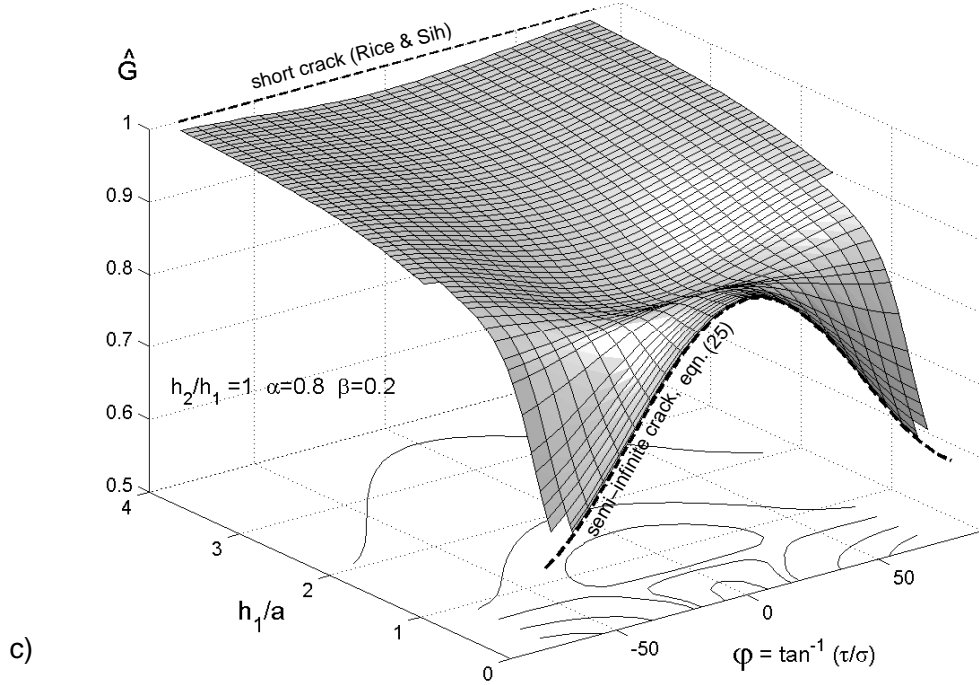


Figure 5.5: continued

that when $h_m/a \rightarrow 0$, the derivative $\partial \hat{G} / \partial (h_m/a)$ for the periodic composite is significantly less than for the corresponding sandwiches. Consequently, the semi-infinite crack asymptote (4.37) can be employed in a relatively broad range of the crack lengths.

The influence of parameter β , as was pointed out in Chapter 4, cannot be disregarded when the crack is long. In order to illustrate this fact, the \hat{G} graphs for the periodic composite with thickness ratio $h_2/h_1 = 0.2$ and material mismatch $\alpha = 0.8$ for the cases $\beta = 0$ and $\beta = 0.2$ are presented in Fig. 5.6. Large gradients in the h_2/a direction are observed when crossing over from the moderate crack length region (where the influence of β is weak), to the one of long cracks. The limiting straight line defined for $\beta = 0$ by (4.37) replaces the concave curve in Fig. 5.5c for $\beta = 0.2$. The observed behavior of

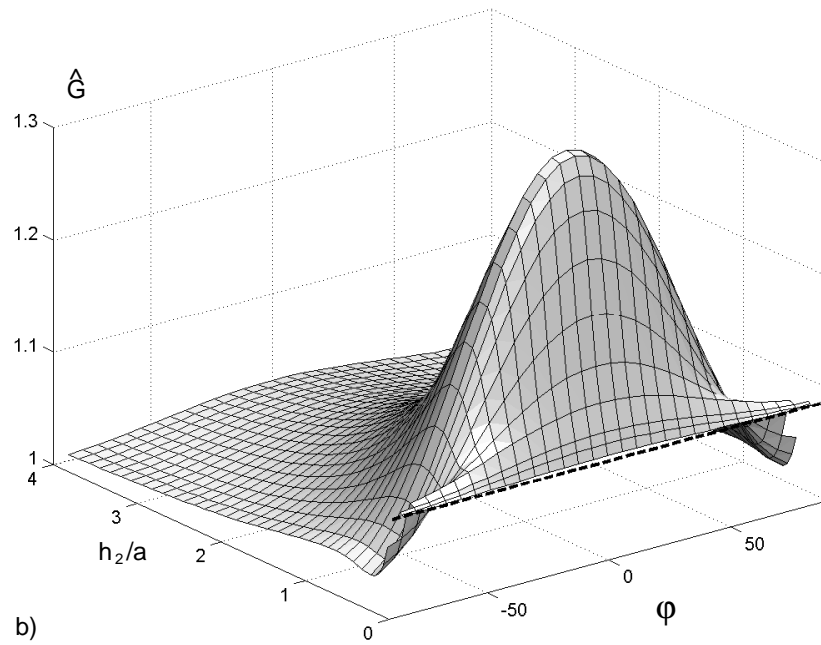
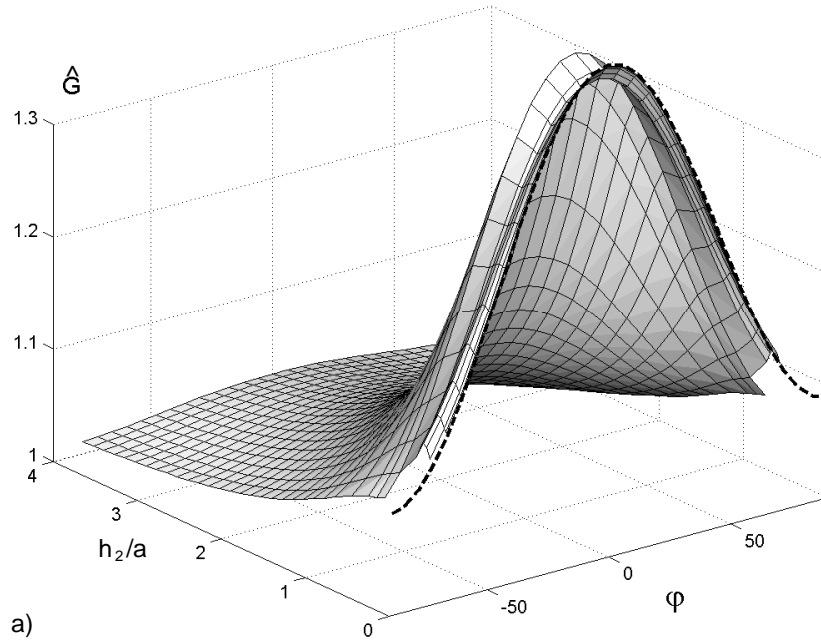


Figure 5.6: Normalized ERR vs. relative crack length h_2/a and loading angle φ , for thickness ratio $h_2/h_1 = 0.2$ and elastic mismatch $\alpha = 0.8$ with $\beta = 0$ a) and $\beta = 0.2$ b).

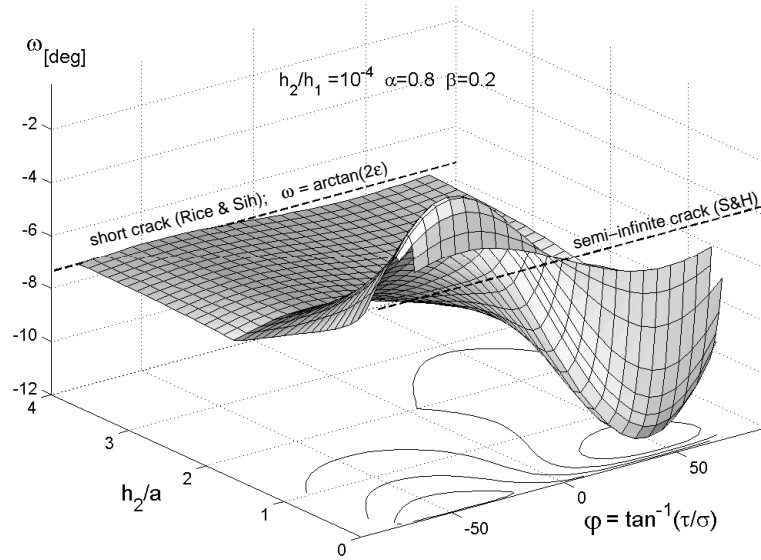


Figure 5.7: Real phase angle vs. relative crack length h_m/a and applied loading angle φ for the sandwich composite with elastic mismatch $\alpha = 0.8$, $\beta = 0$.

the ERR indicates that for long cracks the case $\beta = 0$ cannot be used for the fracture behavior prediction for the periodic multilayers with β distinctly different.

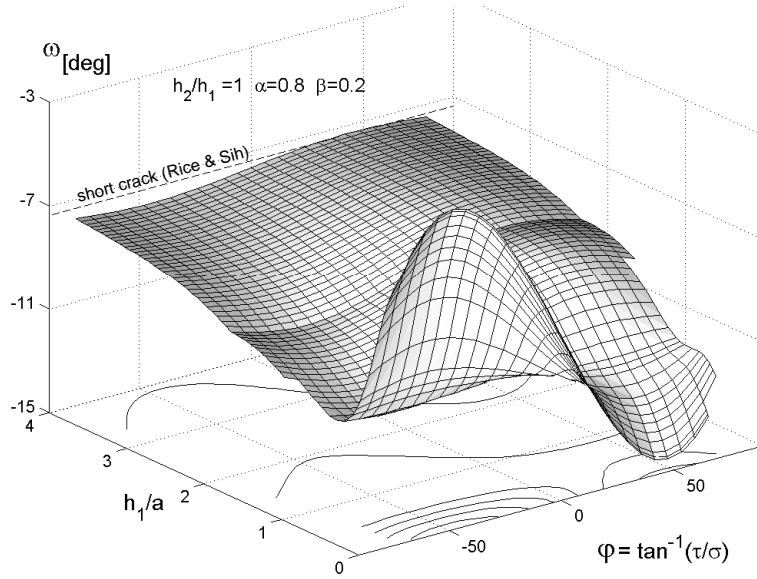


Figure 5.8: Real phase angle vs. relative crack length h_m/a and loading angle φ for the periodically layered composite with thickness ratio $h_2/h_1 = 1$ and elastic mismatch $\alpha = 0.8$, $\beta = 0$.

The behavior of the phase shift angle $\omega(\varphi, h_m/a)$ is illustrated in Figures 5.7 and 5.8. Using (4.20), it is possible to show that the skew symmetry condition

$$\omega(0, h_m/a) = \frac{1}{2}[\omega(\varphi, h_m/a) + \omega(-\varphi, h_m/a)] \quad (5.31)$$

is obeyed. The numerical results meet this stipulation. The jump in the derivative

$\partial\hat{G}/\partial(h_m/a)$ for $h_m/a = 2$ is a result of a change in the length parameter \hat{L} chosen in accordance with (4.10). This enables presentation of the two limiting cases $h_m/a \rightarrow \infty$ and $h_m/a \rightarrow 0$ compatible with the numerical data on the same graph.

For the sandwich composite (Fig. 5.7), both limits are the straight lines. In the first case, this is line $\omega = -7.35^\circ$ defined by the short crack asymptotic $\omega = \tan^{-1}(2\epsilon)$ derived from (4.14) for $\beta = 0.2$. The second limit for the long cracks is in agreement with the result of Suo and Hutchinson (1989b). It can be noted that the behavior of the phase shift for $h_m/a \ll 1$ is characterized by the relatively large gradients. This indicates that employing the asymptotic results obtained in the mentioned paper, for the considered case of large materials mismatch, must be done very carefully.

For the semi-infinite crack in a periodic composite (curve $h_1/a = 0$ in Fig. 5.8), the phase shift, in contrast to the sandwich case, depends upon the loading angle as predicted in Section 4.2. Similar behavior of the phase shift for the case of the non-interface semi-infinite crack in a periodically layered composite was reported by Jha and Charalambides (1998).

Inspecting behavior of the ERR presented earlier in Fig. 5.5c, one can note that except the marginal case $h_1/a \rightarrow \infty$, there is an additional value h_1/a , for which the ERR does not depend upon the loading angle φ . This phenomenon, i.e. existence of some combination of geometric and elastic parameters of the periodic composite, for which the energy release rate and, consequently, the phase shift angle are independent of the loading direction, is illustrated in Fig. 5.9. The fracture characteristics are considered as functions of the parameter h_2/h for the fixed ratio of the cell thickness to the crack length of $h/a = 2$. Families of graphs for different loading angles with $\alpha = 0.8$ and $\beta = 0$ are presented. They have three intersection points. Two limiting cases $h_2/h \rightarrow 0, 1$ correspond to the sandwich composites, consequently, all the curves approach the same values obtained in the asymptotic analysis by Suo and Hutchinson (1988b). The third intersection point is observed only when the crack is not too long in comparison with the cell thickness. For example, in the case $h/a = 0.5$ for the same material mismatch $\alpha = 0.8$ and $\beta = 0$, there is no intermediate intersection point (Fig. 5.10).

A comparison of the graphs for the phase shift angles presented in Fig.5.2b and Fig. 5.9b provides an additional example of the crack length influence on the qualitative effects. As was mentioned earlier, for long cracks (Fig.5.2b), diminishing the thickness of

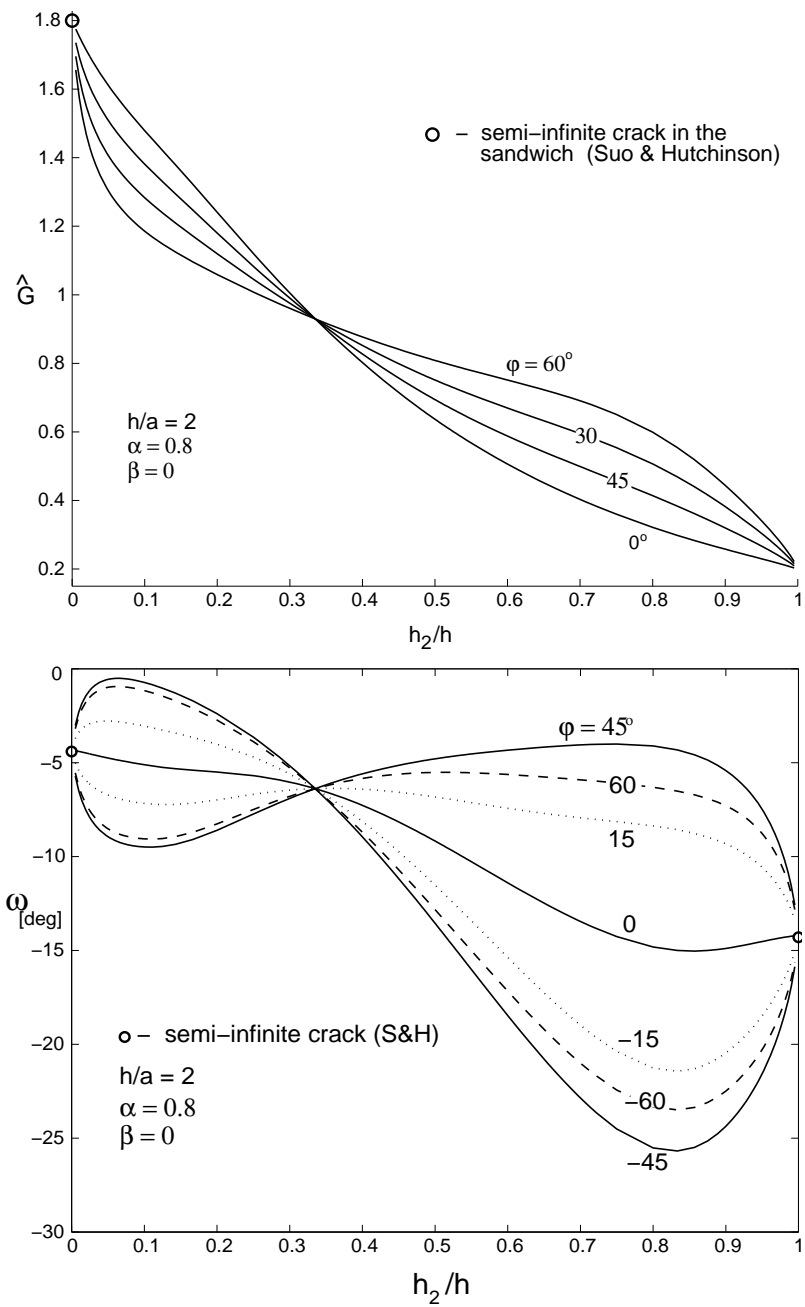


Figure 5.9: Energy release rate (a) and real phase angle (b) vs. volume fraction h_2/h for short cracks with $h/a = 2$.

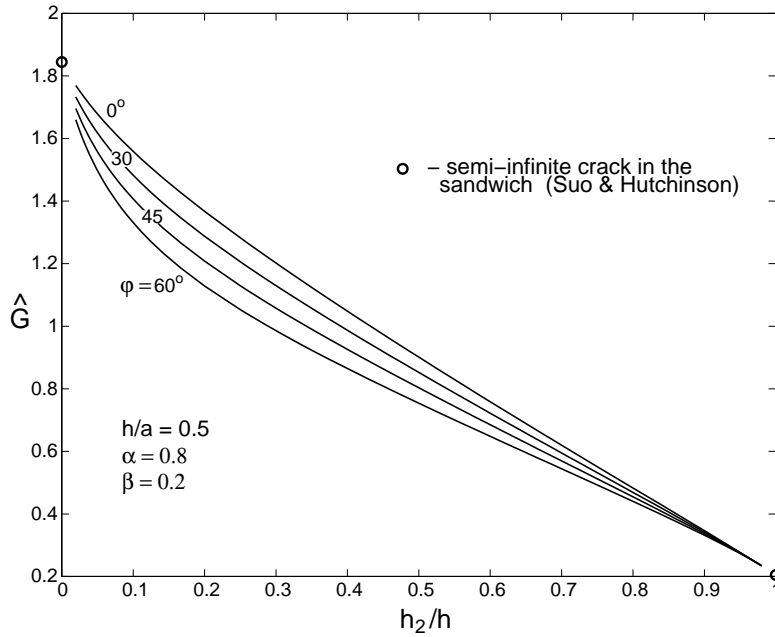


Figure 5.10: Energy release rate vs. volume fraction h_2/h for the long cracks with $h/a = 0.5$.

the more compliant (stiffer) layers increases (decreases) absolute value $|\omega|$ of the phase shift. On the other hand, for relatively short cracks (curve $\varphi = 0$ in Fig. 5.9b), this does not occur. The results for other loading angles for the short cracks (Fig. 5.9b) confirm the general trend that thin compliant layers correspond to the larger shift angles than the thin stiff ones. However, in contrast to the case of long cracks, there are some parameter combinations when this is not true (see, for example, cases $h_2/h = 0.1$ and $h_2/h = 0.9$ for $\varphi = 45^\circ$).

5.4 Conclusions

The singular stress field for an interface delamination crack in a periodically layered composite has been examined. Phenomena different from the known results for the simpler models of three layered sandwich composites have been observed. In particular, it appeared that the ERR and the real phase angle depend upon the direction of the applied loading. The ERR is an even function of φ and, consequently, it has an extremum at $\varphi = 0$ corresponding to the pure normal loading. For most material combinations in periodic multilayers this extremum is found to be maximum for the semi-infinite and, consequently, for sufficiently long cracks and minimum for the short ones. There is a

borderline case of specific parameter combination when the ERR together with the real phase angle is independent of the direction of the applied loading. The above phenomena is not observed in sandwiches, where the above extremum is always maximum (minimum) for the case of a stiffer (more compliant) middle layer.

It was found that in a periodic bi-material composite, only when the layers of both types have the same thickness, the ERR is always smaller than that in the corresponding reference problem of a crack between two dissimilar half planes. The divergence from the reference problem in this case grows monotonically with the increasing of the material mismatch. For the case of different thicknesses, if the thinner layers are more compliant, the increase of their stiffness always increases the SIF and the normalized ERR. When the layers become sufficiently stiff, further increase of their stiffness results in the non-monotonic behavior. Consequently, the ERR approaches some maximum, which may significantly exceed the corresponding value in the reference problem.

The phase angle for the specific case of the pure normal loading ($\varphi = 0$) and the elastic mismatch with $\beta = 0$ has the same general trend as for the known case of the semi-infinite crack in a sandwich. Namely, when the thinner layers are the more compliant ones, the magnitude of this angle is usually larger than in the opposite situation.

On the other hand, for long cracks, the phase shift angle as well as the ERR is found to be very sensitive to the value of β and to the direction of the applied loading. Consequently, one should be careful when using the results obtained for $\beta = 0$ and for $\varphi = 0$ in order to predict the fracture behavior in more general cases.

Chapter 6

Non-interface delamination crack in the periodically layered plane

The problem of the cracked bi-material periodically layered composite is considered. A single crack parallel to the interfaces is loaded by normal opening tractions. The non-symmetric position of the crack results in a mixed mode singular stress field in the crack tip vicinity, characterized by the two stress intensity factors K_I and K_{II} . By following the solution scheme presented in Chapter 2, with certain reduction as in the previous chapter, and some modification for the present case, the problem is reduced to a system of singular integral equations of the first kind, coefficients of which are derived in the closed form by the use of the Green's function for a single intra-layer dislocation. For the specific case of midplane intra-layer Mode I crack, this approach has been implemented by Ryvkin (1999).

In the following section, the boundary value problem on an arbitrary located non-interface crack in a periodically layered composite is formulated and solved. In Section 6.2 the parametric study of the obtained results is presented. The dependence of the SIFs upon the problem parameters is analyzed and the probable crack propagation path is discussed.

6.1 Statement of the problem

Consider a multilayered bi-material space consisting of perfectly bonded periodically alternating dissimilar isotropic elastic layers (Fig. 6.1). A crack of length $2a$ parallel to the interfaces is located arbitrarily within the layer number 1 of the cell number 0 at distance c above the layer midline. The systems of the local Cartesian coordinates are

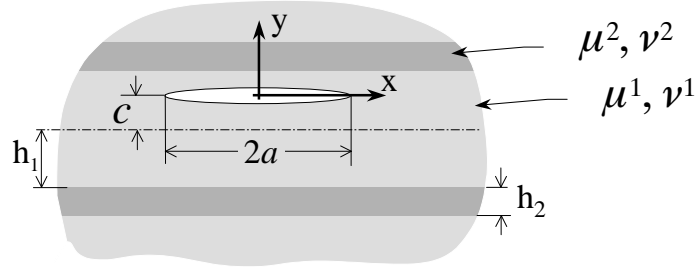


Figure 6.1: Periodically layered space with non-interface delamination crack.

introduced in all cells in an identical manner with the origins in the points corresponding to the center of the crack and x axes parallel to the layering. It is convenient to consider domains $-h_1/2 - c < y < 0$ and $0 < y < h_1/2 - c$ as different layers with the same elastic properties. Consequently, each cell consists of the three layers $r = 1, 2, 3$ defined by thicknesses $h_1/2 + c, h_1/2 - c, h_2$, shear moduli μ_1, μ_1, μ_2 and the Poisson ratio's ν_1, ν_1, ν_2 respectively.

The loading is uniform normal tractions σ applied to the crack faces. When employing the solution of the considered problem for the analysis of an elastic response to the uniform remote tension in the y -direction with the traction free crack, the existence of a non-singular T -stress acting parallel to the crack is to be taken into account. This stress, of course, does not influence magnitudes of the stress intensity factors but plays an important role in the prediction of the crack propagation path (Fleck *et al.*, 1991).

After introducing the vector $\mathbf{U}_r^k(x, y)$ $r = 1, 2, 3; k = 0, \pm 1, \pm 2, \dots$ of the elastic field in the r -th layer of the k -th cell, defined by (2.1), the boundary value problem for the layered space is given by the following infinite system of equations

$$\mathcal{L}_r[u_r^{(k)}, v_r^{(k)}] = 0, \quad k = 0, \pm 1, \pm 2, \dots; \quad r = 1, 2, 3, \quad (6.1)$$

$$\mathbf{U}_1^{k+1}(x, -\frac{h_1}{2} - c) - \mathbf{U}_3^k(x, \frac{h_1}{2} - c + h_2) = 0, \quad k = 0, \pm 1, \pm 2, \dots, \quad (6.2)$$

$$\mathbf{U}_3^k(x, \frac{h_1}{2} - c) - \mathbf{U}_2^k(x, \frac{h_1}{2} - c) = 0, \quad k = 0, \pm 1, \pm 2 \dots \quad (6.3)$$

$$\mathbf{U}_2^k(x, 0) - \mathbf{U}_1^k(x, 0) = 0, \quad k = \pm 1, \pm 2 \dots \quad (6.4)$$

$$\mathbf{U}_2^0(x, 0) - \mathbf{U}_1^0(x, 0) = 0, \quad |x| \geq a \quad (6.5)$$

$$\sigma_j^0(x, 0) = -\sigma, \quad \tau_j^0(x, 0) = 0, \quad |x| < a \quad j = 1, 2. \quad (6.6)$$

Here Eqns. (6.1) are the Lamé field equations, and the relations (6.2)–(6.6) define the boundary conditions at the interfaces between the cells and on the lines $y = h_1/2 - c$ and $y = 0$ within the cells. The mirror symmetry of the formulated boundary value problem (6.1)–(6.6) with respect to line $x = 0$ allows consideration of only the half-space $x > 0$ with an additional stipulation (5.10).

As before, the crack is considered as an assemblage of the distributed dislocations with unknown amplitudes $f_1(t), f_2(t)$. The Green's function $\check{\mathbf{U}}_r^k(x, 0, t)$ is generated by the single dislocation (2.9)–(2.10) located on the line $y = 0$ in the cell number zero ($n = 0$) of the non-cracked periodically layered plane. Consequently, the stress conditions (6.6) on the crack faces are presented by (2.15) with the help of the corresponding Green's functions $\check{\sigma}_1^0(x, 0, t)$ and $\check{\tau}_1^0(x, 0, t)$.

The Green's functions are derived by following the solution scheme presented in the previous chapter. The only significant distinction now is that the representative cell formally consists of three layers. The corresponding boundary value problem is given by conditions (6.1)–(6.3), (5.10), where symbol "◡" is to be added to all the stress strain components in order to distinguish the problem on the Green's functions from the original one, and by conditions

$$\check{\mathbf{U}}_2^k(x, 0, t) - \check{\mathbf{U}}_1^k(x, 0, t) = \mathbf{F}(t)H(x - t) \delta_{k0}, \quad k = 0, \pm 1, \pm 2 \dots \quad (6.7)$$

Note, that in the present problem functions $\check{\mathbf{U}}_2^k(x, 0, t)$ and $\check{\mathbf{U}}_1^k(x, 0, t)$ are the vectors of the elastic fields of the sub-layers with identical elastic properties.

By employing the discrete Fourier transform (2.34) the formulated problem for a single dislocation in the periodically layered plane is reduced to the boundary value problem for representative cell $-\infty < x < \infty, -h_1/2 - c < y < h_1/2 - c + h_2$

$$\mathcal{L}_r[\check{u}_r^*, \check{v}_r^*] = 0, \quad (6.8)$$

$$\check{\mathbf{U}}_1^*(x, -\frac{h_1}{2} - c) - e^{i\phi} \check{\mathbf{U}}_3^*(x, \frac{h_1}{2} - c + h_2) = 0, \quad (6.9)$$

$$\check{\mathbf{U}}_3^*(x, \frac{h_1}{2} - c) - \check{\mathbf{U}}_2^*(x, \frac{h_1}{2} - c) = 0 \quad (6.10)$$

$$\check{\mathbf{U}}_2^*(x, 0) - \check{\mathbf{U}}_1^*(x, 0) = \mathbf{F}(t)H(x - t) . \quad (6.11)$$

$$\check{u}_r^*(0, y, t) = 0, \quad \frac{\partial \check{v}_r^*(0, y, t)}{\partial x} = 0, \quad (6.12)$$

where $\check{\mathbf{U}}_r^*(x, y) \equiv \check{\mathbf{U}}_r^*(x, y, t, \phi)$. The solution of the latter problem by the use of the Fourier integrals is straightforward. The displacements in the r -th layer, in view of the symmetry condition (6.12), are taken in the form (5.12)-(5.13) with $r = 1, 2, 3$, $\kappa_r = 3 - 4\nu_1$, $r = 1, 2$, and $\kappa_3 = 3 - 4\nu_2$. By deriving the stresses from the Hooke's law and satisfying boundary conditions (6.9)-(6.11), the system of twelve linear algebraic equations with respect to the unknown functions $A_j = A_j(z, t, \phi)$, $j = 1, \dots, 12$ is obtained. In the matrix form it can be presented as follows

$$\mathbf{BA} = \mathbf{R} , \quad (6.13)$$

with the right hand side

$$\mathbf{R} = \{0, 0, 0, 0, 0, 0, 0, 0, f_1(t) \cos zt, f_2(t) \sin zt, 0, 0\} .$$

Consequently, the expressions for the A_j have the form

$$A_j = \frac{P_{j1}(z, \phi)f_1(t) \cos(zt) + P_{j2}(z, \phi)f_2(t) \sin(zt)}{\det(\mathbf{B})} , \quad (6.14)$$

where the symbols $P_{ji}(z, \phi)$ denote some known, rather cumbersome functions, derivation and analysis of which have been carried out with the help of symbolic computation. Denominator $\det(\mathbf{B})$, being the determinant of matrix \mathbf{B} is presented in Appendix A.4. It is interesting to note that it equals within a normalizing coefficient to the determinant of the eighth order matrix \mathbf{M} derived for the case of the interface dislocation (see (2.42) in subsection 2.2.2). This results because equations (6.9)–(6.11) and (2.31)–(2.32) are, actually, the systems of boundary conditions for the same representative cell subjected to the different loading.

By substituting A_j in (5.12), (5.13) and employing Hooke's law one obtains the expressions for the stress transforms within the representative cell. The originals, i.e. the stresses in any point of the periodically layered plane generated by the single dislocation (2.9), (2.10), are found by the inverse DFT

$$\{\check{\sigma}_r^k(x, y, t), \check{\tau}_r^k(x, y, t)\} = \frac{1}{2\pi} \int_{-\pi}^{\pi} \{\check{\sigma}_r^*(x, y, t, \phi), \check{\tau}_r^*(x, y, t, \phi)\} e^{-ik\phi} d\phi , \quad (6.15)$$

$$k = 0, \pm 1, \pm 2, \dots; \quad r = 1, 2, 3.$$

Note that this result provides an opportunity to formulate different fracture problems on cracked periodically layered composites for the cases where the considered mirror symmetry (5.10) takes place. The sought stress components $\check{\sigma}_1^0(x, 0, t)$, $\check{\tau}^0(x, 0, t)$ of the Green's function are given by (6.15) with $k = 0$, $r = 1$ and $y = 0$.

Substituting the obtained expressions into boundary conditions (6.6), after some manipulation, the system of two singular integral equations of the first kind in terms of the unknown dislocation densities is obtained. These equations are similar to those obtained by Erdogan and Gupta (1971a) in the problem of the sandwich composite and after normalization by half the crack length a are presented as follows

$$\frac{1}{\pi} \int_{-1}^1 \frac{f_2(t)dt}{t-x} + \int_{-1}^1 f_1(t)K_{11}(x,t)dt + \int_{-1}^1 f_2(t)K_{12}(x,t)dt = \sigma_0, \quad (6.16)$$

$$\frac{1}{\pi} \int_{-1}^1 \frac{f_1(t)dt}{t-x} + \int_{-1}^1 f_1(t)K_{21}(x,t)dt + \int_{-1}^1 f_2(t)K_{22}(x,t)dt = 0, \quad i = 1, 2,$$

where $\sigma_0 = -2(1 - \nu_1)\pi\sigma\mu_1^{-1}$, and the unknown functions $f_i(t)$ are continued for the negative values of the argument $f_1(t) = -f_1(-t)$, $f_2(t) = f_2(-t)$ with the additional restriction (2.11). The four Fredholm kernels $K_{ij}(x, t)$, $i, j = 1, 2$ have the form

$$K_{ij}(x, t) = \frac{1}{\pi} \int_0^\infty \sin z(t-x) k_{ij}(z, \phi) dz, \quad (i \neq j) \quad (6.17)$$

$$K_{ii}(x, t) = \frac{1}{\pi} \int_0^\infty \cos z(t-x) k_{ii}(z, \phi) dz, \quad i = 1, 2.$$

Functions $k_{ij}(z, \phi)$ are rather cumbersome (see Appendix A.4), nevertheless, it appeared that the integration in ϕ can be carried out analytically. The final result obtained after exchanging the integration order is not exhibited for the sake of brevity.

The most effective method for solution of singular integral equations of the obtained type has been developed by Erdogan and Gupta (1972). In view of the singular behavior of the dislocation densities in the vicinity of the crack tip, auxiliary unknown functions $\hat{F}_i(t)$ defined by the relations

$$f_i(t) = \frac{\sigma_0 \hat{F}_i(t)}{(1-t^2)^{1/2}}, \quad i = 1, 2 \quad (6.18)$$

are employed. Substitution of these functions approximated by the truncated series of Chebyshev polynomials in Eqn. (6.16) yields the system of $2n$ linear algebraic equations with respect to the values $\hat{F}_i(t_k)$, $t_k = \cos((\pi/2n)(2k-1))$, $k = 1, \dots, n$; $i = 1, 2$

$$\sum_{k=1}^n \frac{1}{n} \left\{ \hat{F}_2(t_k) \left[\frac{1}{t_k - x_r} - \pi K_{12}(x_r, t_k) \right] + \hat{F}_1(t_k) \pi K_{11}(x_r, t_k) \right\} = 1,$$

$$\sum_{k=1}^n \frac{1}{n} \left\{ \hat{F}_1(t_k) \left[\frac{1}{t_k - x_r} - \pi K_{21}(x_r, t_k) \right] - \hat{F}_2(t_k) \pi K_{11}(x_r, t_k) \right\} = 0, \quad (6.19)$$

$$\sum_{k=1}^n \hat{F}_1(t_k) = 0, \quad \sum_{k=1}^n \hat{F}_2(t_k) = 0,$$

where $x_r = \cos(\pi r/n)$, $r = 1, \dots, n-1$. Having defined the values of $\hat{F}_i(t_k)$ one can determine the entire normalized dislocation densities $\hat{F}_i(t)$, $0 \leq t \leq 1$ by interpolation. By employing the previously derived analytical expression for the Green's function corresponding to the single dislocation, the stress state in any point of the periodically layered composite with the crack is obtained.

6.2 Numerical Results

In this section the dependence of the SIFs K_I , K_{II} upon the geometric and elastic problem parameters is examined. In accordance with (4.12), (4.16) and (4.17), the following normalized quantities

$$\hat{K}_I = \frac{K_I}{\sigma \sqrt{\pi a}}, \quad \hat{K}_{II} = \frac{K_{II}}{\sigma \sqrt{\pi a}}, \quad \hat{G} = \frac{K_I^2 + K_{II}^2}{\sigma^2 \pi a} \quad (6.20)$$

are employed. The relations between the normalized stress intensity factors and normalized dislocation distributions \hat{F}_i have been obtained by Erdogan and Gupta (1971a)

$$\hat{K}_I = \hat{F}_1(1), \quad \hat{K}_{II} = \hat{F}_2(1). \quad (6.21)$$

The normalized SIFs may be considered as functions of three variables h_1/a , h_2/h_1 , c/h_1 defining the geometry of the problem and three others specifying the elastic properties of the materials ν_1 , ν_2 and $\mu = \mu_2/\mu_1$.

In the same way as in the previous interface crack problem, in the present case, elastic properties of the composite can be completely defined by the use of two Dundurs' mismatch parameters α , β . The values of these parameters considered in all the numerical examples correspond to the practically most plausible situation when the cracked layer is more compliant with respect to the outer ones. (We denote hereafter the layers identical to the cracked one as *inner* and the layers of the second type as *outer*.)

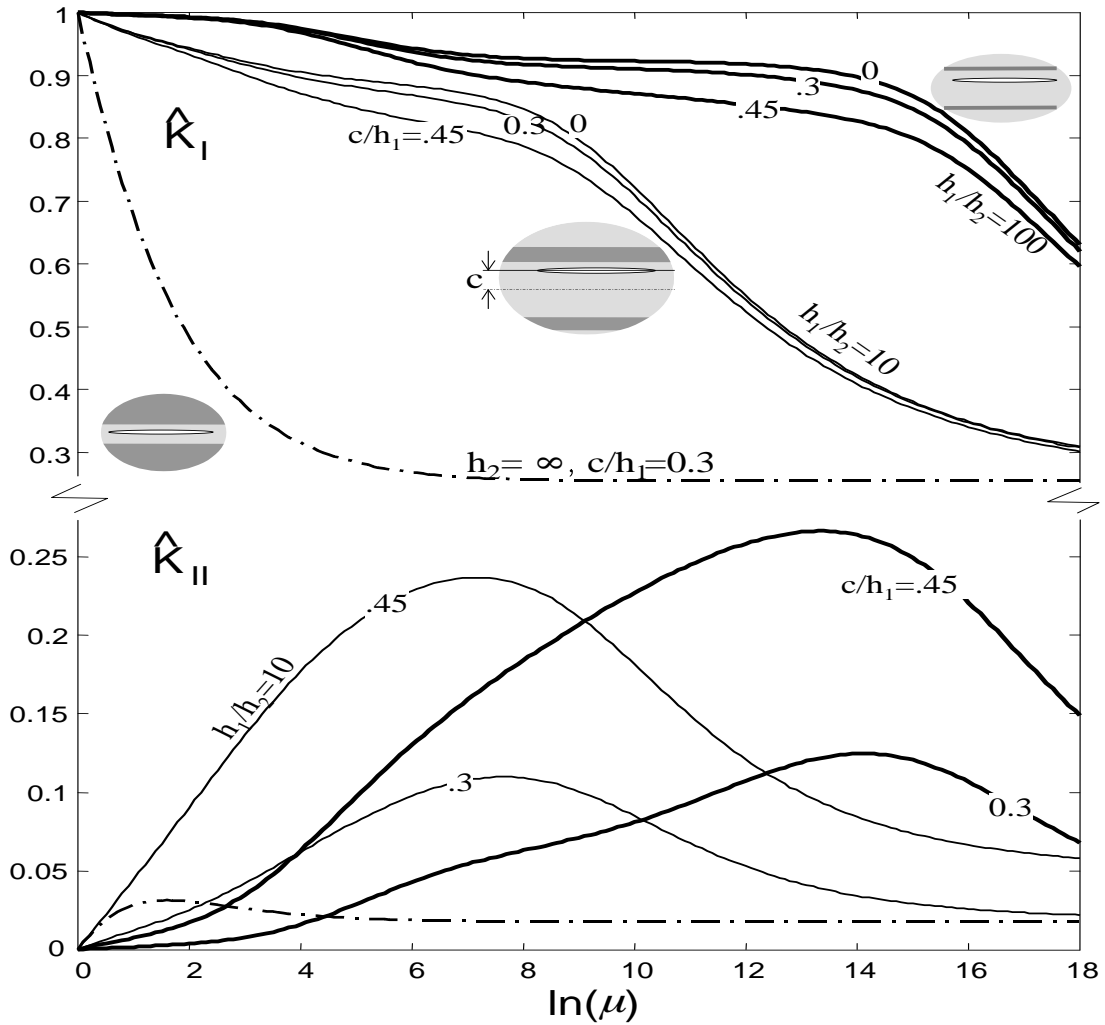


Figure 6.2: SIF K_I and K_{II} vs. stiffness ratio $\mu = \mu_2/\mu_1$ for the crack of relative length $h_1/a = 0.5$ located in the compliant layer of thickness h_1 . Poisson ratios are $\nu_1 = \nu_2 = 0.3$

6.2.1 Influence of the materials mismatch

It is interesting to examine the dependence of the considered fracture characteristics upon the material properties of the composite constituents and to compare the results with those for the interface crack. As was pointed out in Chapter 5, for the considered case this dependency is completely defined by the Dundurs' elastic mismatch parameters. However, in order to attain more "engineering filling" of the problem and to distinguish more details, the stiffness ratio μ is taken as independent variable. A simple unique dependence between the stiffness ratio and parameter α

$$\alpha = \frac{\mu - 1}{\mu + 1}. \quad (6.22)$$

exists when the Poisson ratios are equal. In view of this their values are chosen to be $\nu_2 = \nu_1 = 0.3$. The normalized stress intensity factors \hat{K}_I and \hat{K}_{II} as functions of μ are presented in Fig. 6.2 for two thickness ratios $h_1/h_2 = 10, 100$; and different crack locations $c/h_1 = 0, 0.3, 0.45$ in the layer of the first type, which for considered values of $\mu > 1$ is the more compliant one. Consequently, the stiff layers are rather thin. The crack is four times as long as the cracked layer. The results for the limiting case of sandwich $h_1/h_2 \rightarrow 0$ with the crack located at $c/h_1 = 0.3$ are presented by the dashed-dotted line for comparison.

It can be seen from the figure that $K_I(\mu)$ is a monotonically decreasing function, which has, however, a flat gradient interval. Within this interval the increase of the stiffness ratio almost does not reduce the mode I SIF.

The function $K_{II}(\mu)$ opposite to $K_I(\mu)$ is not monotonic. Its maximum for a certain value of μ several times exceeds the corresponding asymptotic value for the rigid outer layer ($\mu \rightarrow \infty$), which is the same for any thickness ratio. The "sandwich curve" $h_2 = \infty$ meets this value for $\ln(\mu) > 6$. The above non-monotonic behavior results from the "beam effect" produced by a thin layer of a stiffer material located near the crack which increases the SIF in a certain range of problem parameters. A similar phenomenon for the case of Mode III crack in a bi-material periodically layered composite was noted by Ryvkin (1998). An additional demonstration of the above effect will be presented further when examining the thickness ratio influence.

Calculations carried out for the considered and several additional combinations of parameters $\nu_1, \nu_2, h_1/a$ show that, contrary to the interface crack case, for the intra-layer delamination crack in periodic composites, the absolute value $|K|$ of the complex SIF (4.7) is always less than that in the corresponding problem of the crack in a homogeneous plane. When the sub-interface crack verges towards interface, the far field ERR approaches the corresponding value for the interface crack. This does not happen to the corresponding absolute values of stress intensity factors $K_I + i K_{II}$ and $K_1 + i K_2$, since the sub-interface crack singular stress field does not tend to that of the interface crack, but remains confined in the shrinking K-dominance zone (Ryvkin *et al.*, 1995). The issue of the relation between the stress intensity factors for the interface and sub-interface crack was considered in detail by Hutchinson *et al.* (1987).

6.2.2 Fineness of the layering

As was noted in the previous chapter, the ratio of the crack length to the thickness of a layer may be considered as a parameter of the layering fineness. In order to examine the dependence of the stress intensity factors upon this parameter, the layered space with elastic properties specified by $\alpha = 0.8$ and $\beta = 0.2$ is considered. The graphs for the normalized stress intensity factors \hat{K}_I and \hat{K}_{II} are presented in Figs. 6.3a and 6.3b respectively. The results for two periodically layered composites $h_2/h_1 = 1, 3$ with different positions of the crack plane defined by the parameter $c/h_1 = 0, 0.3, 0.45$ (see insert in Fig. 6.3a) are exhibited. The value $c/h_1 = 0$ corresponds to the crack in the midplane of the layer and the value $c/h_1 = 0.45$ to the crack close to the interface. In addition, the three curves for the degenerate sandwich case $h_2/h_1 = \infty$ are given for reference (dashed lines).

From Fig. 6.3 it is seen that in the considered case of relatively thick outer layers, for the short cracks when $h_1/a > 4$, the stress intensity factor K_I is defined mainly by the crack location and is weakly affected by the thickness ratio h_2/h_1 . The presented results together with additional calculations have shown that the sandwich approximation can be employed with less than 5% error for the cases when $h_2/a > 4$. An expected decrease of the SIF when the crack verges towards the stiffer neighboring layer (i.e. when c/h_1 increases) is observed.

On the other hand, when the crack becomes sufficiently long $h_1/a < 2$ the SIF seems to be almost independent of the crack plane location, being controlled only by the thickness ratio. Consequently, the results for the non-symmetric cracks are fairly good approximated by those obtained in the symmetric case $c/h_1 = 0$, considered in detail by Ryvkin (1999). In that work the non-monotonic "wavy" behavior of the stress intensity factor was explained by progressive disturbance of the increasing number of the neighboring layers by the growing crack. An explicit analytical expression for the ERR in terms of the layers parameters for a Mode I semi-infinite midline crack also can be found in the above paper. The corresponding values, which can be obtained directly from (4.37)-(4.38) for $\varphi = 0$

$$\hat{K}_I^\infty = \lim_{a \rightarrow \infty} \frac{K_I}{\sigma \sqrt{\pi a}} = \left[\frac{a_1}{a_2} \left(\sqrt{\frac{a_1}{a_3}} + \frac{a_4}{a_3} \right) \right]^{\frac{1}{4}}, \quad (6.23)$$

are denoted on the ordinate axis by asterisks. The above results meet also those obtained

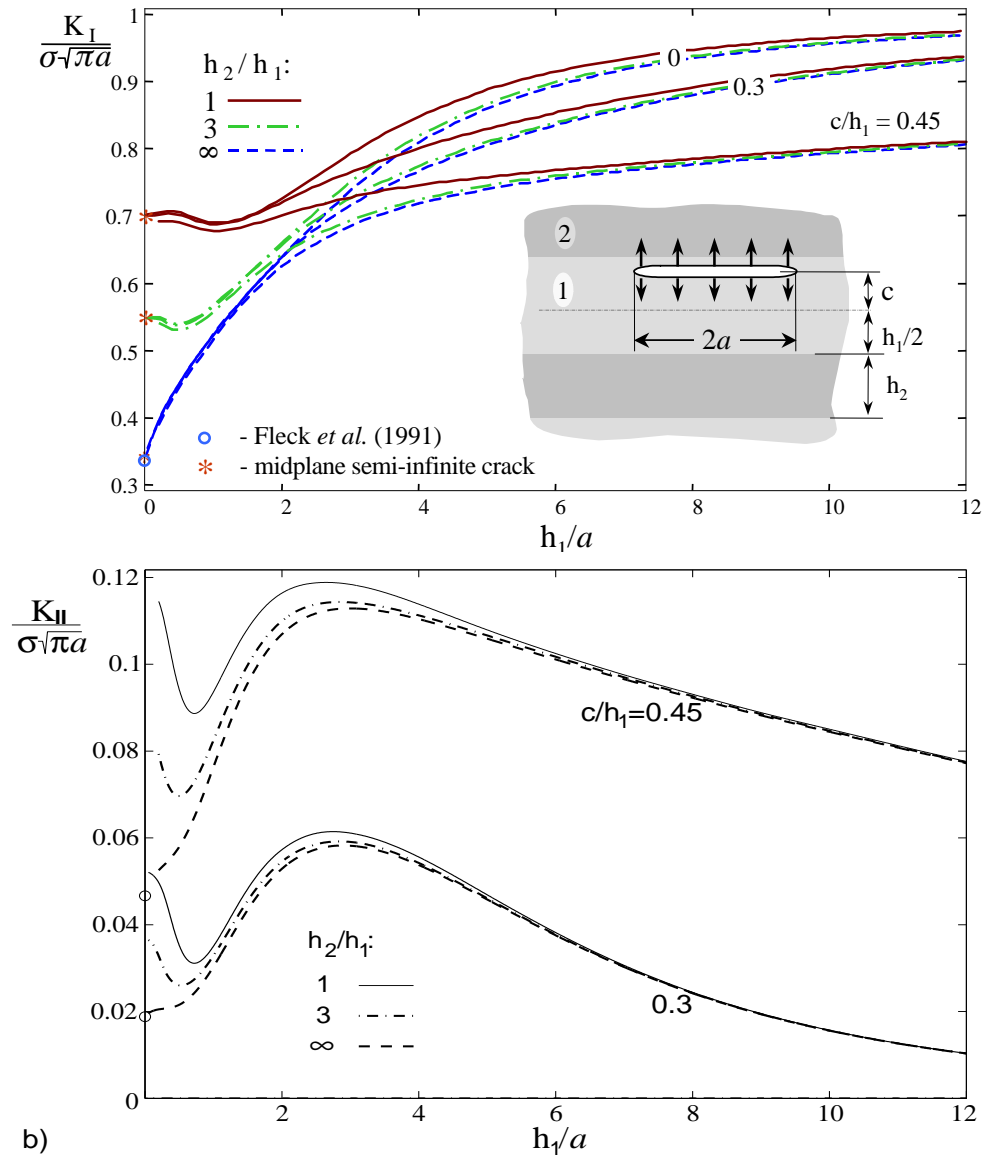


Figure 6.3: SIF K_I and K_{II} vs. normalized crack length h_1/a with the elastic mismatch specified by $\alpha = 0.8$ and $\beta = 0.2$. Crack is located in the compliant layer of thickness h_1 .

by Jha and Charalambides (1998), who examined a long intra-layer delamination crack in the periodic bi-material plane, computed the fracture parameters by the use of the FE method and compared them with the corresponding values (obtained analytically) for the homogenized anisotropic plane.

The above mentioned possibility to use the results obtained for the symmetric mid-plane crack, in order to estimate the stress intensity factor \hat{K}_I in the present problem for small ratios h_1/a , is of prime importance. In fact, analysis of the expressions for

integrands k_{ij} in (6.17) shows that for large z their decaying is defined by the relation

$$k_{ij}(z, \phi) \sim O \left[\exp\left(-z \frac{2h_m}{a}\right) \right], \quad z \rightarrow \infty, \quad (6.24)$$

where $h_m = h_1/2 - c$ is the distance from the crack to the nearest interface. Consequently, when the ratio h_m/a as well as h_1/a diminishes, the computation time required for evaluating the coefficients of the system grows. Furthermore, the oscillations of the dislocation densities $f_i(t)$ near the crack tip become sharper, calling for a rise of the number of the Chebyshev interpolation points, that may be attributed to the known behavior of the interface crack solution. Thus, the analysis of the cases when the crack is very long or is located too close to the interface becomes a difficult task.

The above numerical problem is to be expected. As mentioned earlier, when the crack verges toward the interface, the K-dominance zone shrinks. Consequently, the transition from the far-field to the near-field dislocation distribution becomes sharper. Therefore, for the case of a sub-interface crack, i.e. when the values h_m/a and h_m/h_1 are small, the analysis of the stress distribution and extracting the stress intensity factors become troublesome.

The case of a semi-infinite crack arbitrarily located within a layer sandwiched between two half-spaces was considered by Fleck *et al.* (1991). This result, denoted in the figure by a circle, is seen to agree with the obtained numerical data. It may be predicted that for the smaller values h_2/h_1 the graphs for \hat{K}_I will approach the line $\hat{K}_I = 1$, corresponding to the case of a homogeneous plane.

The stress intensity factor \hat{K}_{II} in front of the crack loaded by the normal tractions is non-vanishing only for the non-symmetric crack location when $c/h_1 = 0.3, 0.45$ and, clearly, significantly less than the corresponding values for \hat{K}_I (Fig. 6.3b). It is observed that for short cracks \hat{K}_{II} , similar to \hat{K}_I , is also defined mainly by the crack location within the layer, independently of the outer layers thickness. At the same time when the crack is positioned closer to the interface, \hat{K}_{II} , in contrast to \hat{K}_I , grows. The latter property, which may be explained by the increasing of the "non-symmetry" in the system, holds true for other crack lengths also. For the limiting case of a semi-infinite crack the observed opposite behavior of \hat{K}_I and \hat{K}_{II} meets the asymptotic relation obtained in Subsection 4.3 from the energy arguments. For the present case it may be written as

follows

$$\hat{K}_I^2 + \hat{K}_{II}^2 = \frac{2\mu_1}{1-\nu_1} Q_1, \quad h_1/a \rightarrow 0, \quad (6.25)$$

where Q is a known function of the elastic parameters and the thickness ratio h_2/h_1 but not of the crack plane location within the layer. The general behavior of \hat{K}_{II} for the sandwich composite (dashed line), characterized by a single maximum, is analogous to that observed in the similar problem by Erdogan and Gupta (1971a). The limiting values for the case $h_1/a \rightarrow 0$ have been derived by Fleck *et al.* (1991). In the figure they are denoted by the circles. One can see the satisfactory agreement with the results obtained in the present work. With the crack extension in the periodically layered composite, the behavior of \hat{K}_{II} is found to be close to the sandwich case up to certain crack length when the influence of the remote layers emerges. Then the curves turn to the limiting values which must satisfy relation (6.25). It may be noted, that unlike \hat{K}_I the behavior of \hat{K}_{II} for sufficiently long cracks is significantly influenced by both the crack location and the thickness ratio h_2/h_1 .

6.2.3 Mode I crack locations

It is of interest to examine the dependence of the stress intensity factors upon the distance from the interface in more detail. The numerical results for the composite with very thin ($h_2/h_1 = 0.01$) and stiff ($\alpha = 0.8, \beta = 0.2$) outer layers are presented in Fig. 6.4. Four crack lengths $h_1/a = 1, 2, 3, 10$ are considered. Since the outer layers are thin, the obtained values of \hat{K}_I and \hat{K}_{II} are close to unity and to zero respectively.

The mentioned general trend that the stress intensity factor \hat{K}_I (\hat{K}_{II}) for the crack located close to the interface is less (more) than that for the crack near the midplane of the layer, is also observed here. On the other hand, existence of a thin outer layer with different elastic properties in the crack vicinity causes non-monotonic behavior. The small variations in the values of \hat{K}_I may be of limited importance but behavior of \hat{K}_{II} is of interest, since its sign changes for some parameter combinations. Consequently, for the crack with the given length, there may be one or two locations within the cracked layer, in addition to the symmetric case $c/h_1 = 0$, where \hat{K}_{II} vanishes. Condition $\hat{K}_{II} = 0$ is often accepted as a criterion for the crack propagation direction (e.g. Hutchinson and Suo, 1991). Since, for the certain problem parameter range, several alternate $\hat{K}_{II} = 0$

locations exist, this may indicate general instability of a straight-line propagation.

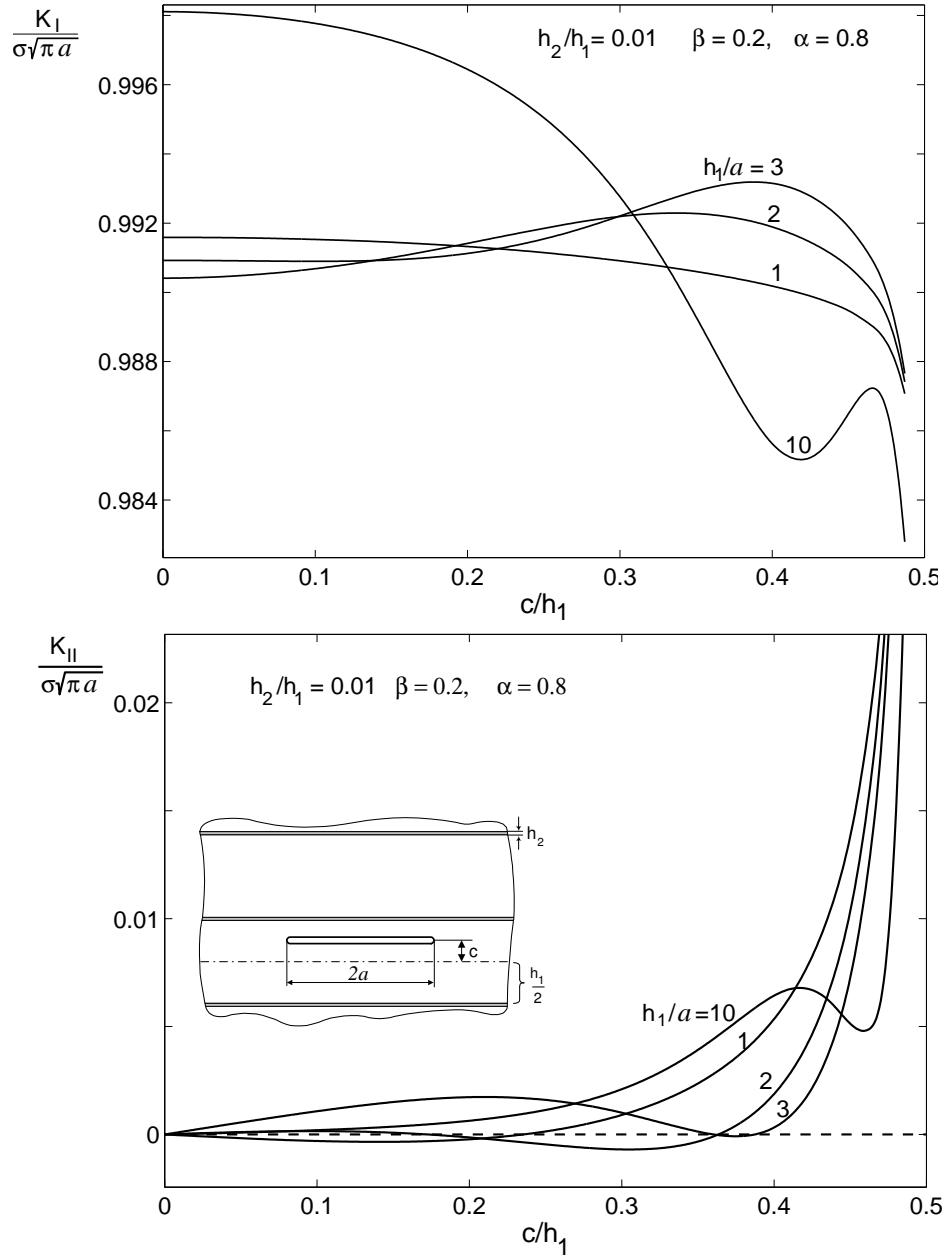


Figure 6.4: Dependence of the stress intensity factors \hat{K}_I and \hat{K}_{II} upon the crack location for the case of thin stiff non-cracked layers.

The dependence of critical crack locations c^*/h_1 defined by the condition $\hat{K}_{II} = 0$ upon the crack length is depicted in Fig. 6.5. The results are presented for composites with the same geometry as in the previous example $h_2/h_1 = 0.01$ but different elastic properties $\alpha = 0.7, 0.8, 0.85, 0.9$ with $\beta = \alpha/4$. The latter relation corresponding to the condition $\nu_1 = \nu_3 = 1/3$ is used in the literature (e.g. Fleck *et al.*, 1991) as a good approximation for many bi-material systems. It is seen that non-zero values of c^*/h_1

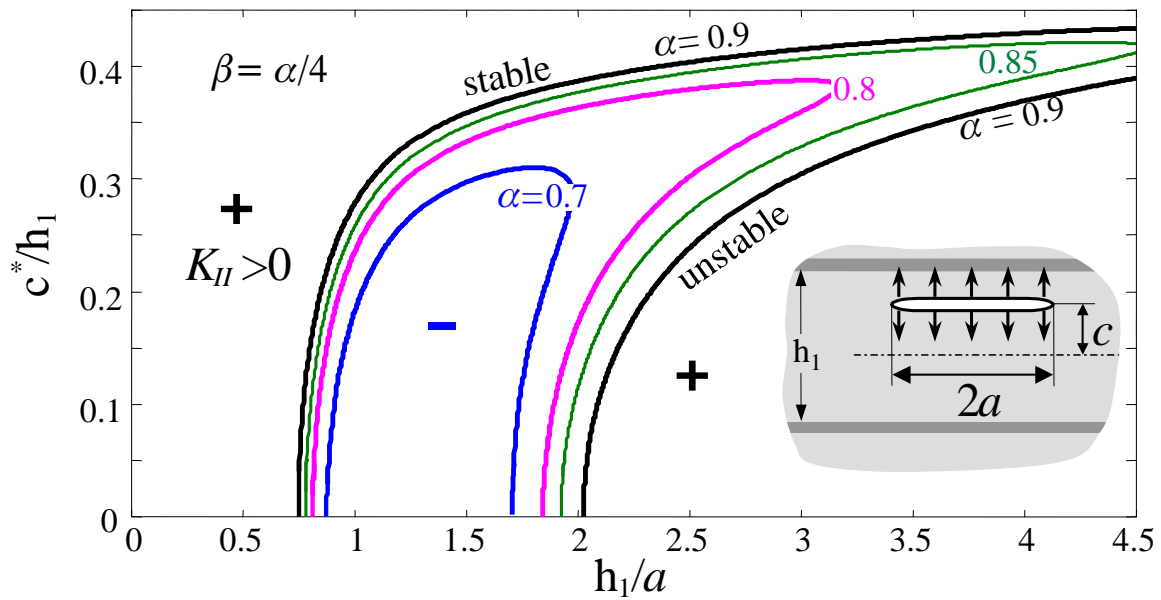


Figure 6.5: Crack location c^*/H corresponding to $\hat{K}_{II} = 0$ vs. crack length for different material mismatch with $\beta = \alpha/4$. The stiffer layers are thin $h_1/h_2 = 100$.

exist only when the crack is neither too long nor too short. The corresponding range of crack length parameter h_1/a expands with the increase of the material mismatch. The whole midline $c^*/h_1 = 0$ corresponds to the crack location satisfying condition $\hat{K}_{II} = 0$.

Parameter combination domains, where \hat{K}_{II} takes on positive or negative values, are denoted by signs "+" or "-", respectively. Following the arguments used by Fleck *et al.* (1991) for the case of pure mode II loading, suppose the crack is displaced from the midline upwards. Since the right tip of the crack is considered, the positive sign indicates, as consistent with the $\hat{K}_{II} = 0$ criterion, that the crack has a trend¹ to propagate towards the midline of the layer. From the symmetry considerations it follows that the same will occur for the crack displaced downwards. Thus, the midline of the layer can be a stable propagation path if it borders the upper "+" region, and an unstable one in the case of the "-" upper region. As can be seen from the figure, the only path within the layer which can be stable for a sufficiently long or rather short crack, is the midline. However, for any material combination there is an interval of the crack lengths, for which this path is not stable.

¹Clearly, this trend is not sufficient to conclude about the crack trajectory. When using such arguments the existence of so-called T-stress (σ_{xx}) having a great effect on the crack path stability, is not taken into consideration. A more complete stability analysis and prediction of another propagation morphology (kinking, wavy propagation) should be carried out, for example, by following the guidelines of Fleck *et al.* (1991).

Concerning the curves depicted in the figure, it can be noticed that they probably may be considered as a near straight $\hat{K}_{II} = 0$ propagation path in the region where they have flat gradients. The upper branch may be called "stable" while the lower one "unstable" in the context of the previous paragraph.

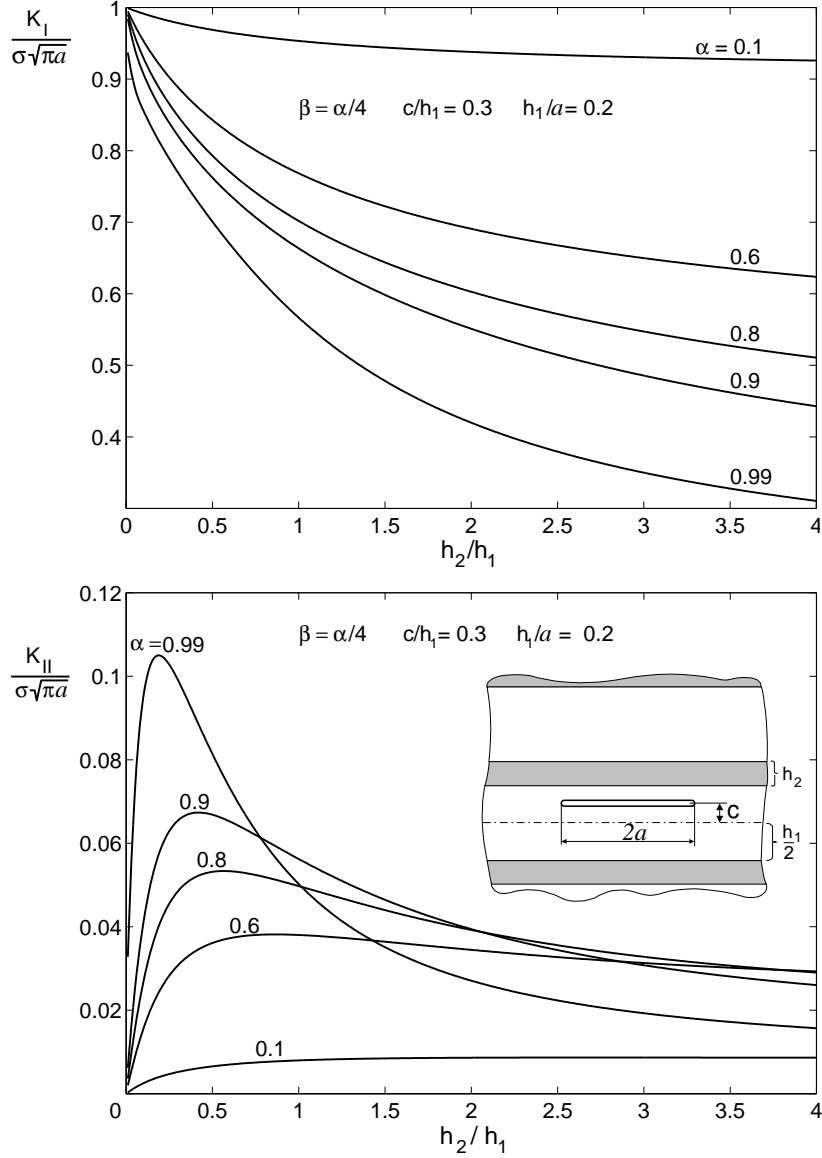


Figure 6.6: Dependence of the stress intensity factors \hat{K}_I and \hat{K}_{II} upon the outer layers thickness for different material combinations with $\beta = \alpha/4$.

6.2.4 Thickness ratio of the layers.

In Fig. 6.6 the dependence of the stress intensity factors upon the outer layers thickness is illustrated. The case of a rather long crack $h_1/a = 0.2$ with $c/h_1 = 0.3$ for five

material combinations is considered. The results are presented in the interval between $h_2/h_1 = 0$ when the composite becomes a homogeneous body and $h_2/h_1 = 4$ when all the perturbation in the stress state generated by the crack is localized within the three layers and the stress intensity factors may be found from the sandwich model with sufficient accuracy. Consequently, the curves for \hat{K}_I and \hat{K}_{II} begin from unity and zero, respectively, and for $h_2/h_1 \rightarrow 4$ approach the asymptotic values corresponding to the sandwich case. For \hat{K}_I the observed monotonic decreasing is more significant for small values of h_2/h_1 .

The behavior of the stress intensity factor \hat{K}_{II} , contrastingly, is non-monotonic with a clear maximum for small values of h_2/h_1 . Here one can see the result of the same "beam effect" pointed out earlier. The observed sensitivity of the solution upon the thickness of a thin layer of dissimilar material located near the crack was emphasized by Suo and Hutchinson (1989a) in the problem on substrate cracking beneath adherent film.

6.3 Conclusions

The dependence of the SIFs upon the distance from the crack to the nearest interface, the thickness of the nearby layers and the mismatch of the materials have been examined. The numerical study allowed to point out the cases when the simplified models can be employed.

As expected, for the considered normal loading on the crack faces, SIF K_I is found to be considerably larger than K_{II} . As opposed to the interface case, increase of the relative stiffness of the thin rigid layers always reduces singular stresses at the tip of the crack located in the more compliant layer.

It appeared that if the thicknesses of the layers with significant materials mismatch are of the same order, then the sandwich approximation of the stress intensity factors may be used with accuracy better than 4% only for the crack lengths below one fourth of the layers thickness. This observation holds true independently of the crack location within the layer. On the other hand, for sufficiently long cracks, when $h_1/a < 2$, the stress intensity factor K_I becomes very close to that for the symmetric midplane crack. Consequently, this SIF can be estimated by the use of the analytic result (4.37) obtained for the semi-infinite crack.

The study of the SIFs behavior for the case of very thin and rigid outer layers revealed an interesting and somewhat unexpected phenomenon. Namely, the stress intensity factor K_{II} is found to be zero not only for the symmetric midplane crack location but also for some additional ones. This fact, together with existence of the crack length interval where the midline is unstable location, points to existence of a wavy crack propagation path. Another important phenomenon for the case of thin outer layers is the non-monotonic behavior of K_{II} as a function of the outer layer thickness. The above results may be understood as the influence of a beam-like element that is generated by the layer, neighboring the cracked one.

It should be noted that significant numerical difficulties in the solution of the system of singular integral equations arise only for cracks located very close to the interface. However, this disadvantage must not be overestimated since, when the distance from the interface is so small that it becomes comparable with the fracture process zone of the material, the total stress intensity factor approach to the fracture analysis fails (Ryvkin *et al.*, 1995).

Chapter 7

Strip with an interface debonding

In this chapter an interface debonding in an infinite periodically layered strip is analyzed. Two problems are considered. In the first problem the crack in the strip with the fixed base and the tractions-free upper edge, is subjected to the internal pressure. In this case derivation of a new Green's function for the free-clamped strip edges is required. Therefore, the solution will be derived below by following the guidelines presented in Chapter 2. In the second problem the both edges of the strip are subjected to collinear equilibrated point forces; while the crack faces are tractions-free. The solution of this problem is easily derived by following the scheme presented in Chapter 2, in which the edge tractions should be substituted for point forces.

7.1 Delamination crack in a strip on a rigid foundation

Consider a strip Ω of thickness H consisting of N identical bi-layered cells Ω_k , $k = 0, \dots, N-1$, depicted in Fig. 7.1. Following the description used in Chapter 2 the thickness, shear modulus and Poisson ratio of the layers of r -th type are denoted as h_r , μ_r and ν_r , respectively. The perfect bonding of the layers is violated by the delamination crack of length $2a$ located at the inner interface in the cell number n . Consider the case when the crack is loaded by the uniform pressure σ . The upper edge of the strip is traction free

$$\sigma_2^{N-1}(x, h_2) = \tau_2^{N-1}(x, h_2) = 0, \quad (7.1)$$

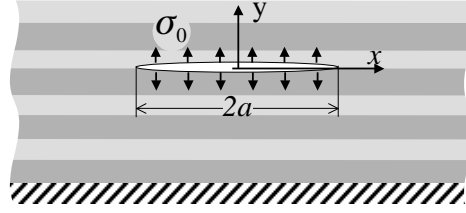


Figure 7.1: Clamped base strip with an interface crack under the internal uniform pressure.

while the lower one is clamped, i.e. the condition

$$u_1^0(x, -h_1) = v_1^0(x, -h_1) = 0 . \quad (7.2)$$

takes place. The reducing of the initial problem for a crack to the singular integral equation hinges on the deriving of the Green's function for a single dislocation in the non-cracked body. The corresponding boundary problem is defined by equations (2.2)–(2.7), with

$$\sigma(x) = \sigma , \quad \tau(x) = 0 , \quad (7.3)$$

$$\sigma^u(x) = \tau^u(x) = 0 , \quad (7.4)$$

and a new bonding condition (7.2) at the bottom, instead of stress condition (2.8).

In the considered case of homogeneous boundary conditions (7.1)–(7.2) the solution $\hat{\mathbf{U}}_r^k(x, y)$ for the perfectly bonded strip is zero. Therefore, the Green's function coincides with the solution of the auxiliary problem

$$\tilde{\mathbf{U}}_r^k(x, y, t) = \check{\mathbf{U}}_r^k(x, y, t) , \quad (7.5)$$

which is formulated with the help of the unknown stress jumps.

The stress jumps are derived from a 4-th order system similar to (2.44):

$$\mathbf{S}^C \bar{\mathbf{\Delta}} = e^{-zt} \left[f_1(t) \mathbf{b}^{C,1} + f_2(t) \mathbf{b}^{C,2} \right] , \quad (7.6)$$

where the upper index C indicates the clamped bottom case. In the right-hand side of (7.6) only the terms proportional to the dislocation amplitudes $f_1(t)$, $f_2(t)$ are retained. The sought Green's function being expressed in terms of the stress jumps has exactly the same form as that in Chapter 2. Therefore, it is obtained by replacing symbol " \sim " with " \smile " in formula (2.48). Coefficients A_j , $j = 1 \dots 8$ defining the elastic field vector are

calculated by the use of (2.47), in which a_j^0 are set to zero and the components of vector $\bar{\Delta}$ are determined from system (7.6). Calculation of $\bar{\Delta}$ can be carried out by the use of symbolic computation or numerically, but its explicit expression is too cumbersome and is not exhibited here.

Hence, the analytical expression of the Green's function for the single interface dislocation has been determined. Execution of the steps described in Section 2.3, for

$$\sigma_1^n(x, 0) = \sigma_2^n(x, 0) = -\sigma, \quad (7.7)$$

$$\tau_1^n(x, 0) = \tau_2^n(x, 0) = 0, \quad -a < x < a, \quad (7.8)$$

leads to the following integral equation

$$\frac{1}{\pi i} \int_{-1}^1 \frac{f(t)dt}{t-x} - \beta f(x) + \int_{-1}^1 [f(t)K_1(t,x)dt + \bar{f}(t)K_2(t,x)]dt = p. \quad (7.9)$$

Here, the right hand side is defined by the prescribed tractions

$$p = \frac{i(\mu_1 - \mu_2)(1 - \beta^2)}{2\mu_1\mu_2(\alpha - \beta)}\sigma, \quad (7.10)$$

and the kernels are given by (2.56), and (2.54) with

$$d_i^k = \bar{\Delta}_i^k + \gamma_m^N \bar{\Delta}_{i+1}^k, \quad i = 1, 3; \quad k = 1, 2 \quad (7.11)$$

associated with the components of the stress jump vector obtained from (7.6). (Recall, that the upper index k indicates the solution component corresponding to the dislocation f_k , $k = 1, 2$)

The solution of such systems of singular integral equations by the use of Jacobi orthogonal polynomials and derivation of the SIF is carried out by following the scheme presented in Section 5.2.

Numerical results. The parameters of the multilayered strip are chosen in order to verify the developed technique by comparing the results obtained in limiting cases with those known from the literature. The crack in an aluminium/epoxy composite consisting of $N = H/h = 50$ bi-layers with thick aluminium layers ($h_1/h_2 = 9$) is examined (see insert in Fig. 7.2). The normalized ERR is defined by (4.15), where $q = \sigma$.

The dependence of \hat{G} upon the crack length is presented in Fig. 7.2. The upper curve corresponds to the interface separated from the free upper edge by a single epoxy layer

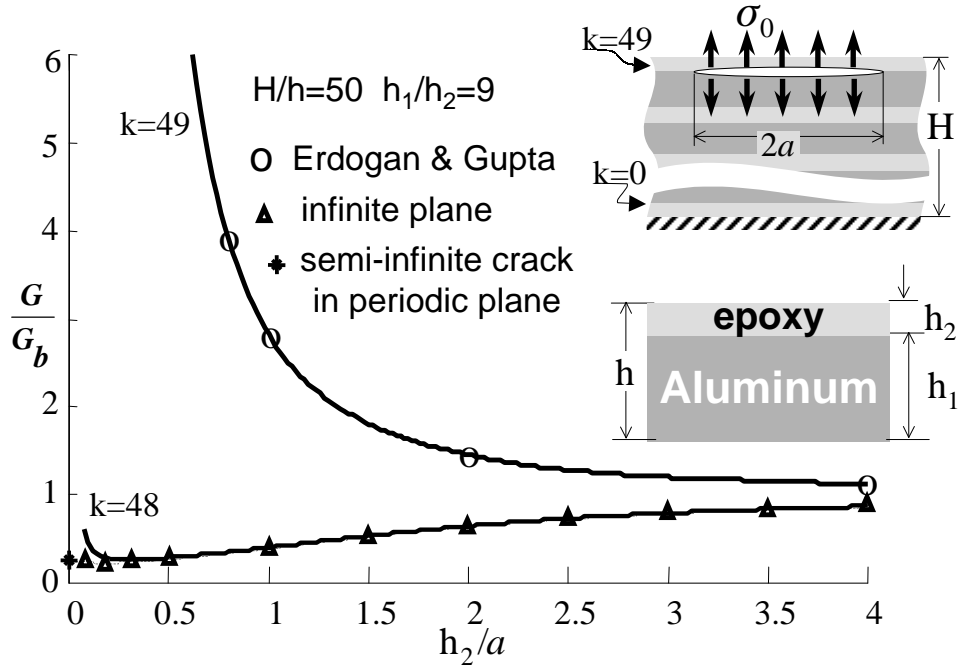


Figure 7.2: Clamped base strip with an interface crack under the internal pressure. Normalized ERR \hat{G} upon the relative crack length.

($k = 49$). Since the underlying aluminium layer is significantly thicker and stiffer than the epoxy one, the results, as expected, meet the data obtained by Erdogan and Gupta (1971b) in the corresponding problem on a crack at the interface between the layer and the half plane.

On the other hand, for the crack at the interface located deeper into the strip with $k = 48$, the observed behavior looks vastly different. Within the broad range of the crack length when the crack is not too long compared to the strip thickness, ERR is found to be very close to the corresponding value for the crack in the periodically layered plane (Chapter 5), which smoothly reaches the limit corresponding to the semi-infinite crack. Only when the crack length exceeds some critical value, which is about the distance to the upper edge of the strip (for the considered interface this distance is approximately equal to $11h_2$) the influence of the free boundary emerges, the ERR deviates from the layered plane asymptotic and unlimitedly increases.

7.2 Tractions-free crack in the strip subjected to point forces at the edges

In the next example, the cracked strip is loaded by two collinear self-equilibrated point forces applied at the external strip boundaries (see insert in Fig. 7.3). For this case, the general solution presented in Chapter 2 can be employed directly. Since the edge boundary conditions are defined by

$$\sigma_2^{N-1}(x, h_2) = \sigma_1^0(x, -h_1) = -Q\delta(x) , \quad (7.12)$$

$$\tau_2^{N-1}(x, h_2) = \tau_1^0(x, -h_1) = 0 , \quad (7.13)$$

vector \mathbf{b}^0 in (2.44), containing applied traction transforms, takes the form

$$\mathbf{b}^0 = \begin{bmatrix} Q \\ 0 \\ Q \\ 0 \end{bmatrix} \quad (7.14)$$

After calculating from (2.44) the stress jumps transforms, integral equation (2.55) is derived. Note, that crack faces are free of tractions, consequently, the value of p in the right hand side of the integral equation is zero. Its solution is obtained as described in Chapter 5.

Numerical results. In the first configuration, the crack is located at the interface closest to the upper edge of the strip consisting of 50 bi-layers. The absolute value of the stress intensity factor is examined. Its dependence upon the crack length for different material combinations with $\beta = 0$ and various shear modulus ratio $\mu = \mu_2/\mu_1$ is depicted in Fig. 7.3.

The general trend is similar to what was observed previously in the case of the uniformly loaded crack near the free edge. The rapid increase of the stress intensity factor with the increase of the crack length indicates the beam-like behavior of the upper layer separated from the strip by the crack. In fact, the beam asymptotic (the dashed line), derived for the specific case $\mu = 1$ of the homogeneous strip by Dyskin et al. (2000), is found to be a very good approximation for sufficiently long cracks.

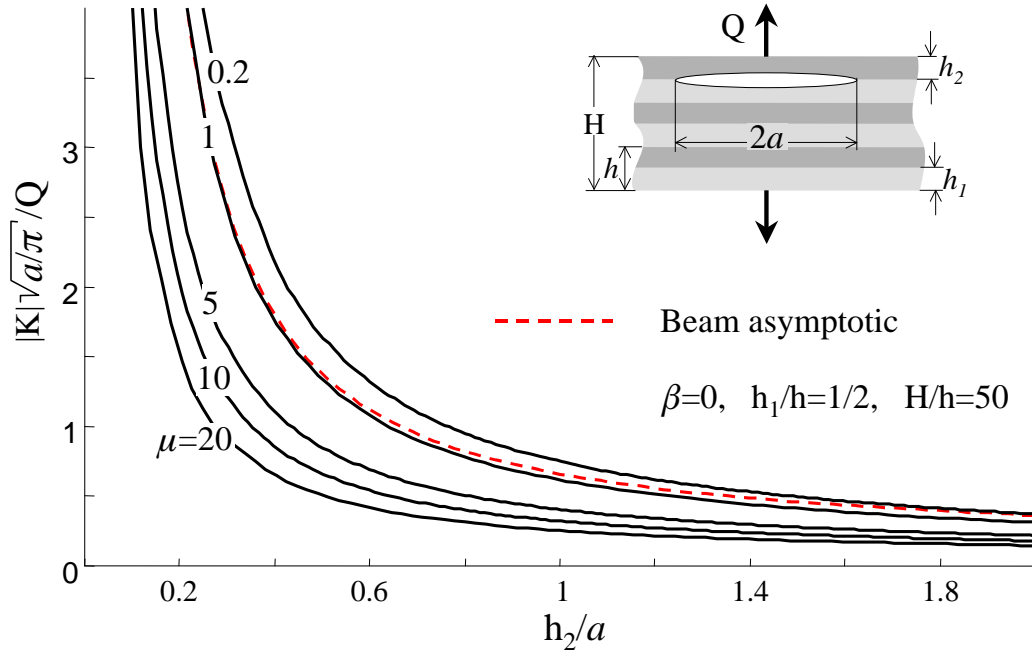


Figure 7.3: The absolute value of the SIF upon the crack length parameter h_2/a for different material combinations with $\beta = 0$ and various shear modulus ratio $\mu = \mu_2/\mu_1$.

The increase of the upper layer stiffness leads to a monotonic decrease of the stress intensity factor. Note, that when the crack is located deeper inside the strip and the thicknesses of the layers, contrary to the considered case are not equal, the influence of the elastic mismatch on the stress intensity factor can be more complicated. This issue is illustrated below.

In the problem presented in Fig. 7.4a the crack is placed in the midplane of the strip. The dependence of the absolute value of the normalized SIF upon elastic mismatch parameter α is exhibited for the case $\beta = \alpha/4$. Consequently, the value $\alpha = 0$ corresponds to the case when the materials properties coincide, i.e. to the case of homogeneous strip. The solid lines are related to the strip with eleven bi-layers and the crack length $a/h = 2$. For all the curves the thickness of the layers of the first type is more or equal than that of the second type. So, the increase of α from zero for the curves with $h_1/h = 0.7, 0.9$ may be understood as further increasing of the stiffness of the stiff thinner layers. It is seen that similar to the case of the crack in an infinite layered plane (Chapter 5), the above increase may lead to increasing as well as to decreasing of the stress intensity factor. Consequently, it approaches a maximum value for some materials combination.

Only in the particular case of equal thicknesses of the layers $h_1/h = 0.5$ the increase of

the elastic mismatch always leads to the decrease of the SIF. Hence, only in this case the absolute value of the stress intensity factor for the interface crack is less than the stress intensity factor for the crack in a homogeneous material. Note, that for the case $\beta = 0$

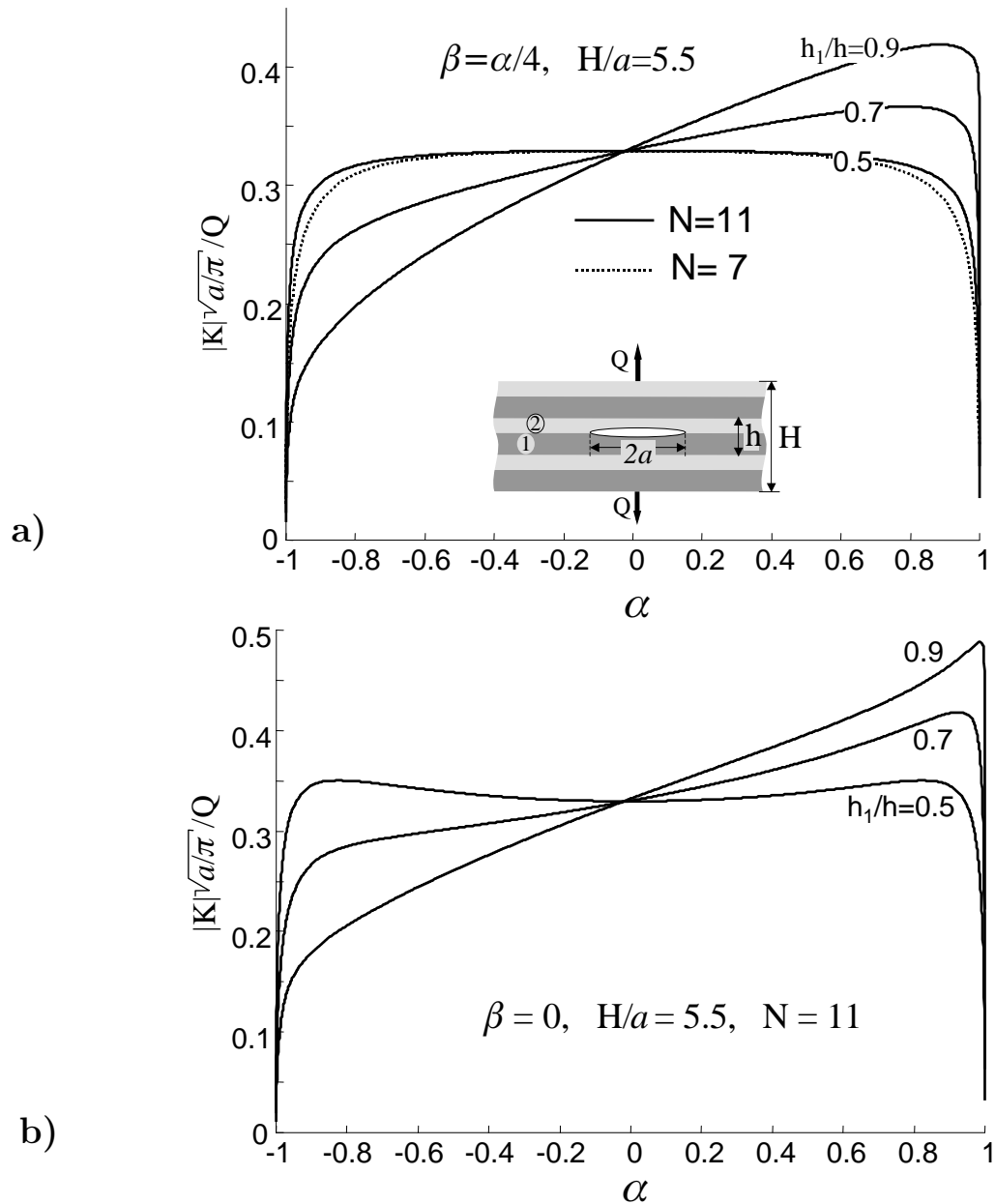


Figure 7.4: Normalized absolute value SIF upon elastic mismatch parameter α for the case $\beta = \alpha/4$ a) and $\beta = 0$ b) and the crack length $a/h = 2$, when the strip is loaded by two point forces.

the observed phenomenon does not hold true as it is seen from Fig. 7.4b. Therefore, the general conclusions about the interface fracture based on the analysis of the relatively simple case $\beta = 0$ must be done very carefully.

It is of the interest to elucidate the influence of the scale parameter h/a on the stress intensity factor. This can be done by comparing two composites with the same volume fraction defined by the ratio h_2/h_1 and different thicknesses h of the repetitive cell. To this end the calculations for the strip with the diminished number of bi-layers ($N = 7$, $h/a = 0.786$) have been carried out. The results presented in Fig 7.4a by the dotted line show, that for any elastic mismatch the stress intensity factor is weakly affected by the change in the layering scale h/a .

7.3 Conclusions

In the study of the cracked composite strips with the interface debonding, two types of fracture behavior have been observed. When the crack is near the strip edge, the separated layer acts like a beam and the SIF may be found from the beam asymptotic. Alternatively, when the crack is located far from the strip boundaries, the behavior typical for the crack in an infinite periodically layered plane emerges in a surprisingly broad range of parameters. As in the case of a layered plane, it was found that if the thinner layers are stiff, then further increase of their stiffness may lead to the enlarging as well as to the diminishing of the absolute value of the stress intensity factor. The essential length scale of each periodically layered composite is the thickness of the repetitive cell. The influence of this parameter on the SIF has been examined and found to be limited.

Chapter 8

Conclusions

Delamination in periodically layered composites consisting of an arbitrary number of layers is considered. Combined use of the representative cell method based on the discrete Fourier transform and of the dislocation approach has enabled obtaining analytical and semi-analytical solutions to a number of problems without any simplifying assumptions. The method is found to be a powerful, convenient tool providing accurate results in both cases of interface and non-interface cracks. In contrast to the known numerical methods, the suggested approach is insensitive to the number of layers, their thickness and elastic mismatch between the composite constituents. Rather cumbersome analytic expressions appearing during the solution procedure have been successfully treated by the use of symbolic computation. In this research bi-material composites with the repetitive cell consisting of two isotropic elastic layers were considered. The employed method is applicable also to the more complicated cases of anisotropic materials and increased number of layers in the cell, which seems to be an essential next step in the topic.

Several specific problems on a perfectly bonded periodically layered composite strip without cracks have been solved. The stress analysis of the three point bending strip has shown, as expected, that in the vicinity of the point forces the cross section of the strip does not remain plane after the deformation and, consequently, the approximate plate theory is not valid. On the other hand, it appeared that for a large elastic material mismatch, the strain distribution is linear in each individual layer except the nearest to the force application point. The investigation of the protective properties of the periodically layered strip bonded to the rigid substrate indicates that there is an optimal ratio

between the layers thicknesses, providing the minimal normal (shear) contact stresses induced by the shear (normal) tractions at the upper strip edge.

When studying the finite thickness composites with the interface crack, two types of behavior have been observed. When the crack is near the strip edge, the separated layer acts like a beam and the stress intensity factor can be found from the beam asymptotic. Alternatively, when the crack is located not too close to the strip boundary, the behavior typical for the crack in an infinite periodically layered plane emerges in a surprisingly broad range of parameters.

A new phenomena differing from that observed for the simpler sandwich models of multilayers has been revealed. In particular, it appeared that the ERR and the phase angle shift generally depend upon the angle φ defining the direction of the applied loading. It has been shown analytically, that the opposite can occur only simultaneously for both fracture parameters when some mathematical condition holds true, namely, when the ERR for the normal and for the shear uniform tractions on the crack faces is identical.

In the rest of the cases, the ERR appeared to be an even function of φ , and consequently, to have an extremum at $\varphi = 0$ corresponding to pure normal loading. The long crack asymptotic formula provides a simple condition for determining the character of this extremum for both the interface and the intra-layer cracks. For most material combinations in periodic multilayers this extremum is found to be maximum for sufficiently long cracks while minimum for the short ones. There is a borderline case when the ERR is independent of the loading angle. The phenomena mentioned is not observed in sandwiches, where the above extremum is always maximum (minimum) for the case of a stiffer (more compliant) middle layer.

In the specific case $\beta = 0$, when the crack is long, the results are found to be significantly different from those for arbitrary β . Thus, the phase shift angle, as well as the ERR, is found to be very sensitive to the value of β and to the direction of the applied loading. Consequently, results obtained for $\beta = 0$ and for $\varphi = 0$ should be used cautiously for predicting the fracture behavior in more general cases.

Further, for both interface and non-interface cracks in a periodically layered plane, the normalized ERR governing the stress intensity has been found to be a non-monotonic function of the crack length. This effect becomes more noticeable for the case when the layer thickness ratio is large. If the thicknesses of the layers with significant materials

mismatch are of the same order, then the sandwich approximation may be used with accuracy better than 4% only for the crack lengths below one fourth of the sandwiched layer thickness. This observation holds true independently of the crack location within the layer. On the other hand, for sufficiently long cracks, the ERR can be estimated by the use of the analytic formula obtained for the asymptotic semi-infinite crack case.

For a layered composite of finite or infinite thickness with an interface debonding, as opposed to the case of non-interface delamination, it appeared that increase of the thin layers stiffness can lead to increase of the absolute value of the SIF as well as to its decrease. Consequently, for a given geometric configuration there is a combination of elastic parameters corresponding to the maximal value. For the case of large material mismatch between sufficiently thin stiff layers and thick compliant ones, this maximum can significantly exceed the corresponding value for a crack in homogeneous material.

For the non-interface mixed-mode cracks in an infinite layered composite, the study of the SIFs behavior for the case of very thin stiff non-cracked layers revealed an interesting and somewhat unexpected phenomenon. Namely, it was found that K_{II} may vanish not only for the symmetric crack position at the layer midline but also in several additional ones, which are functions of the crack length. This, together with the fact that the midline can be an unstable location for some crack lengths, points out the possibility of wavy crack propagation. Another interesting phenomenon is the non-monotonic behavior of K_{II} as a function of the thickness of the thin non-cracked neighboring layers. It may be understood as the influence of a beam-like elements generated by these layers.

The semi-analytical solution of the fracture problem on a delamination crack in periodically layered composites presented herein, allows the implementation of the complete study of the fracture characteristics upon the geometric and elastic parameters. The closed form analytical expression for the Green's function employed in the solution of the present problems is very cumbersome but can be effectively worked out by the use of symbolic computation. Numerical difficulties in the solution of the system of singular integral equations arise only when the crack is long compared to the distance to the nearest interface. However, this disadvantage must not be overestimated, since when the distance is so small that it becomes comparable with the fracture process zone of the material, the total SIF approach to the fracture analysis fails (Ryvkin *et al.*, 1995).

Bibliography

- [1] Allix O. Ladeveze P, Corigliano A. (1995), Damage analysis of interlaminar fracture specimens. *Compos. Struct.*, **31**, 1, 6174.
- [2] Arata JJM, Kumar KS, Curtin WA, Needleman A. (2001) Crack growth in lamellar titanium aluminide *Int. J. Fract.*, **111**, 2, 163–189
- [3] Babuska I, Szabo BA, Actis RL. (1992) Hierarchy models for laminated composites. *Int J Numer Meth Eng*, **33**, 3, 503–535.
- [4] Barbero EJ, Reddy JN (1991) Modelling of delamination in composite laminates using a layer-wise plate-theory *Int. J. Solids Structures*, **28**, 3, 373–388
- [5] Barenblatt G.I. (1962), The mathematical theory of equilibrium cracks in brittle fracture. *Adv. Appl. Mech.*, **7**, 55129.
- [6] Bolotin V.V., Novitchkov Ju.N. (1980) Mechanics of multilayered structures. Moscow: Mashinostroenie. (in Russian)
- [7] Bolotin VV (1996), Delaminations in composite structures:its origin, buckling, growth and stability. *Composites*, **27B**, 129–145.
- [8] Bossavit A. (1986) Symmetry, groups, and boundary value problems—a progressive introduction to non-commutative harmonic analysis of partial differential equations in domain with geometric symmetry. *Comp Meth Appl Mech Engng*, **56**, 167–215.
- [9] Brillouin L. (1946) Wave Propagation in Periodic Structures. New York, Dover.
- [10] Budiansky B, Wu TT (1961) Transfer of load to sheet from a rivet-attached stiffener. *J. Math. Phys.*, **40**, 142-162.
- [11] Bufler H. (1998) The arbitrarily and the periodically laminated elastic hollow sphere: exact solutions and homogenization. *Archive of Applied Mechanics*, **68**, 9, 579–588
- [12] Bufler H. (2000) Planar elastic laminates and their homogenization *Acta Mechanica*, **141**, (1–2), 21–36.
- [13] Buryshkin ML. (1978) A general periodic problem in elasticity theory. *Prikladnaya Matematika i Mekhanika. transl. Applied Mathematics and Mechanics*, **42**, 3, 521–31.
- [14] Cao H. C. and Evans A.G. (1989) An experimental study of fracture resistance of bimaterial interfaces. *Mech. Mater.*, **7**, 295–305.
- [15] Carrera E and Demasi L (2002) Classical and advanced multilayered plate elements based upon PVD and RMVT. Part 1: Derivation of finite element matrices *Int J Numer Meth Eng*, **55**, 2, 191–231.

- [16] Charalambides P.G. (1991) Steady-state mechanics of delamination cracking in laminated ceramic-matrix composites. *Journal of American Ceramics Society* **74**, 3066–3080.
- [17] Chatterjee SN (1987) Three- and two-dimensional stress fields near delaminations in laminated composite plates. *Int J Solids Structures*, **23**, 11, 1535–1549.
- [18] Chai H. (1987), A note on crack trajectory in an elastic strip bounded by rigid substrates. *Int J Fract*, /bf32, 211–213.
- [19] Chai H. (2003) Fracture mechanics analysis of thin coatings under plane-strain indentation *Int J Solids Struct*, **40**, 3, 591–610.
- [20] Chen E.P. and Sih G.C. (1971) Interfacial delamination of a layered composite under anti-plane strain *Journal of Composite Materials*, **5**, 12–23.
- [21] Corigliano A, Ricci M. (2001), Rate-dependent interface models: formulation and numerical applications. *Int. J. Solids Struct*, **38**, 547-576.
- [22] Davies GAO, Robinson P, Robinson J, Eady D. 1997 Shear driven delamination propagation in two dimensions *Composites Part A*, **28A**, 757–765.
- [23] Davi G and Milazzo A (1999) Bending stress fields in composite laminate beams by a boundary integral formulation *Computers and Structures*, **71**, 3, 267–276.
- [24] Dean DL (1976) Diskrete field analysis of structural systems. CISM, Courses and Lectures No. 203, Udine
- [25] Dinkevich S. (1991) Finite symmetric systems and their analysis. *Int. J. Solids Structures*, **27**, 10, 1215–1253.
- [26] Drory M.D. and Thouless M.D. and Evans A.G. (1988) On the decohesion of residually stressed thin films. *Acta Met*, **36** 2019–2028.
- [27] Dugdale DS (1960), Yielding of steel sheets containing slits. *J. Mech. Phys. Solids*, **8**, 100104
- [28] Dyskin AV, Germanovich LN, Ustinov KB (2000) Asymptotic analysis of crack interaction with free boundary. *Int. J. Solids Struct.*, **37**, 857–886.
- [29] Eatwell GP, Willis JR (1982) The excitation of a fluid-loaded plate stiffened by a semi-infinite array of beams. *J Appl Math*, **29**, 247–270.
- [30] England AH (1965) A crack between dissimilar media *J Appl Mech*, **32**, 2, 400–402.
- [31] Erdogan F. (1969) Approximate solutions of systems of singular integral equations. *SIAM Journal of Applied Mathematics* **17**, 1041–1059.
- [32] Erdogan F, Gupta GD (1972) On the numerical solution of singular integral equations. *Quarterly of Applied Mathematics*, January, 525–534.
- [33] Erdogan F. and Gupta G. (1971a). The stress analysis of multi-layered composites with a flaw. *Int. J. Solids Struct*. **7**, 39–61.
- [34] Erdogan F. and Gupta G. (1971b). Layered composites with an interface flaw. *Int. J. Solids Struct.*, **7**, 1089–1107

- [35] Evans AG, Ruhle M, Dalgleish BJ, Charalambides PG. (1990), The fracture energy of bimaterial interfaces. *Mater Sci Engng*, **A 126**, 53–64
- [36] Fleck N.A., Hutchinson J.W. and Suo Z. (1991) Crack path selection in a brittle adhesive layer. *Int. J. Solids Struct.*, **27**, 13, 1683–1703.
- [37] Fuchs M.B. and Ryvkin M.(2002) Explicit exact analysis of infinite periodic structures under general loading. *Struct Multidisc Optim*, **23**, 268–279
- [38] Garg A.C. (1988) Delamination—a damage mode in composite structures. *Eng. Fract. Mech.* **29**, 557–584.
- [39] Gaudenzi P (1997) On delamination buckling of composite laminates under compressive loading. *Compos. Struct.*, **39**, 21–30.
- [40] Griffith AA, The theory of rupture. *Proceedings of the First International Congress of Applied Mathematics, Delft*, 1924, 5593.
- [41] Gutkowski W. (1974) Mechanical problems of elastic lattice structures. In: Kucheman, D. (ed.) Progress in aerospace science, Vol.15, Oxford, Pergamon.
- [42] Hao TH, Gong X and Suo Z (1996) Fracture mechanics for the design of ceramic multilayer actuators. *J Mech Phys Solids*, **44**, 1, 23–48
- [43] Healey TJ and Treacy JA (1991) Exact block diagonalization of large eigenvalue problems for structures with symmetry. *Int. J. Numer. Meth. Engng*, **67**, 257–296.
- [44] Her SC (2000) Fracture analysis of interfacial crack by global–local finite element Int J Fracture **106**, 2, 177–193.
- [45] Holleck H. and Schier V. (1995) Multilayer PVD coatings for wear protection, *Surface and Coatings Technology*, **76–77**, 328–336
- [46] Holleck H, Lahres M, Woll P. (1990) Multilayer coatings – influence of fabrication parameters on constitution and properties. *Surface and Coatings Technology*, **41**, 179–190.
- [47] Howard SJ, Pateras SK, Clyne TW (1998) Effect of interfacial adhesion on toughness of metal/ceramic laminates. *Materials Science and Technology*, **14**, 6, 535–541.
- [48] Hu M.S., Thouless M.D. and Evans A.G. (1988) The decohesion of thin films from brittle interface. *Acta Met*, **36**, 1301–1307
- [49] Huang H, Kardomateas GA (2001) Stress intensity factors for a mixed mode center crack in an anisotropic strip *Int. J. Fract.*, **108**, 367–381.
- [50] Hutchinson JW, Mear ME, Rice J.R. (1987) Crack paralleling an interface between dissimilar materials, *Journal of Applied Mechanics*, **54**, 828–832
- [51] Hutchinson JW, Suo Z. (1991) Mixed mode cracking in layered materials. *Advances in Applied Mechanics*, **29**, J.W. Hutchinson and T.Y. Wu (eds.), 63–191.
- [52] Irwin G.R.(1957) Analysis of stresses and strains near the end of a crack traversing a plane. *J. Appl. Mech.*, **24**, 361–364.
- [53] Jha M., Charalambides P.G. (1998) Crack–tip micromechanical fields in layered elastic composites: crack parallel to the interfaces. *Int. J. Solids Struct.*, **35**, 149–79.

- [54] Kaczyński A., Matysiak S. (1988) On crack problems in periodic two-layered elastic composites. *Int. J. Fract.*, **37**, 31–45.
- [55] Kaczyński A., Matysiak S. (1989) A system of interface cracks in a periodically layered composite, *Engineering Fracture Mechanics*, **32**, 5, 745–756
- [56] Kaczyński A., Matysiak SJ. (1995), Analysis of stress intensity factors in crack problems of periodic two-layered elastic composites. *Acta Mechanica*, **110**, 1–4, 95–110.
- [57] Kaczyński A., Matysiak S.J. and Pauk V.I. (1994) Griffith crack in a laminated elastic layer. *Int. J. Fract.*, **67**, R81–R86.
- [58] Kamysheva GA, Nuller BM, Ryvkin MB. (1982) Deformation of an elastic plane reinforced by a periodic system of nonperiodically loaded oblique semi-infinite stringers. *Mechanics of Solids*, **17**,3 104–109
- [59] Kangwai RD, Guest SD and Pellegrino S. (1999) An introduction to the analysis of symmetric structures *Computers and Structures*, **71**, 6, 671–688
- [60] Kant T, Kommineni JR (1994) Large-amplitude free-vibration analysis of cross-ply composite and sandwich laminates with a refined theory and c(0) finite-elements. *Computers and Structures*, **50**, 1, 123–134
- [61] Karpenko L.N. (1966) Approximate solution of a singular integral equation by means of Jacobi polynomials. *Journal of Applied Mathematics and Mechanics (PMM)*, **30**, 668–675.
- [62] Karpov EG, Dorofeev DL and Stephen NG (2002a) Characteristic solutions for the statics of repetitive beam-like trusses. *Int. J. Mech. Sciences*, **44**, 7, 1363–79.
- [63] Karpov EG, Stephen NG and Dorofeev DL. (2002b) On static analysis of finite repetitive structures by discrete Fourier transform. *Int. J. Solids Struct.*, **39**, 16, 4291–310.
- [64] Klein CA (2001) Normal and interfacial stresses in thin-film coated optics: the case of diamond-coated zinc sulfide windows. *Optical Engineering*, **40**, 6, 1115–1124
- [65] Konishi Y, Atsumi a. 1973, Crack problem of transversely isotropic strip. *Int J Eng Sci*, **11**, 1, 9–20.
- [66] Kovar D., Thouless M.D. and Halloran J.W. (1998) Crack deflection and propagation in layered silicon nitride/boron nitride ceramics. *J. of the American Ceramic Society*, **81**, 1004–12.
- [67] Kriven WM, Lee SJ. (2001) Toughened Oxide Composites Based on Porous Alumina-Platelet Interphases. *J. Am. Ceram. Soc.*, **84**, 4, 76774.
- [68] Kucherov LV, Chebakov MI. (1991) Generalized periodic contact problem of elasticity for a ring. *Mechanics of Solids*, **4**, 108–115.
- [69] Kucherov L. and Ryvkin M. (2002) Interface crack in periodically layered bimaterial composite, *Int. J. Fract.*, **117**, 2, 175–194.
- [70] Langley RS, Bardell NS, Ruivo HM (1997) The response of two-dimensional periodic structures to harmonic point loading: a theoretical and experimental study of a beam grillage. *J. Sound Vib.* **207**, 521–535

- [71] Langley RS (1999) Wave evolution, reflection, and transmission along inhomogeneous waveguides *J. Sound Vib.*, **227**, 1, 131–158.
- [72] Lax Melvin (1974), Symmetry principles in solid state and molecular physics, New York: Wiley, 499 p.
- [73] Li D. and Benaroya H. (1996) Wave propagation and localization in disordered periodic laminated materials, *Composite Structures*, **36**, 1–2, 59–70.
- [74] Li Jia. (2000) Debonding of the interface as ‘crack arrestor’. *Int J Fract*, **105**, 1, 57–79.
- [75] Lin H.J. and Lee Y.J. (1990) Impact induced fracture of laminated plates and shells. *J. Compos. Mater.*, **24** 1179–1199.
- [76] Liu DS, Lan X, Lu XQ (1994) Stress–analysis of imperfect composite laminates with an interlaminar bonding theory *Int J Numer Meth Eng*, **37**, 16, 2819–2839.
- [77] Loader CB, Howard SJ, Kulikowski Z, Dunford DV and Ward–Close CM (1996) Iron and aluminium micro– and nano–laminates produced by high rate physical vapour deposition. Synthesis/Processing of Lightweight Metallic Materials II. Proceedings of a Symposium held during TMS Annual Meeting. 137–48.
- [78] Lu XC, Shi B, Li M, et al. (2001) Microstructure and properties of Fe–N/Ti–N magnetic multilayers *Surf Interface Anal*, **32**, 1, 66–69
- [79] Malishev B.M. and Salganik, R.L. (1965) The strength of adhesive joints using the theory of crack. *Int. J. Fract. Mech.*, **1**, 114–128.
- [80] Markaki AE, Clyne TW (2002) Energy absorption during failure of layered metal foam/ceramic laminates. *Mat Sci Eng A–Struct*, **323**, (1–2), 260–269.
- [81] Mead DJ (1996) Wave propagation in continuous periodic structures: research contributions from Southampton, 1964–1995. *Journal of Sound and Vibration*, **190**, 3, 495–524.
- [82] Melin LG, Schon J (2001) Buckling behaviour and delamination growth in impacted composite specimens under fatigue load: an experimental study. *Compos Sci Technol*, **61**, 13, 1841–52.
- [83] McNaney J.M., Cannon R.M., Ritchie R.O. (1994) Near–interfacial crack trajectories in metal–ceramic layered structures *Int. J. Fract.* **66**, 3, 227–240
- [84] Mi Y, Crisfield MA, Davies GAO. (1998) Progressive delamination using interface elements. *J. Compos. Mater.*, **32**, 1246–272.
- [85] Moses E, Ryvkin M, Fuchs MB 2001, A finite element methodology for the static analysis of infinite periodic structures under general loading. *Comput Mech* **27**, 5, 369–377
- [86] Nakhmein EL, Nuller BM, Ryvkin MB. (1981) Deformation of a composite elastic plane weakened by aperiodic system of the arbitrarily loaded slits. *J Appl Math Mech*, **45**, 6, 821–826.
- [87] Nilsson KF, Thesken JC, Sindelar P, Giannakopoulos AE, Storakers B. (1993) A theoretical and experimental investigation of buckling induced delamination growth. *J. Mech. Phys. Solids* **41**, 749–782.

- [88] Noor A.K. (1988) Continuum modelling for repetitive lattice structures. *Applied Mechanics Reviews*, **41**, 7, 285–296.
- [89] Nuller B. (1981) On the elastic deformation of a layered plate and a half-space. In *Proceedings of the State Hydraulic Institute*, **151**, 25–30. Energia, Leningrad, in Russian.
- [90] Nuller B., Ryvkin M. (1980) On boundary value problems for elastic domains of a periodic structure deformed by arbitrary loads. Proc. of the State Hydraulic Institute, Vol. 136, 49–55. Leningrad: Energia (in Russian)
- [91] Nuller BM, Ryvkin MB. (1983), Nonsymmetric bending of a plate reinforced by a symmetric system of radial ribs. *J Appl Math Mech*, **47**, 3, 395–402.
- [92] O'Brien MJ. Capaldi FM. Sheldon BW. (2000) A layered alumina composite tested at high temperature in air. *Journal of the American Ceramic Society*, vol.83, no.12, 3033–40.
- [93] Ohashi Y., Wolfenstine J., Koch R. and Sherby, O.D.,(1992) Fracture behavior of a laminated steel–brass composite in bend tests. *Mat Sci Eng A–Struct*, **151**, 1, 37–44.
- [94] Pagano NJ. 1978. Stress fields in composite laminates. *Int J Solids Struct*, 14 , 385–400.
- [95] Postma G.W. (1955) Wave propagation in stratified medium, *Geophysics*, **20**, 780–806.
- [96] Pritchard J, Bowen CR, Lowrie F (2001) Multilayer actuators: review *Brit. Ceram. T* **100**, 6, 265–273.
- [97] Renton JD (1964) A finite difference analysis of the flexural–torsional behavior of grillages. *Int. J. Mech. Sciences*, **6** , 209–224.
- [98] Renton JD (1996) Generalized beam theory and modular structures *Int. J. Solids Struct.* **33**, 10, 1425–1438.
- [99] Rice J.R. (1988) Elastic fracture mechanics concepts for interfacial cracks. *Journal of Applied Mechanics*, **55**, 98–103.
- [100] Rice J.R. and Sih, G.C. (1965) Plane problems of cracks in dissimilar media. *Journal of Applied Mechanics*, **32**, 418–423.
- [101] Roeder BA and Sun CT (2001) Dynamic penetration of alumina/aluminum laminates: experiments and modeling. *International Journal Of Impact Engineering*, **25**, 2, 169–185.
- [102] Ryvkin M. (1996) Mode III crack in a laminated medium. *Int. J. Solids Struct.* **33**, No.24, 3611–3625.
- [103] Ryvkin M. (1998) Antiplane deformation of a periodically layered composite with a crack. A non–homogenization approach. *Int. J. Solids Struct.*, **35**, 522–526.
- [104] Ryvkin M.(1999) A mode I crack paralleling interfaces in a periodically layered composite. *Int. J. Fract.*, **99**, 3, 173–188.
- [105] Ryvkin M. (2000) K–Dominance zone for a semi-infinite mode I crack in a sandwich composite. *Int. J. Solids Struct.*, **37**, 35 , 4825–4840.

- [106] Ryvkin M, Fuchs MB, Nuller B (1999) Optimal design of infinite repetitive structures *Struct Optimization* **18**, (2–3), 202–209.
- [107] Ryvkin M., Kucherov L. (2000) Mixed mode crack in a periodically layered composite. *Int. J. Fract.*, **106**, 373–389.
- [108] Ryvkin M., Kucherov, L. (2001) An inverse shielding effect in a periodically layered composite. *Int. J. Fract.*, **108**, L3–L8.
- [109] Ryvkin M.B., Nuller B.M. (1987) Boundary–Value problems for the domains contained in Non–homogeneous Translation–Symmetric Space, *Izvestia VNIIG*, **202**, 11–14, (in Russian)
- [110] Ryvkin M., Nuller, B. (1997) Solution of Quasi–Periodic Fracture Problems by Representative Cell Method. *Computational Mechanics*, **20**, 145–149.
- [111] Ryvkin M, Slepyan L, Banks–Sills L. (1995) On the scale effect in the thin layer delamination problem. *Int. J. Fract.*, 71, 247–271.
- [112] Sackman JI, Kelly Jm and Javid Ae (1989) A Layered Notch Filter For High–Frequency Dynamic Isolation. *J Pressure Vessel Technology – T ASME* **111**, 1, 17–24.
- [113] Samartin A. (1988) Analysis of spatially periodic structures application to shell and spatial structures. Proc. Int. Symp. on Innovative Applications of Shells and Spatial Forms (held in Bangalore, India), 205221. New Delhi: Oxford IBH Publishing
- [114] Sbaizero O. and Evans A.G. (1986) Tensile and shear properties of laminated ceramic matrix composites. *Journal of American Ceramic Society*, **69**, 481–486.
- [115] Schoeppner GA, Pagano NJ (1998) Stress fields and energy release rates in cross–ply laminates *Int J Solids Structures*, **35**, 11, 1025–1055.
- [116] Schreiber J, Melov V and Dietsch R (2002) Stress development in Ni/C–multilayers on Si–substrates with increasing period number. ECRS 6: Proceedings Of The 6th European Conference On Residual Stresses Materials Science Forum 404–4, 797–802.
- [117] Selvadurai APS, Lan Q. (1998) Axisymmetric mixed boundary value problems for an elastic halfspace with a periodic nonhomogeneity, *Int J Solids Struct*, **35**, 15, 1813–1826
- [118] Sheinman I, Kardomateas GA (1997) Energy release rate and stress intensity factors for delaminated composite laminates *Int J Solids Struct*, **34**, 4, 451–459.
- [119] Shen S, Kuang ZB and Hu S (1999) On interface crack in laminated anisotropic medium. *Int J Solids Structures*, **36**, 4251–4268.
- [120] Short GJ, Guild FJ and Pavier MJ (2002) Delaminations in flat and curved composite laminates subjected to compressive load. *Composite Structures*, **58**, 2, 249–258.
- [121] Sih, G.C. and Chen, E.P. (1981) Cracks in composite materials. In *Mechanics of Fracture* (Edited by Sih G.C.), **6**, Martinus Nijhoff, the Hague.
- [122] Sih G.C., Paris P.C. and Irwin G.R. (1965) On cracks in rectilinearly anisotropic bodies. *Int. J. Fract.*, **1**, 189–203.

- [123] Slepyan L (1974) Crack in a layered medium. Selected Problems of Applied Mechanics, pp.557–54. Viniti, Moskow (in Russian)
- [124] Slepyan L (1988) Some basic aspects of crack dynamics. In Cherepenov G (ed) Fracture: A Topical Encyclopedia of Current Knowledge Dedicated to Alan Arnold Griffith, pp.620–621. Krieger Publishing Company, Melbourne.
- [125] Soldatos KP and Shu XP (2002) Improving the efficiency of finite element formulations in laminated composites *Communications In Numerical Methods In Engineering*, **18**, 9, 605–613.
- [126] Suga T., Elssner G. and Schmauder S. (1988) Composite parameters and mechanical compatibility of material joints. *Journal of Composite Materials*, **22**, 917–934.
- [127] Suo Z (1990), Delamination specimens for orthotropic materials. *J Appl Mech*, **57**, 627–634.
- [128] Suo Z and Hutchinson JW. (1989a) Steady–state cracking in brittle substrates beneath adherent films. *Int. J. Solids Struct.*, **25**, 11, 1337–1383.
- [129] Suo Z and Hutchinson JW (1989b) Sandwich test specimens for measuring interface crack toughness. *Mater Sci Engng*, **A107**, 135–143.
- [130] Suo Z and Hutchinson JW (1990) Interface crack between two elastic layers. *Int J Fract*, **43**, 1–18.
- [131] Thouless M.D., Evans A.G. and Ashby M.F. and Hutchinson, J.W. (1987) The edge cracking and spalling of brittle plates. *Acta Met*, **35**, 1333–1341.
- [132] Toya M., Aritomi M., Chosa M. Energy release rates for an interface crack embedded in a laminated beam subjected to three–point bending. *J Appl Mech –Trans ASME*, **64**, 2, 1997, 375–82.
- [133] Uflyand I.S. (1968) Integral Transforms in Problems of the Theory of Elasticity. Nauka, Leningrad. (in Russian).
- [134] Vaamonde AJV (1993) Impact Properties Of Multilayered Materials. *Journal De Physique*, IV 3 C7, 773–781 Part 1
- [135] Vel SS, Batra RC (2000) The generalized plane strain deformations of thick anisotropic composite laminated plates. *Int J Solids Struct* **37**, 5, 715–733.
- [136] Voleti SR, Chandra N and Miller JR (1996) *Computers and Structures*. **58**, 3, 453–464.
- [137] Vorovich I.I., Kucherov LV, Chebakov MI. V–resonances in the problem of steady–state stamp oscillations on the periodic layer surface. Mechanics of Solids, N3, 1992. p.95–100. (in Russian)
- [138] Vorovich I.I., Kucherov LV. and Chebakov MI.(1994) Dynamic characteristics of the periodic layer. *Izv. VYZov North–Caucasian region. Special edition*, 87–89. (in Russian)
- [139] Wah T, Calcote LR (1970) Structural Analysis by Finite Difference Calculus. Van Nostrand, NY

- [140] Wang J.-S and Suo Z. (1990) Experimental determination of interfacial toughness curves using brazil nut sandwiches. *Acta Metall. Mater.*, **38**, 1279–1290.
- [141] Wang YM, Tarn JQ and Hsu CK (2000), State space approach for stress decay in laminates. *Int J Solids Struct*, **37**, 26, 3535–3553.
- [142] Whitney J.M., (1987) Structural Analysis of Laminated Anisotropic Plates. Technomic, Lancaster, PA.
- [143] Williams JF, Stouffer DC, Ilic S, Jones R (1986) An analysis of delamination behaviour. *Compos. Struct.*, **5**, 203–216.
- [144] Williams JG (1988) On the calculation of energy–release rates for cracked laminates. *Int. J. Fract.*, **36**, 2, 101–119.
- [145] Williams M.L. (1959) The stress around a fault or crack in dissimilar media. *Bull Seismol Soc Am*, **49**, 199–204.
- [146] Williams M.L. (1957) On the stress distribution at the base of a stationary crack. *J Appl Mech*, **24**, 109–114.
- [147] Williams TO, Addessio FL (1997) A general theory for laminated plates with delaminations *Int J Solids Struct*, **34**, 16, 2003–24.
- [148] Yang J, Kahn H, He A-Q, Phillips SM, Heuer AH. (2000) A New Technique for Producing Large–Area as–Deposited Zero–Stress LPCVD Polysilicon Films: The Multipoly Process, *J. MEMS*, **9**, 485–494.
- [149] Zhong W.X. and Williams F.W. (1995) On the direct solution of wave propagation for repetitive structures. *Journal of Sound and Vibration*, **181**,3, pp485–501.
- [150] Zhuang SM, Ravichandran G. and Grady DEW (2003) An experimental investigation of shock wave propagation in periodically layered composites, *J. Mech. and Phys. of Solids*, **51**, 2, 245–265.
- [151] Zou Z, Reid SR, Soden PD, et al. (2001) Mode separation of energy release rate for delamination in composite laminates using sublaminates *Int J Solids Struct*, **38**, 15, 2597–2613
- [152] Zou Z, Reid SR, Li S. (2003), A continuum damage model for delaminations in laminated composites. *J Mech Phys Solids*, **51**, 2, 333–356.

Appendix A

A.1 Matrix M

The following is the expression for the eighth order square matrix \mathbf{M} of the system (2.42,) of algebraic equations in A_j , $j = 1, \dots, 8$, obtained when satisfying the boundary conditions for the representative bi-layered cell (2.31), (2.32).

$$\mathbf{M} = \begin{bmatrix} \mu c_1 & -\mu s_1 & -\mu z_1 c_1 & \mu z_1 s_1 & -\gamma_m c_2 & -\gamma_m s_2 & -\gamma_m z_2 c_2 & -\gamma_m z_2 s_2 \\ \mu s_1 & \mu c_1 & -\mu d_1 & \mu e_1 & \gamma_m s_2 & -\gamma_m c_2 & \gamma_m d_2 & \gamma_m e_2 \\ -\hat{\mu} c_1 & \hat{\mu} s_1 & \hat{\mu} z_1 c_1 + \frac{\eta_1}{2} s_1 & \frac{\eta_1}{2} c_1 - \hat{\mu} z_1 s_1 & 0 & 0 & \frac{\gamma_m \eta_2}{2} s_2 & -\frac{\gamma_m \eta_2}{2} c_2 \\ \hat{\mu} s_1 & \hat{\mu} c_1 & -\hat{\mu} z_1 s_1 - \check{\eta} c_1 & \check{\eta} s_1 - \hat{\mu} z_1 c_1 & 0 & 0 & \frac{\gamma_m \eta_1}{2} c_2 & \frac{\gamma_m \eta_1}{2} s_2 \\ -\mu & 0 & 0 & 0 & 1 & 0 & 0 & 0 \\ 0 & -\mu & \mu k_1 & 0 & 0 & 1 & -k_2 & 0 \\ -2 & 0 & 0 & -\eta_1 & 2 & 0 & 0 & \eta_2 \\ 0 & 2 & -\zeta_1 & 0 & 0 & -2 & \zeta_2 & 0 \end{bmatrix}$$

where

$$\begin{aligned} z_i &= h_i z, & c_i &= \cos z_i, & s_i &= \sin z_i \\ \eta_i &= \kappa_i + 1, & \zeta_i &= \kappa_i - 1, & \check{\eta} &= \mu \kappa_1 - \zeta_1 / 2, & \hat{\mu} &= \mu - 1 \\ d_i &= \kappa_i c_i + z_i s_i, & e_i &= \kappa_i s_i - z_i c_i, & i &= 1, 2 \end{aligned}$$

A.2 Matrix S for the stress boundary conditions

The stress jump transforms in the case of the prescribed tractions at the strip edges are determined from the system of equations (2.44). The elements of corresponding matrix \mathbf{S} are presented on the imaginary axis $z = it$

$$s_{ij} = \frac{\hat{s}_{ij}}{\det(\mathbf{M})}$$

where

$$\begin{aligned} \det(\mathbf{M}) &= \eta_4 (\gamma_m^4 + 1) + 4 \eta_4 (\hat{\mu} (\lambda_0 - 2 h_1 h_2 \hat{\mu} t^2) C_3 - \lambda_{12} C_4) g_1 \gamma_m \\ &\quad - (4 \lambda_{12} \lambda_0 (C_2 + C_1) \hat{\mu} - 2 \lambda_{12}^2 C_6 - 2 \hat{\mu}^2 \lambda_0^2 C_5 \\ &\quad - 4 (\lambda_0 \hat{\mu} + (\kappa_2 \kappa_1 + 1) \mu) (\mu^2 \kappa_1 + \kappa_2) - 4 \mu^2 ((\kappa_2^2 + \eta_2) (\kappa_1^2 + \eta_1) + 3 \kappa_2 \kappa_1) \\ &\quad - 4 t^2 (4 h_{12}^2 t^2 + \lambda_7 - 2 (h_1^2 C_2 \lambda_1^2 + h_2^2 C_1 \lambda_2^2) \hat{\mu}^2)) \gamma_m^2 \end{aligned}$$

and

$$\begin{aligned}
\hat{s}_{11} &= \eta_4 \gamma_m (2t \hat{\mu} ((h_1 \kappa_2 - h_2) \gamma_m^2 + \mu (h_1 - \kappa_1 h_2)) S_3 + 2t (\lambda_1 h_1 + \lambda_2 h_2) (\gamma_m^2 - \mu) S_4 \\
&\quad - (n_2 g_1 + 2 \lambda_{12}) C_4 - (4 h_1 h_2 \hat{\mu} (\hat{\mu} - g_1) t^2 + n_3 g_1 - 2 \lambda_0 \hat{\mu}) C_3) + (\\
&\quad 2t \hat{\mu} \eta_4 (\lambda_2 h_2 S_1 + h_1 \lambda_1 S_2) - 4 \hat{\mu} (h_2^2 \lambda_2 \lambda_8 C_1 + \lambda_1 n_1 h_1^2 C_2) t^2 \\
&\quad + (C_2 + C_1) (\lambda_1 (\lambda_2^2 + \hat{\mu} \eta_2) + (-\hat{\mu} \kappa_2 \lambda_0 + n_1 \lambda_1) \lambda_2) + \lambda_{12} n_2 C_6 - \lambda_0 \hat{\mu} n_3 C_5 \\
&\quad - 16 h_1^2 h_2^2 \hat{\mu}^3 t^4 + 4 \hat{\mu} (\lambda_1 n_1 h_1^2 - \eta_4 h_1 h_2 (3 - \mu) + \lambda_2 \lambda_8 h_2^2) t^2 + 2 \eta_4^2 \\
&\quad - \eta_4 \lambda_0 - \hat{\mu} (\kappa_2 \lambda_2 - \lambda_0) (\lambda_1 - \lambda_0) \gamma_m^2 + \eta_4^2 \\
\hat{s}_{13} &= i \eta_4 \gamma_m ((4 h_1 h_2 \hat{\mu} (\gamma_m^2 + \mu) t^2 + \mu g_1 (\kappa_2 - \kappa_1)) S_3 - \mu g_1 (\kappa_2 \kappa_1 - 1) S_4 \\
&\quad - 2t (\lambda_1 h_1 + \lambda_2 h_2) (\gamma_m^2 + \mu) C_4 - 2t \hat{\mu} ((h_2 + h_1 \kappa_2) \gamma_m^2 - \mu (\kappa_1 h_2 + h_1)) C_3) + \\
&\quad i \mu \gamma_m^2 (\eta_1 ((4 t^2 h_2^2 - \kappa_2) \lambda_2 \hat{\mu} + \lambda_1 \lambda_0) S_1 - \eta_2 ((4 t^2 \lambda_1 h_1^2 - \kappa_1) \lambda_1 \hat{\mu} + \lambda_0 \lambda_2) S_2 \\
&\quad + \lambda_0 \hat{\mu} (\kappa_2 - \kappa_1) S_5 + \lambda_{12} (\kappa_2 \kappa_1 - 1) S_6 + \\
&\quad 2t (\hat{\mu} h_1 \zeta_2 \lambda_1 \eta_1 C_2 - \hat{\mu} \eta_2 \lambda_2 \zeta_1 h_2 C_1 + 4 h_{12} (\eta_1 h_2 + h_1 \eta_2) t^2 + \eta_5)) \\
\hat{s}_{21} &= -\hat{s}_{13} + 4I t \gamma_m (-\eta_4 (\lambda_1 h_1 + \lambda_2 h_2) (\gamma_m^2 + \mu) C_4 \\
&\quad - \eta_4 \hat{\mu} ((\kappa_2 \gamma_m^2 - \mu) h_1 + (\gamma_m^2 - \mu \kappa_1) h_2) C_3 + \\
&\quad \gamma_m \mu (\hat{\mu} h_1 \zeta_2 \lambda_1 \eta_1 C_2 - \hat{\mu} \eta_2 \lambda_2 \zeta_1 h_2 C_1 + 4 h_{12} (\eta_1 h_2 + h_1 \eta_2) t^2 + \eta_5)) \\
\hat{s}_{23} &= \hat{s}_{11} - 4t \gamma_m \eta_4 (\hat{\mu} ((\mu + \kappa_2 \gamma_m^2) h_1 - (\mu \kappa_1 + \gamma_m^2) h_2) S_3 \\
&\quad + (\gamma_m^2 - \mu) (\lambda_1 h_1 + \lambda_2 h_2) S_4 + \hat{\mu} \gamma_m (\lambda_2 h_2 S_1 + h_1 \lambda_1 S_2))
\end{aligned}$$

with

$$\begin{aligned}
g_1 &= 1 + \gamma_m^2, & h_{12} &= h_1 h_2 \hat{\mu}^2, & \eta_4 &= \mu \eta_1 \eta_2, \\
\lambda_0 &= \mu \kappa_1 - \kappa_2, & \lambda_1 &= \mu + \kappa_2, & \lambda_2 &= \mu \kappa_1 + 1, \\
\lambda_7 &= 2 \hat{\mu}^2 (\lambda_1^2 h_1^2 + 2 \eta_4 h_2 h_1 + \lambda_2^2 h_2^2), & \lambda_8 &= \hat{\mu} - \lambda_2, & \lambda_{12} &= \lambda_1 \lambda_2, \\
n_1 &= \hat{\mu} \kappa_2 - \lambda_1, & n_2 &= \kappa_2 \lambda_2 + \lambda_1, & n_3 &= \lambda_0 + \hat{\mu} \kappa_2, & C_1 &= \cosh 2th_1, \\
C_2 &= \cosh 2th_2, & C_3 &= \cosh t(h_1 - h_2), & C_4 &= \cosh th, & C_5 &= \cosh 2t(h_1 - h_2), \\
C_6 &= \cosh 2th, & S_1 &= \sinh 2th_1, & S_2 &= \sinh 2th_2, & S_3 &= \sinh t(h_1 - h_2), \\
S_4 &= \sinh th, & S_5 &= \sinh 2t(h_1 - h_2), & S_6 &= \sinh 2th, \\
\eta_5 &= \eta_1 (\mu \eta_2^2 + \lambda_1^2 - \hat{\mu}^2 \kappa_2) h_1 + \eta_2 (\mu \eta_1^2 + \lambda_2^2 - \hat{\mu}^2 \kappa_1) h_2
\end{aligned}$$

A.3 Fredholm kernels. Interface debonding

The coefficients defining expression (5.18) in the kernels of the integral equation for the interface crack in the periodically layered space are given by following:

$$\begin{aligned}
e_{11}^2 &= -\beta, & e_{12}^2 &= 1, & e_{22}^2 &= 0, \\
d_0 &= 4(4h_{12}^2 z^4 + \lambda_7 z^2 + \eta_3(\lambda_1^2 + \hat{\mu}^2) - \hat{\mu}\lambda_5\lambda_6 - \lambda_{12}\hat{\mu}\lambda_1)E^2 + \lambda_{12}^2(E^4 + 1) \\
&\quad - 2\hat{\mu}\lambda_2\hat{E}_1(2h_2^2\hat{\mu}\lambda_2 z^2 + \lambda_1\lambda_0) - 2\hat{\mu}\lambda_1\hat{E}_2(2h_1^2\hat{\mu}\lambda_1 z^2 + \lambda_2\lambda_0) + \hat{\mu}^2\lambda_0^2 e \\
d_1 &= -4\eta_4(E_4(2h_{12}z^2 - \hat{\mu}\lambda_0) + \lambda_{12}E_3), & d_2 &= 2\eta_4^2 E^2 \\
e_{11}^0 &= \beta\{\lambda_2\eta_2(4z^2\hat{\mu}\lambda_2^2 h_2^2\lambda_4 - \lambda_6)\hat{E}_2 + \lambda_6(4z^2\hat{\mu}\lambda_1^2 h_1^2\lambda_4 - \lambda_2\eta_2)\hat{E}_1 + \hat{\mu}\eta_4\lambda_0 e \\
&\quad - 8\hat{\mu}z^2\lambda_4[2(h_{12}(\lambda_2\eta_2 + \lambda_6)z^2 + \eta_4\lambda_6^-)h_2 h_1 + h_1^2\lambda_1^2\lambda_6 + \lambda_2^3\eta_2 h_2^2]E^2 \\
&\quad - 2\eta_2(\lambda_5\lambda_6 - 2\eta_3\hat{\mu})E^2\} \\
e_{12}^0 &= 2\lambda_{12}^2 E^4 + 4[4h_{12}^2 z^4 + \lambda_7 z^2 + (\eta_3 - \lambda_2\hat{\mu})\lambda_1^2 - \hat{\mu}\lambda_5\lambda_6 + \eta_3\hat{\mu}^2]E^2 \\
&\quad + \lambda_3\{\lambda_2\eta_2(4z^2\hat{\mu}\lambda_2^2 h_2^2 + \lambda_8\lambda_1^2 + \lambda_6\lambda_2)e_2 \\
&\quad - \lambda_2[2\lambda_2 h_2^2\hat{\mu}(2\lambda_5\lambda_1 + 2\lambda_2\hat{\mu})z^2 - \lambda_2^+\lambda_1^3 + (\eta_3 + 2\hat{\mu}^2)\lambda_1^2 + 3\hat{\mu}\lambda_6\lambda_2]e_1 E^2 \\
&\quad - \lambda_1[4\hat{\mu}\lambda_1 h_1^2(\lambda_8\lambda_1 + 2\lambda_2\hat{\mu})z^2 + \lambda_2(\lambda_2^-\lambda_1^2 + \lambda_8\lambda_2^+\lambda_1 + 3\mu\eta_1\hat{\mu}\lambda_2)]e_2 E^2 \\
&\quad - \lambda_6(4z^2\hat{\mu}\lambda_1^2 h_1^2 + \lambda_2\lambda_9)e_1 - \eta_2\hat{\mu}(\lambda_8\lambda_1 + \mu\eta_1\lambda_2)\lambda_0 e_2^2 + \mu\eta_1\hat{\mu}\lambda_9\lambda_0 e_1^2\} \\
e_{22}^0 &= 4\lambda_{12}z\lambda_3\{4h_{12}(\eta_2 h_1 + h_2\mu\eta_1)z^2 E^2 + \eta_2 h_2[2\eta_3 E^2 + \lambda_2\hat{\mu}(\hat{E}_2 - 2E^2)]\} \\
&\quad + \mu\eta_1 h_1[\hat{\mu}\lambda_1(2E^2 - \hat{E}_1) + 2\eta_2^2 E^2]\} \\
e_{11}^1 &= 2\beta\mu\eta_2\eta_1[(4h_1 h_2\hat{\mu}\lambda_6^- z^2\lambda_4 - 2\hat{\mu}\lambda_0 + \lambda_{12})E_4 + \lambda_{12}E_3] \\
e_{12}^1 &= 2\eta_4\{[-4\hat{\mu}h_2 h_1\lambda_6^+ z^2 + (\lambda_{12} - 2\lambda_6 + \eta_3 + \hat{\mu}^2)\lambda_1]\lambda_3 e_1 E + 2\mu\eta_1\hat{\mu}\lambda_2\lambda_3 E_4 \\
&\quad + [4h_1 h_2\hat{\mu}(\lambda_{12} - \frac{\hat{\mu}}{\lambda_3})z^2 + (\lambda_{12} - 2\hat{\mu}\lambda_1 + 3\hat{\mu}^2 - \eta_3)\lambda_1]\lambda_3 e_2 E - \lambda_{12}(2E^3 + E_3)\} \\
e_{22}^1 &= -4\lambda_6\lambda_2\lambda_3 z\eta_2[(\lambda_1 h_1 + \lambda_2 h_2)E_3 - \hat{\mu}(h_1 - h_2)E_4]
\end{aligned}$$

with

$$\begin{aligned}
\eta_3 &= \eta_1^2 \mu^2, & \lambda_2^\pm &= \lambda_2 \pm 3\hat{\mu} & \lambda_3 &= (\lambda_1 + \lambda_2)^{-1}, & \lambda_4 &= (\lambda_1 - \lambda_2)^{(-1)}, \\
\lambda_5 &= \lambda_2 + 2\hat{\mu}, & \lambda_6 &= \mu\lambda_1\eta_1, & \lambda_6^\pm &= \lambda_6 \pm \lambda_2\hat{\mu}, & \lambda_9 &= \lambda_6^+ - \lambda_1^2, \\
E &= e^{-zH}, & e_i &= e^{-2zh_i}, & E_i &= e_i E, & E_3 &= E + E^3, \\
E_4 &= E_1 + E_2, & e &= e_1^2 + e_2^2, & \hat{E}_i &= e_i + e_{3-i}E^2, & & i = 1, 2
\end{aligned}$$

A.4 Fredholm kernels. Intra-layer delamination

The kernels (6.17) of the integral equation for the non-interface crack in the periodically layered space contain functions $k_{ij}(z, \varphi)$, which have the structure similar to that in the interface crack case.

$$k_{ij}(z, \phi) = \frac{1}{\pi} \int_0^\pi \frac{a_{ij} + b_{ij} \cos \phi + c_{ij} \cos 2\phi}{d_0 + d_1 \cos \phi + d_2 \cos 2\phi} d\phi, \quad i, j = 1, 2; \quad (\text{A.1})$$

where

$$\begin{aligned} d_0 &= 4\hat{\mu}^2 \lambda_0^2 \cosh 2z(h_1 - h_2) + 8\lambda_2 \hat{\mu} (2\lambda_2 h_2^2 z^2 \hat{\mu} + \lambda_0 \lambda_1) \cosh 2zh_1 \\ &\quad + 8\hat{\mu} \lambda_1 (2z^2 h_1^2 \hat{\mu} \lambda_1 + \lambda_2 \lambda_0) \cosh 2zh_2 - 4\lambda_{12}^2 \cosh 2zh \\ &\quad - 32h_{12}^2 z^4 - 8\lambda_7 z^2 - 8\mu^2 [\eta_1 \eta_2 (\kappa_2 + \kappa_1) + 1 + 4\kappa_2 \kappa_1 + \kappa_1^2 \kappa_2^2] \\ &\quad - 32\mu \bar{\nu}_1 \bar{\nu}_2 (\mu^2 \kappa_1 + \kappa_2) - 8\kappa_1^2 \mu^4 - 8\kappa_2^2, \\ d_1 &= 16\eta_4 \{ \hat{\mu} (2\hat{\mu} h_2 h_1 z^2 - \lambda_0) \cosh z(h_1 - h_2) + \lambda_{12} \cosh zh \}, \\ d_2 &= -(2\eta_4)^2. \end{aligned}$$

The explicit expressions of the coefficients a_{ij} for the case $i = j = 1$ are

$$\begin{aligned} a_{11} &= -8(\hat{\mu} \lambda_1 (h_2^c z)^2 + \bar{\lambda}_3) [\hat{\mu} \lambda_0 \cosh 2z(h_2 - h_1^c) + \lambda_{12} \cosh 2z(h_2 + h_1^c)] \\ &\quad + 8(\hat{\mu} \lambda_1 (h_1^c z)^2 + \bar{\lambda}_3) [\hat{\mu} \lambda_0 \cosh 2z(h_2 - h_2^c) + \lambda_{12} \cosh 2z(h_2 - h_2^c)] \\ &\quad - 32z^2 \hat{\mu}^2 c \{ 2h_1 h_2^2 z^2 \hat{\mu}^2 + \eta_4 h_2 + h_1 \lambda_1^2 (1 - \cosh 2zh_2) \} \\ &\quad - 16\{ h_2 \lambda_2 \hat{\mu} (\eta_4 h_1^c + h_2 \bar{\lambda}_5) z^2 - \bar{\lambda}_3 \bar{\lambda}_4 + 2\lambda_2 \hat{\mu}^3 (h_2 h_1^c z^2)^2 - \hat{\mu} \lambda_1 \bar{\lambda}_4 (h_1^c z)^2 \} \cosh 2zh_2^c \\ &\quad + 16\{ h_2 \lambda_2 \hat{\mu} (\eta_4 h_2^c + h_2 \bar{\lambda}_5) z^2 - \bar{\lambda}_3 \bar{\lambda}_4 + 2\lambda_2 \hat{\mu}^3 (h_2 h_2^c z^2)^2 - \hat{\mu} \lambda_1 \bar{\lambda}_4 (h_2^c z)^2 \} \cosh 2zh_1^c, \\ b_{11} &= 16\eta_4 \{ 2z^2 \hat{\mu}^2 h_2 c \cosh z(h_1 - h_2) + [h_1^c \hat{\mu} (h_2 \lambda_2 + \lambda_1 h_2^c) z^2 - \bar{\lambda}_3] \cosh z(h_2 - 2c) \\ &\quad - [h_2^c \hat{\mu} (h_2 \lambda_2 + \lambda_1 h_1^c) z^2 - \bar{\lambda}_3] \cosh z(h_2 + 2c) \}, \\ c_{11} &= 0, \end{aligned}$$

where

$$\begin{aligned} h_1^c &= \frac{h_1}{2} + c, & h_2^c &= \frac{h_2}{2} - c \\ \bar{\lambda}_3 &= 2\mu(1 - \nu_1)(\mu \bar{\nu}_1 - \bar{\nu}_2), & \bar{\lambda}_4 &= -\kappa_1 \mu^2 - 2\bar{\nu}_2 \bar{\nu}_1 \mu - \kappa_2, \\ \bar{\lambda}_5 &= \mu \eta_1 (\mu \bar{\nu}_1 + 1), & \bar{\nu}_i &= 1 - 2\nu_i \quad i = 1, 2. \end{aligned}$$